U. S. DEPARTMENT OF COMMERCE
NATIONAL OCEANIC AND ATMOSPHERIC ADMINISTRATION
NATIONAL WEATHER SERVICE
NATIONAL METEOROLOGICAL CENTER

OFFICE NOTE 311

THE EFFECT OF INITIAL UNCERTAINTY IN TROPICAL ANALYSES UPON 5-DAY FORECASTS WITH NMC'S GLOBAL SPECTRAL MODEL

EDWARD A. O'LENIC, PETER J. WEBSTER
AND
ARTHUR N. SAMEL

AUGUST 1985

ABSTRACT

The effect of initial perturbations in the tropical portions of the global optimum interpolation (OI) analysis scheme used at the National Meteorological Center (NMC) upon 5-day forecasts in both the tropics and in middle latitudes is examined.

Systematic tropical mass and wind field differences at 850 and 200 mb between analyses produced at NMC and the European Center for Medium-range Weather Forecasting (ECMWF) during the FGGE year are first shown to exist and to persist during February and June of 1979. Subsets of the ECMWF mass and wind field analyses at all levels in regions where the systematic difference or "uncertainty" is largest between the analysis are used to construct initial fields which are perturbed in isolated portions of the tropics. Five-day forecasts are then run from these initial data as well as from unperturbed "control" NMC analyses, and the results compared.

The response to initial tropical perturbations takes 2 forms: a local response and a teleconnection response to middle latitudes. Pertubations propagate in the tropics fairly slowly via Kelvin modes and mixed Rossby gravity modes. Propagation to middle latitudes occurs rapidly via ultra long wave length barotropic Rossby modes. The middle latitude response is similar regardless of the location of the initial perturbation, and the response is strongest when the initial perturbation lies near regions of tropical westerlies, suggesting that an initial tropical disturbance escapes to middle latitudes through these westerly wind ducts.

1. Introduction

Interest in improving the tropical portions of global data assimilation systems has grown in the face of mounting experimental and observational evidense that links disturbances in the tropical oceans and atmosphere with middle latitude weather systems. A direct result of this awareness is the recent appearance of initialization and analysis schemes aimed at improving global forecasts by properly representing the tropics (Puri, 1983; Julian, 1984). Bjerknes (1966, 1969) first proposed and then documented an apparent relationship between the sea surface temperature in the equatorial Pacific Ocean and sea level pressure in the subtropical Pacific. The oceanic and atmospheric systems were coupled via the Hadley circulation, which is, he suggested, strengthened during periods of anomalously warm ocean temperatures, resulting in stronger than normal middle latitude westerlies. The occurence of anomalously warm SST over the eastern equatorial Pacific has been found to occur with a quasi-regular period of 3-5 years has since become widely known as the El Nino - Southern Oscillation, or ENSO, phenomenon.

During the most recent occurence in 1982-1983, the ENSO reached its most intense level in recorded history and was accompanied by highly anomalous weather, both in the tropics and in middle latitudes (Rasmusson and Carpenter, 1982). Rowntree (1972) performed the first numerical experiment to investigate the SST - atmosphere relationship. Using a hemispheric version of the GFDL model with an equatorial wall, he found that anomalously warm SSTs in the eastern equatorial Pacific gave rise to a weakened Walker (East-West) Circulation not unlike that documented in Rasmusson and Carpenter (1982). Julian and Chervin (1978) substantiated Rowntree's results, using a version of the NCAR global circulation model to reproduce many of his middle latitude responses using initial SST anomalies identical to his.

Webster (1972), using a linear, global, baroclinic model to simulate the response of the tropical atmosphere to tropical forcing, found that the response takes two forms: Kelvin modes which form in the equatorial esterlies, and Rossby modes, which form in the middle latitude westerlies. Webster (1981) further refined his study of this problem by examining the response of the atmosphere, as simulated by a model similar to that used in Webster (1972), to forcing by warm SST anomalies placed at various latitudes. He found the atmospheric response to be strongest when the SST anomaly was placed in the tropics, where a strong local response, characterized by a positive diabatic heating-dynamic feedback, occurs. Webster further found that tropical SST anomalies also elicit a strong remote (teleconnection) response in middle latitudes. The remote response Webster found was also characterized by barotropy on the poleward side of the middle latitude westerlies and baroclinicity on the equatorward side. Hoskins and Karoly (1981) conducted a similar set of experiments using a linear, spherical, hemispheric, 5-layer baroclinic model. Using negative vorticity anomalies as proxies for heat sources. They found:

(1) largest atmospheric response to localized, steady, thermal forcing occurs when the anomaly is located in the subtropics;

(2) such a low-latitude source causes long waves to propagate poleward and eastward, with shorter waves turning toward the equator at about 35°;

(3) the middle latitude perturbations are barotropic; and

(4) a low latitude anomaly forces a wavetrain comprised of long waves, which lies along a great circle extending poleward and eastward of the source.

These results bear a marked resemblance to those of Wallace and Gutzer (1981) in which observational evidence of teleconnections between the tropics and middle latitudes was found; the teleconnection pattern strongly resembling a wavetrain lying along a great circle.

Anlaysis and forecast systems whose domains extend into the tropics have been found to possess a special set of problems involving the ultralong waves. Here, the term ultralong waves refers to motions whose horizontal scale L, is comparable to the radius of the earth a, i.e., $L/a \sim 1$ and $B = Ro^2Ri<1$, as defined by Phillips (1963). Such motions require that the equations of motion be formulated using spherical geometry. These waves (wave number 1-3) are stationary, or very slow moving. In October 1957, the Joint Numerical Weather Prediction (JNWP) unit extended the computational domain of the non-divergent barotropic model then in use from one of limited area to one of hemispheric proportions extending into the tropics, expecting a resultant large reduction in the gross error of the forecast (Wolff, 1958). Instead, the errors worsened since now, the model was forecasting waves 1-3 to retrogross. While very effective techniques were used to compensate for this shortcoming (Wolff, 1958; Cressman, 1958), the reason for this behavior was not found.

Dickenson and Williamson (1972) pointed out the importance of determining which parts of meteorological data fields should be retained and which should be discarded. They developed a technique for expanding initial data of a model with a finite number of degrees of freedom into the free oscillations of that model. In an example of the application of this technique to a 2 layer model, they found that, in addition to the modes known to be significant for meteorological analyses and forecasts, i.e., the westward propagating Rossby modes, the antisymmetric gravity mode (Kelvin mode) may also be of importance due to their low frequencies. Williamson and Dickinson (1976) expanded data from a 30 day forecast

from the NCAR global circulation model into the normal modes of that model in order to determine the relative importance of the various modes of oscillation present in the model. They compared the amplitudes of the physical modes to the computational, considering the latter to represent the "noise" level which physically meaningful physical modes must exceed in amplitude. They found that the amplitudes of the external Rossby mode, the Kelvin gravity mode, and the large scale internal Rossby modes do exceed the noise level, while the rest of the gravity modes do not. They suggested that these latter gravity modes could be selectively filtered from model data. Furthermore, Williamson and Dickinson (1976) found that the amplitudes of the stationary Kelvin modes exceed those of the transient Kelvin modes in the NCAR GCM, implying the existence long time-scale highly divergent, meteorologically significant eastward motions in this model.

A review of the mathematical techniques involved in finding the eigen solutions (normal modes) of linearized primitive equations on a sphere is presented in Kasahara (1976). The works cited thus far, point to the conclusion that the tropical portions of both the real atmosphere and several global circulation models; (1) contain wave motions which may be important locally, such as Kelvin modes and mixed Rossby-gravity moes, and (2) possess teleconnections with middle latitudes via ultralong wave external Rossby modes. In order to better exploit numerical models to understand complex atmospheric phenomena which they seem to simulate, we must understand better the behavior of the models themselves, especially with regard to the tropical portions of global analyses and forecasts. Somerville (1980), demonstrated that degraded tropical initial data can significantly degrade subsequent middle-latitude forecasts made using these initial fields. He also found that when forecasts made from similarly formulated GCMs and hemispheric models are compared, those forecasts

made using the GCMs tend to be superior to those from the hemispheric forecast models.

The foregoing review of literature suggests that there are two possible types of anomalies in tropical analyses and forecasts:

(1) forcing anomalies (e.g., sea surface temperature, vorticity, heating) as studied by Webster (1972, 1981), Hoskins and Karoly (1981), Rowntree (1972), Bjerknes (1969), Julian and Chervin (1978); and

(2) anomalies due to errors or uncertainties in specifying the initial fields in the tropics. Such anomalies may arise through a lack of radiosonde and rawinsonde data, and the fact that satellite winds are limited to two levels (low and high), and that the use of geostrophic winds derived from satellite mass field measurements is inappropriate in the tropics. It is clear that anomalies in tropical analyses, whether phenomenological or due to uncertainties, do significantly impact GCM forecasts and that it is important to understand the impact such perturbations have upon GCMs, and whether or not the impact is systematic.

The purpose of this paper is to examine the effect of initial uncertainties in tropical analyses upon subsequent global forecasts. To do so, first we will define the uncertainty pattern in the analysis. We then construct an experiment designed to allow the insertion of uncertainties into analyses which are then used as initial data for GCM forecasts out to 5 days. Finally, we give the results of the experiments, showing that, as a direct result of the initial perturbations, orderly propagation occurs in the tropics, the features bearing the appearance of eastward propagating Kelvin waves, and westward propagating mixed Rossby-gravity waves. The middle latitude response tends to be constant,

regardless of the location of the initial perturbation. This result is different than earlier results from simple climate models.

2. Estimates of Uncertainty in the Initial State of the Tropics

We now face the very difficult problem of estimating the uncertainty in analyses of tropical wind and mass fields. The two main sources of uncertainty in tropical analyses arise from data scarcity and from inaccurate initializaton. The latter problem is the subject of ongoing research, and there is reason to believe that progress will be made on it. The observing network, especially in the tropics however, shows signs of continual deterioration. The best global tropical data set ever assembled is that compiled during the first GARP Global Experiment (FGGE). The best estimates we have of the atmospheric state during the FGGE year (1979) consist of carefully prepared analyses of NMC and ECMWF, the FGGE IIIA, and FGGE IIIB analyses. For various reasons, including differences in the analysis codes themselves, different time thresholds for using data which becomes available either before or after the nominal time of the analysis and differing operational constraints, analyses valid simultaneously are slightly different. It is these differences which we use to define analysis uncertainty.

Figure 1a shows the global wind speed differences at 200 mb between pairs of these analyses for 12GMT 17 February and 12GMT 27 June. Note that 200 mb wind speed differences of 5-10 ms^{-1} exist throughout the tropics, but that localized regions where these differences exceed 10 ms^{-1} occur in the tropical eastern Pacific Ocean, the western Pacific Ocean, and the Indian Ocean. Examination of a large number of these maps reveals that these differences are systematic, occuring map after map of analysis differences during February and June 1979. A Hovmoller diagram constructed from the analysis difference maps during these months clearly shows the persistence of these differences. The

cases shown in Figure 1a are those which were thought to be fairly representative of the systematic differences seen in the time series of analysis differences exemplified by Figure 1b.

3. Experimental Design

Five numerical model runs were done for each of the two sets of cases, including a "control" forecast out to 5-days using the unmodified NMC analysis to initialize the global spectral model. The remaining four runs per case were made using specially prepared analyses as initial data. These "test" analyses were prepared by inserting a subset of the ECMWF analysis valid at the same time as the NMC analysis into the NMC analysis. Thus, the only difference between a pair of test and control analyses for a given case would occur in the subset region. The subset insertions were done for u, v, z, and T at all levels. The four different subset regions used are shown in Figure 1. Interpolation was performed in a ten degree wide band surrounding each subset region in such as way as to linearly reduce the difference between the subset boundary points and the surrounding NMC analysis to zero over the band. Following the insertion and blending of the ECMWF subset into the NMC analysis, a non-linear normal model initialization is performed, and the model is integrated out to 120 hours in 17 minute time steps. Figure 2 illustrates the sequence of events involved in performing such an experiment.

The numerical model used for this study is the rhomboidally truncated, 12-layer, 30-zonal wave, -coordinate, global model described in Sela (1982), and used operationally at NMC. Model parameterizations include: orography, which is modeled spectrally; lower boundary friction, and a drag coefficient C_D, which is a function of latitude and longitude; sensible heat transfer from the ground to the air over the oceans only; dissipation, parameterized

by a term of the form $\kappa\nabla^4 F$, where F = a prognostic variable, and $\kappa = 6 \times 10^{15}$. Moisture flux from ocean to atmosphere is parameterized by a formulation in which the flux is a function of wind speed and sea surface temperature. There is no evaporation from land in this model. The model moisture sink consists of convective and large-scale condensation accumulated every time step at each point of the computational grid. Kuo-type convection is used. In all the experiments, the sea surface temperature used was the climatological sea surface temperature field.

Sections 4 and 5 present the results of the winter and summer experiments, respectively. Section 4 presents a discussion of results, and Section 5 contains conclusions.

4.1 The Extratropical Response

We now examine the response of the model atmospere in middle latitudes to initial uncertainty perturbations created by inserting subsets of the ECMWF analysis for a given day into the NMC analysis valid at the same time, as decribed in Section 3. Figure 3 shows the results of the four 120 hour forecast experiments run from 12GMT 17 February 1979 initial data. (Maps such as these showing differences between forecasts initialized from perturbed initial conditions and forecasts from unperturbed initial conditions will be called "perturbation forecasts"). The experiment in which the largest region of uncertainty, the WTT (Winter Total Tropics) run, was inserted also has the largest perturbation forecast amplitude, with 200 mb height differences exceeding 100 meters in the North Atlantic and North Pacific (Figure 3a). The bulk of the impact occurs between 30°N and 60°N. The perturbation forecast for the WEP (Winter Eastern Pacific) experiment (Figure 3b) nearly reproduces the WTT pattern over the North Atlantic, northeast of the location of the initial

perturbation, but includes larger scale differences over the Pole and the Pacific Ocean. The WIO (Winter Indian Ocean) perturbation forecast (Figure 3c) again reproduces the WTT pattern to the northeast of the site of the initial perturbation. It also contains a hint of the WTT difference couplet near 30°W. The WWP (Winter Western Pacific) perturbation forecast (Figure 3d) also contains this couplet, as well as features which appeared in the WTT experiment to the northeast of the site of the WWP initial uncertainties. Figure 3 shows that the northern hemisphere middle latitude response is largest to the north and east of initial uncertainty perturbation, a result similar to that of Hoskins and Karoly (1981). It also clearly shows a tendency for middle latitude perturbations to occur in the same location, though perhaps differing in amplitude from case to case, regardless of the location of the initial perturbation. The summer hemisphere also responds in just this way (Figures 4a-d), but with the maximum response occuring slightly closer to the pole, suggesting perhaps some dependence of the location response upon the baroclinicity of the atmosphere, though Figure 5 clearly indicates that the form of the response is barotropic.

The 120 hour 200 mb forecast height difference for the four experiments run from initial data valid 12GMT 27 June 1979 are shown in Figures 6-8. These maps show a marked tendency for the recurrence of the same difference pattern regardless of the site of the initial perturbation. In this case, the difference couplet extending from the vicinity of Turkey eastward to about 60°E reappears in each of the maps of 120 hour forecast height differences (Figures 6a-d). The tendency, noted earlier, for the largest response to occur poleward and eastward of the initial perturbation is not as marked in Figures 6a-d, nor is there any indication that response in the northern (summer) hemisphere occurs any farther north than it did in the February case. As shown in Figure 7, the response in the southern hemisphere tends to occur closer to the pole than it does in the

northern hemisphere. This effect then is probably attributable to differences in the distribution of land and sea between the hemispheres. The response in the winter hemisphere again shows a tendency to be stronger than that in the summer hemisphere, and to have maximum amplitude poleward and eastward of the initial perturbation.

The evolution of these forecast differences can be illustrated by examining a sequence of successive forecasts from the WEP experiment at 12 hour intervals out to 120 hours (Figure 9). The difference in the initial NMC and ECMWF height fields in the uncertainty region is too small to show with the 20 meter contour interval used in Figure 9a. By 12 hours differences appear in both hemispheres near the site of the initial differences. As the forecast progresses, a wavetrain slowly develops, well defined in the winter hemisphere, and muted, but well defined in the summer hemsiphere, extending poleward and eastward of the site of the initial disturbance. The wavetrains themselves remain quasi-stationary throughout the forecast sequence. The large middle latitude differences between the perturbed and control forecasts develop after about 84 hours. Daley, et.al, (1981), showed that such a middle latitude response is caused in part by the excitation of external large-scale Rossby modes, forced by difference in the rotational component of the tropical wind fields of the control and perturbation forecast initial data.

When the wind field for this same forecast series is examined (Figure 10), it becomes clear that the information of the initial disturbance resides mainly in the wind field. As the forecast progresses, wind field differences propagate both eastward and westward from the initial disturbance, while remaining relatively confined within the tropics out to 24 hours. Then, at 36 hours, the disturbance in the velocity field appears to begin to progress northward over

the southern U.S. Between 36 and 72 hours, the perturbation pattern spreads eastward and westward over the southern U.S., forming an enlongated pattern which coincides with a strong jet. The region poleward and eastward of the original WEP perturbation appears to be the only place on the globe that disturbances can propagate through toward the poles, except for some small amplitude leakage into the southern hemisphere near Australia. This region is the site of a region of westerly winds. Webster (1982) noted that atmospheric waves can propagate meridionally through such "westerly ducts". High amplitude wind speed differences of more than 12 ms^{-1} develop over the north Atlantic by 120 hours, the amplitude increasing very rapidly after 96 hours.

4.2 The Tropical Response

One of the questions we wish to answer is: Does orderly propagation of uncertainty occur in the tropics, and if so, under what conditions? In order to address this question, Hovmoller (longitude versus time) charts of wind speed, height, and rotational and divergent wind component differences were prepared from the model forecast spectral coefficients. In order to simplify the Hovmoller fields, the spectral coefficients were selectively zeroed so that only certain wave numbers were included in the diagrams. A truncation which includes only waves 0-3 gives results in the deep tropics which appear only slightly different from those obtained when zonal waves 0-10 (not shown) are used. This wave number band is also the logical one in which to seek the ultralong waves which have been shown by Webster (1972, 1981, 1982), Somerville (1980), Williamson and Dickinson (1976), Puri (1983), Zangvill and Yanai (1981, 1982), Lu and Lanai (1984), to be of importance in the tropics. Figure 11 shows Hovmoller charts centered on the equator from control analysis of 200 mb height (Z), stream function (ψ), and velocity potential (χ) for both the winter

and summer experiments. A similar set of 850 mb charts is provided in Appendix 1. The significant features of the control Hovmoller are: (1) the change in the scale of the 200 mb height field from a wave number 2 form in the winter case, to a wave number 1 in summer (Figure 11a,b); (2) the clear evidence of an eastward propagating ultralong wavelength feature in the velocity potential forecasts, a feature which also exists, though with a much higher amplitude, in the summer control Hovmoller (Figure 11b,c); and (3) the spatial stationarity of the features in the winter stream function control forecasts, versus the clear existence of a westward propagating feature with wave number two spatial scale.

The perturbed-minus-control forecast difference for the June and February experiments are shown in Figures 12-14. There is a clear tendency for eastward propagation of the different perturbations of height, and especially velocity potential in both the June and February experiments. Stream function differences, on the other hand, propagate westward at a fairly rapid rate. The forecast differences in the June cases generally have much larger amplitude than do those for February. The phase speed of the eastward propagating features is about 40 ms^{-1}, which is approximately the phase speed of the slowest gravity mode for vertical mode 4 and planetary wave number 1 in the NMC spectral model for 12 equally spaced levels (Ballish, 1980). These wave modes strongly resemble those shown by Puri (1983) to be excited by convective adjustment in the ANMRC specral model, and which dominate the model's Tropical irculation. Although the modes excited vary somewhat with the number and spacing of the levels of the model, Puri's results appear to have application to those we obtained from NMC's spectral model (Ballish, personal communication). In comparing forecasts with and without convection, Puri found large differences in the total gravity mode energy in vertical model 4. He relates this to the

existence of very low frequency eastward (Kelvin) and westward (mixed Rossby-gravity) propagating modes. According to Table 1 of Ballish (1980), the phase speed of the gravest eastward propagating internal mode is 36 meters per second. This agrees well with the phase speed (39 ms^{-1}) of the wave number 1 features in Figure 11c,d.

While there is ample evidence of tropospheric Kelvin modes and mixed Rossby-gravity modes in numerical models (Webster, 1972; Dickinson and Williamson, 1972; Williamson and Dickinson, 1976; Kasahara, 1976; Puri, 1983), until recently observational evidence of Kelvin waves has been limited to the lower stratosphere. Wallace and Kousky (1968) discovered eastward propagating disturbances with a period of 15 days, and a downward component of phase velocity in the equatorial stratosphere, Murakami (1971) concluded that these Kelvin modes were forced from below by large-scale diabatic heating in the tropical troposphere, based on numerical experiments using a simple linear primitive equations model. The work of Zangvill and Yanai (1980, 1981) establishes the existence of these wave modes in the equatorical troposphere at 200 mb. Using the solutions of Laplace's tidal equations of Longuet-Higgins (1968), Lu and Yanai (1984) extended the work of Zangvill and Yanai, finding eastward moving waves for zonal wave number one with periods of greater than 20 days, and of about 7 days. They also found westward propagating waves with zonal wave number 4 and period 5 days. They positively identified the former waves as Kelvin waves having no meridional component, and the latter as mixed Rossby-gravity waves, which do possess a meridional component of phase velocity. The large-scale wave number one feature in the divergent component of the forecast wind field differences seen in Figure 12c qualitatively resembles Lu and Yanai's Kelvin waves, while the westward propagating features in the rotational component resembles the faster moving mixed Rossby-gravity modes (5-day periods).

5. Conclusions

Numerical experiments have been conducted, using systematic differences between simultaneous NMC and ECMWF global analyses of wind and mass as "uncertainties", by inserting and blending various subsets of the ECMWF tropical analysis into the NMC analysis. 5-day forecasts using these perturbed analyses as input data were then compared with unperturbed control forecasts. The response of the model to these perturbations takes place both locally (in the tropics) and remotely (in the middle latitudes). In the tropics, eastward propagating, apparently trapped waves result, waves resembling the Kelvin modes found by many investigators in both the real atmosphere and in model atmospheres. A wave resembling a westward propagating mixed Rossby-gravity mode, with a meridional component, is also found. There is evidence that the tropically excited Rossby mode propagates into the westerlies of both hemispheres. The middle latitude response tends to be the same regardless of the location of the initial perturbation. This suggests that the meridional transport of wave energy is highly selective, and supports the notion that the energy of waves excited by the initial disturbance can propagate northward or southward form the tropics only in specific regions as suggested by Webster (1982). The results indicate that differences in the tropical wind fields from two state of the art analysis and forecast systems result in significant forecast differences in as little as five days. Such a result implies the need for improvements in either the data in the tropics, or the analysis system, or both.

Acknowledgements

Thanks are due to Dr. John Ward and Mr. Scott Dennstaedt for devising and coding the transplant technique, and to Dr. Brad Ballish for interesting discussions.

References

Ballish, B. A., 1980: Initialization, theory and application to the NMC spectral model. PhD Dissertation. Dept. Meteoro., Univ. of Maryland, 151 pp.

Bjerknes, J. 1966: A possible response of the atmospheric Hadley circulation to equatorial anomalies of ocean temperature. Tellus, 18, 820-829.

Bjerknes, J., 1969: Atmospheric teleconnections from equatorial Pacific. Mon. Wea. Rev., 108, 1279-1292.

Cressman, G. P., 1958: Barotropic divergence and very long atmospheric waves. Mon. Wea. Rev., 86, 293-297.

Daley, R. J., J. Tribbia, and D. L. Williamson, 1981: The excitation of large-scale free Rosby waves in numerical weather prediction. Mon. Wea. Rev., 109, 1836-1861.

Dickinson, R. E., and D. L. Williamson, 1972: Free oscillation of a discrete stratified fluid with application to numerical weather prediction. Journ. Atmos. Sci., 29, 623-640.

Hoskins, B. J., and D. J. Karoly, 1981: The steady linear response of a spherical atmosphere to thermal and orographic forcing. Journ. Atmos. Sci., 38, 1179-1196.

Julian, P. R., and R. M. Chervin, 1978: A study of the Southern Oscillation and Walker Circulation phenomenon. Mon. Wea. Rev., 106, 1433-1451.

Julian, P. R., 1984: Objective analysis in the tropics: a proposed scheme. Mon. Wea. Rev., 112, 1752-1767.

Kasahara, A., 1976: Normal modes of ultralong waves in the atmosphere. Mon. Wea. Rev., 104, 669-690.

Longuet-Higgins, M. S., 1968: The eigenfunctions of Laplace's tidal equations over a sphere. Phil. Trans., London, A262, 511-607.

Lu, M. M., and M. Yanai, 1984: Equatorically trapped waves at the 200 mb level and their association with meridional wave energy flux and cloud activity. Post-print Volume, 15th Conf. on Hurricanes and Tropical Meteorology, Jan. 9-13, 1984, Miami, FL, Amer. Met. Soc., 45 Beacon St., Boston, MA 02108. pp. 514-521.

Murakami, T., 1971: Equatorial stratospheric waves induced by diabatic heat sources. Journ. Atmos. Sci., 29, 1129-1137.

Phillips, N. A., 1963: Geostrophic motion. Rev. Geophysics. 1, 123-176.

Puri, Kamal, 1983: The relationship between convective adjustment, Hadley circulation and normal modes of the ANMRC spectral model. Mon. Wea. Rev., 111, 23-33.

Rasmusson, E. M., and T. H. Carpenter, 1982: Variations in tropical sea surface temperature and surface wind fields associated with the Southern Oscillation/ El Nino. Mon. Wea. Rev., 110, 354-384.

Rowntree, P. R., 1972: The influence of tropical east Pacific Ocean temperatures on the atmosphere. Quart. J. R. Met. Soc., 98, 290-321.

Sela, J. G., 1982: The NMC spectral model. NOAA Technical Report NWS 30, U.S. Department of Commerce, Washington, D.C.

Somerville, R. C. J., 1980: Tropical influence on the predictability of ultralong waves. Journ. Atmos. Sci., 37, 1141-1156.

Wallace, J. M., and V. E. Kousky, 1968: Observational evidence of Kelvin waves in the tropical stratosphere. J. Atmos. Sci., 25, 900-907.

Wallace, J. M., and D. S. Gutzler, 1981: Teleconnections in the geopotential height field during the Northern Hemisphere winter. Mon. Wea. Rev., 109, 784-812.

Webster, P. J., 1972: Response to the tropical atmosphere to local steady forcing. Mon. Wea. Rev., 100, 518-541.

Webster, P. J., 1981: Mechanisms determining the atmospheric response to sea surface temperature anomalies. Journ. Atmos. Sci., 38, 554-571.

Webster, P. J., 1982: Seasonality in the local and remote atmospheric response to sea surface temperature anomalies. Journ. Atmos. Sci., 39, 41-52.

Webster, P. J., 1982: Cross-equatorial response to middle-latitude forcing in a zonally varying basic state. Journ. Atmos. Sci., 39, 722-744.

Williamson, D. L., and R. E. Dickinson, 1976: Free Oscillations of the NCAR global circulation model. Mon. Wea. Rev., 104, 1372-1391.

Wolff, P. M., 1958: The error in numerical forecasts due to retrogression of ultralong waves. Mon. Wea. Rev., 86, 245-250.

Zangvill, A., and M. Yanai, 1980: Upper tropospheric waves in the tropics. Part I: Dynamical analysis in the wavenumber-frequency domain. Journ. Atmos. Sci., 37, 283-298.

Zangvill, A., and M. Yanai, 1981: Upper tropospheric waves in the tropics. Part II. Association with clouds in the wavenumber-frequency domain. Journ. Atmos. Sci., 38, 939-953.

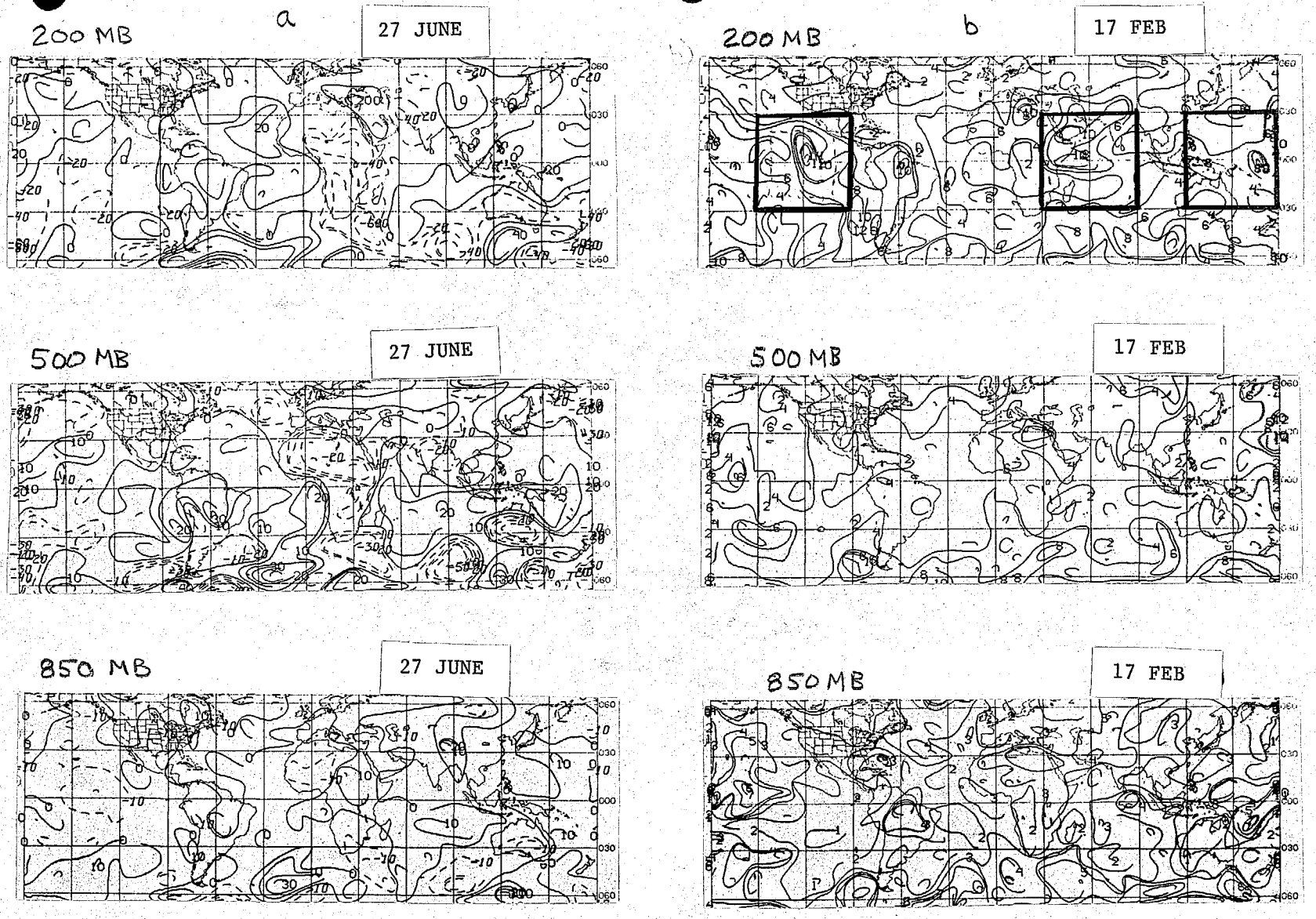

Figure 1. NMC-ECM wind speed differences, meters per second, at 850, 500 and 200 mb for 12 GMT 17 February 1979, and 27 June 1979.

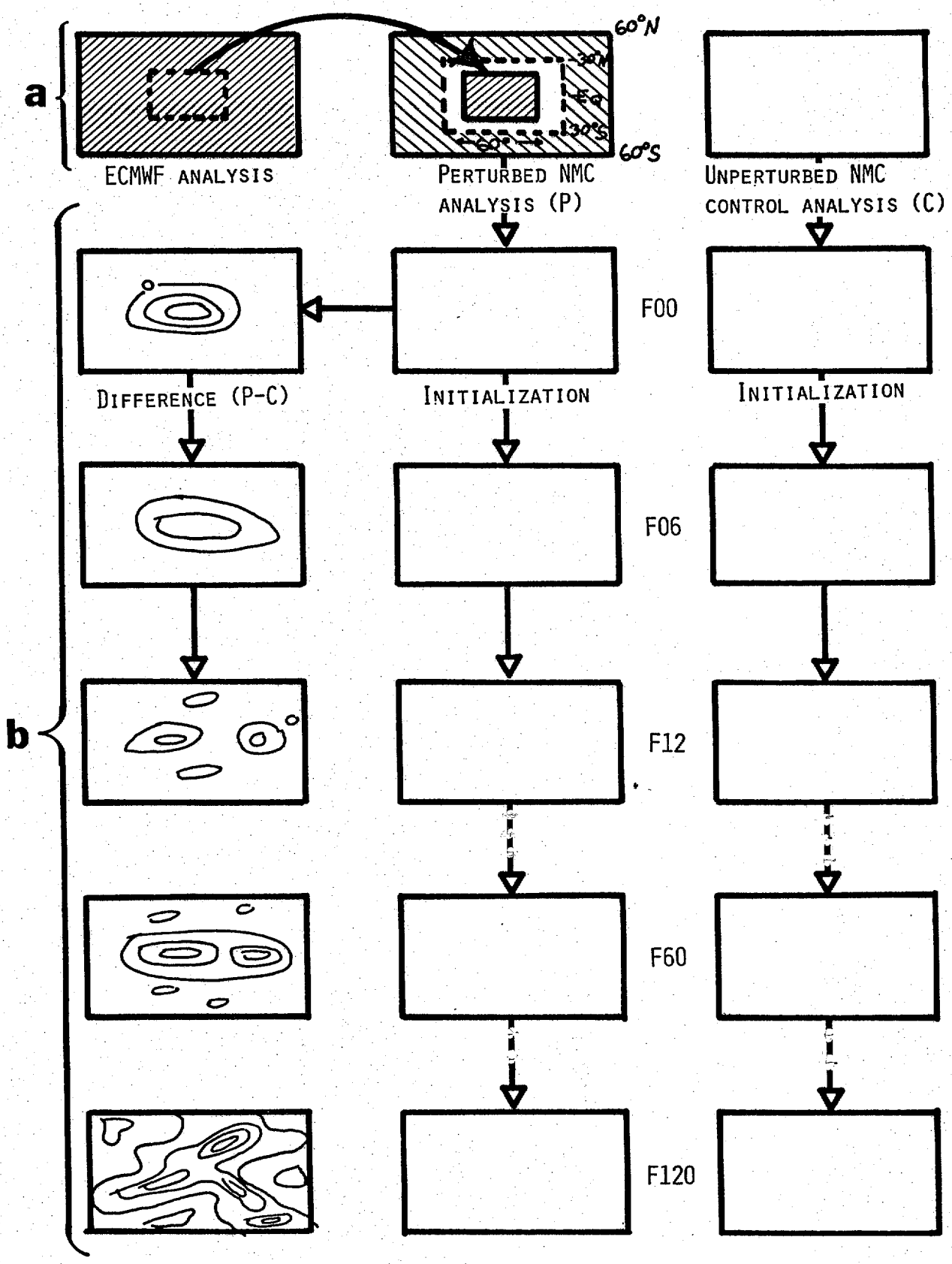

Figure 2. Schematic of design of the perturbation experiments showing (a) insertion and blending of ECMWF analysis subset into the NMC analysis, and (b) initialization and forecast sequence.

a) Total tropics (WIT)

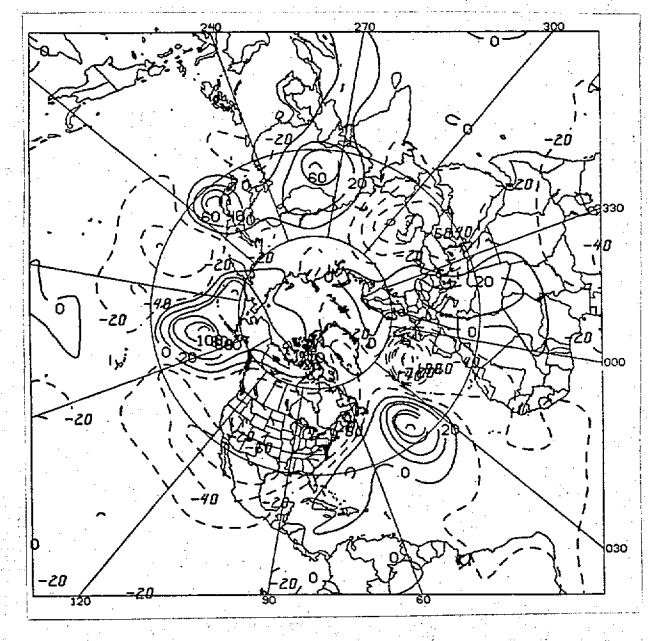

b) Eastern Pacific (WEP)

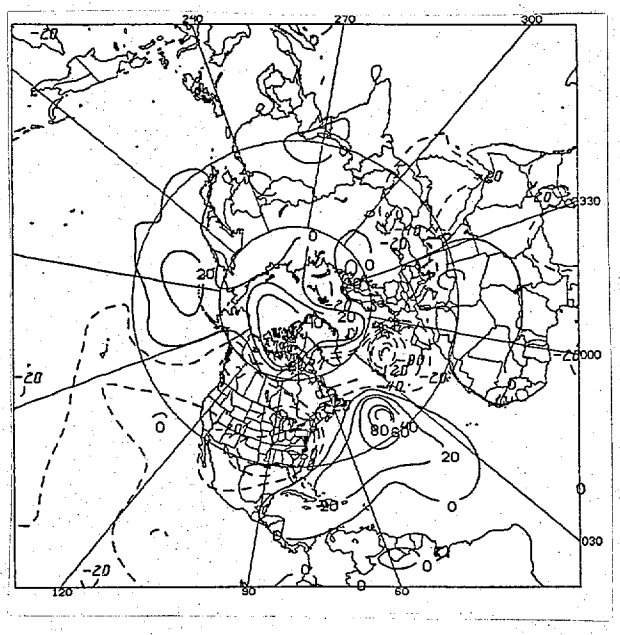

c) Indian Ocean (WIO)

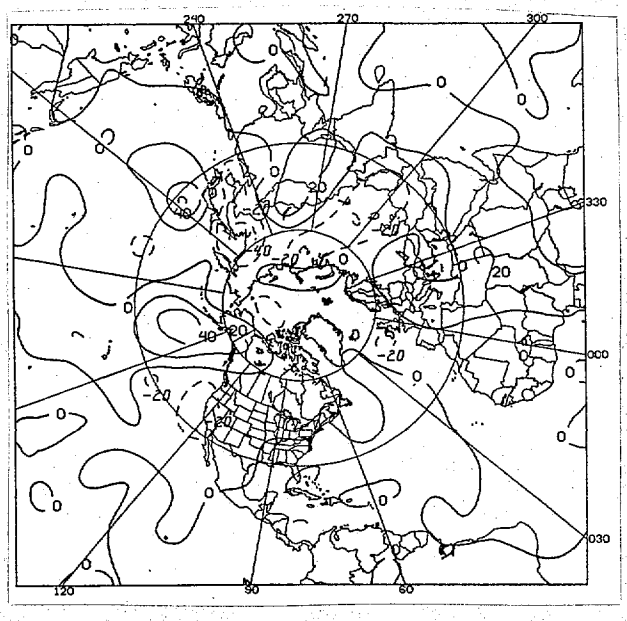

d) Western Pacific (WWP)

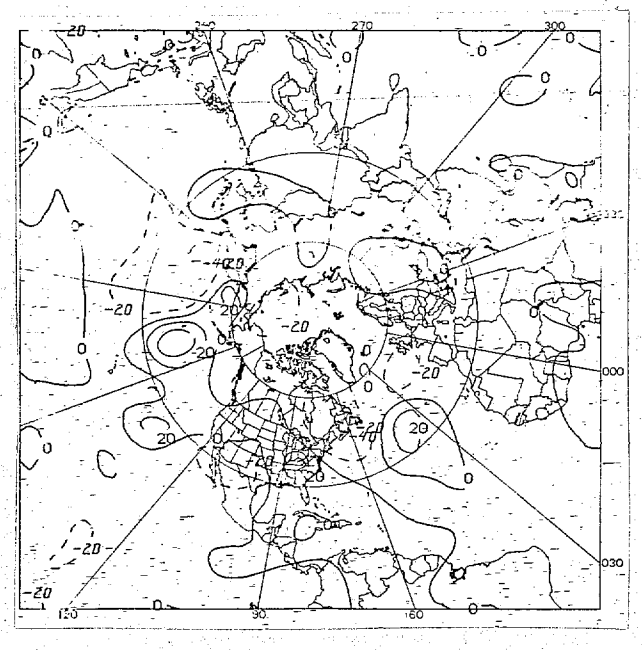

Figure 3. 120 hour differences (P-C), meters, between perturbed (P) and control (C) forecasts of 200 mb height for the winter experiments, northern hemisphere.

a) Total tropics (WTT)

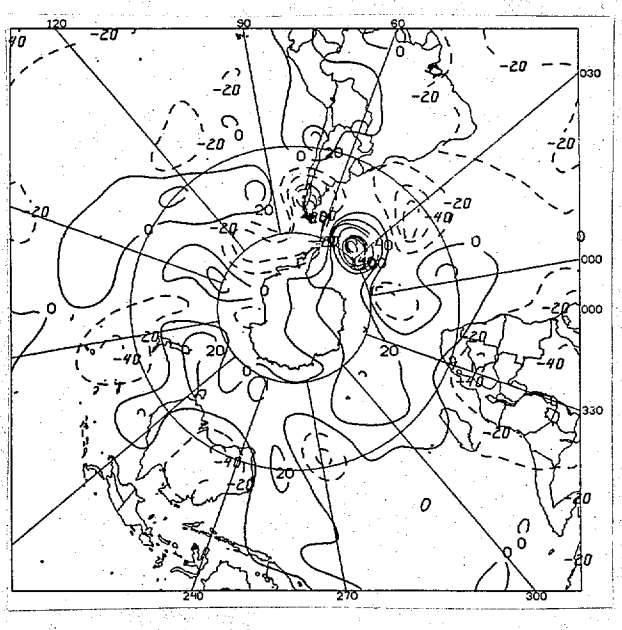

b) Eastern Pacific (WEP)

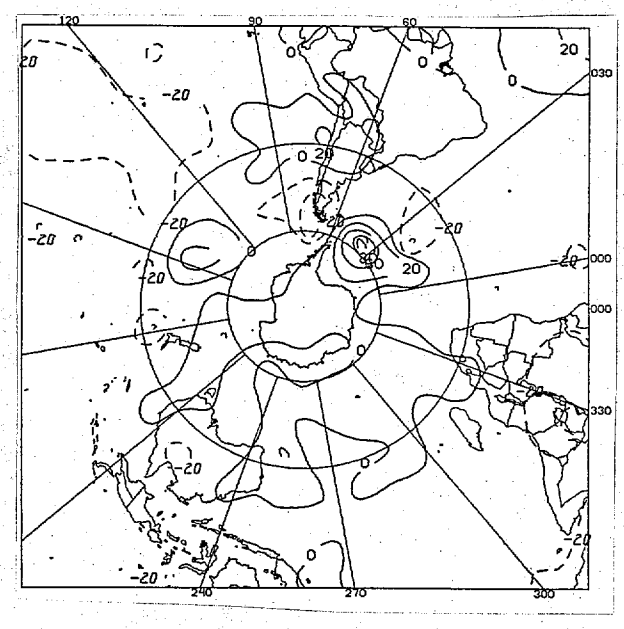

c) Indian Ocean (WIO)

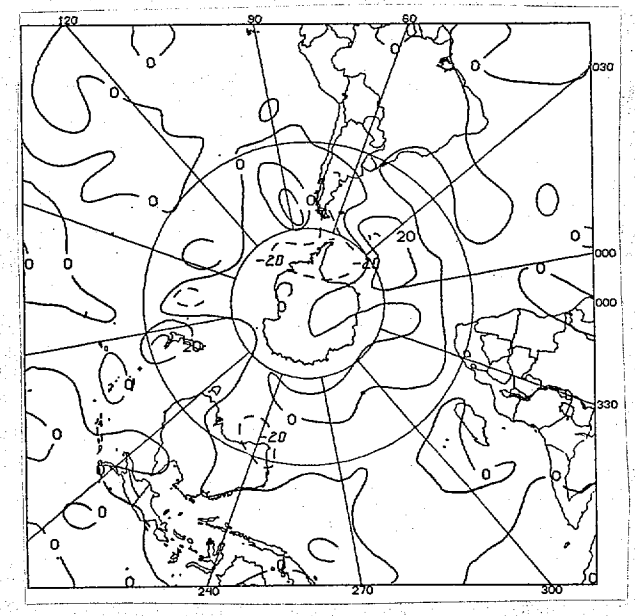

d) Western Pacific (WWP)

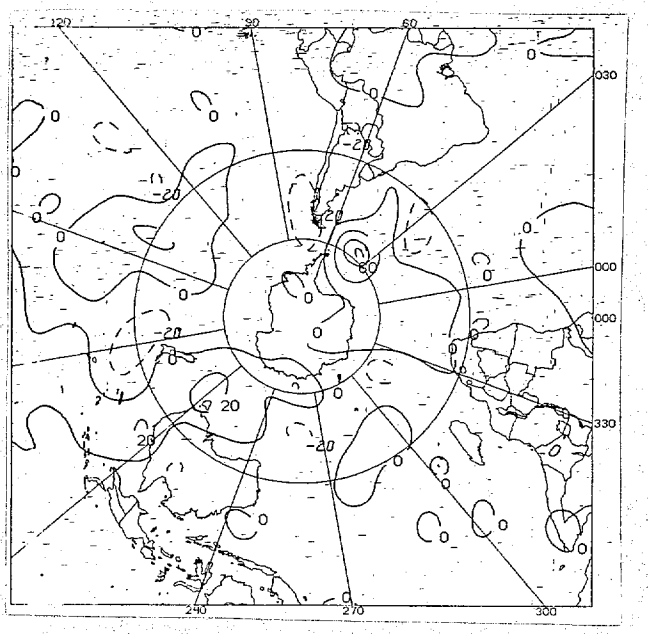

Figure 4. 120 hour differences (P-C), meters, between perterbed (P) and control (C) forecasts of 200 mb height for the winter experiments, southern hemisphere.

a)

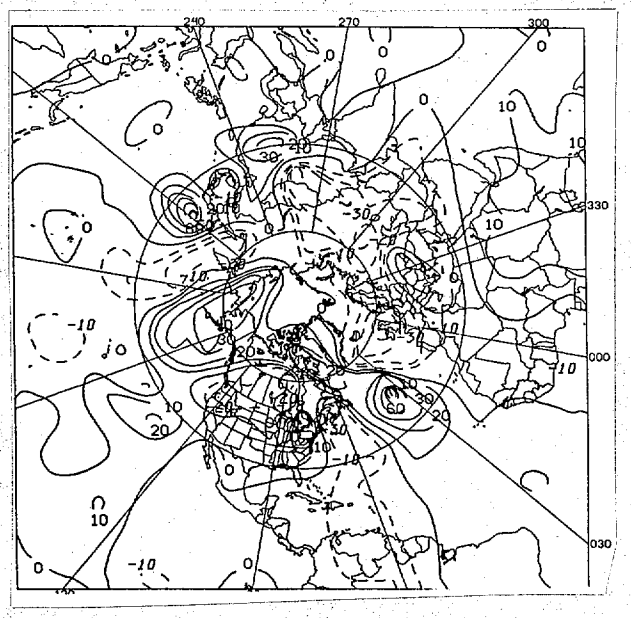

b)

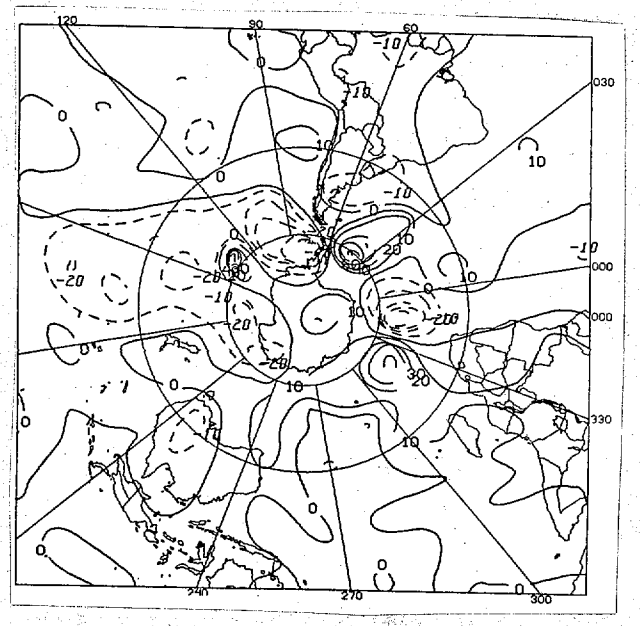

Figure 5. 120 hour differences (P-C), meters, between perturbed (P) and control (C) forecasts of 850 mb height, both hemispheres, winter total tropics experiment.

a) Total tropics STT

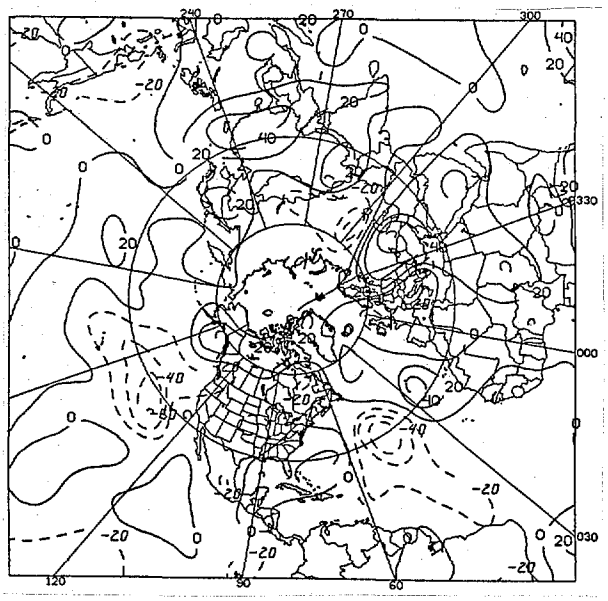

b) Eastern Pacific SEP

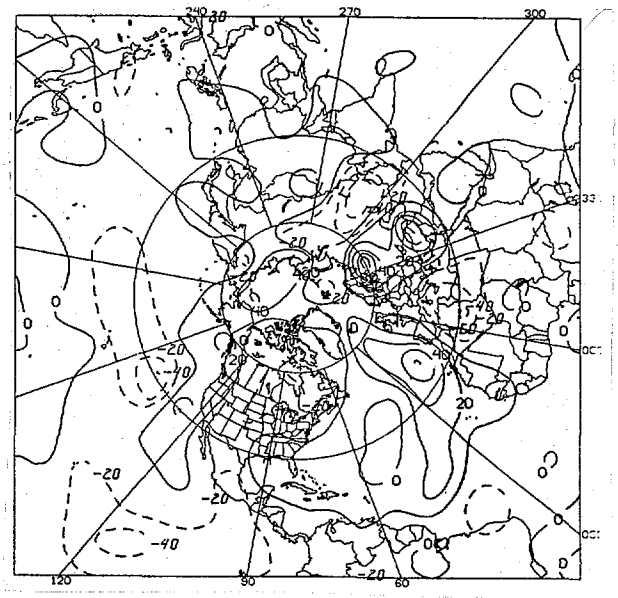

c) Indian Ocean SIO

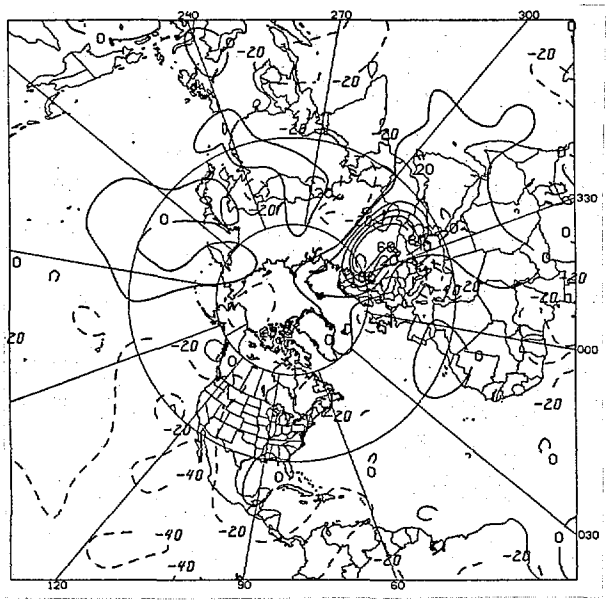

d) Western Pacific SWP

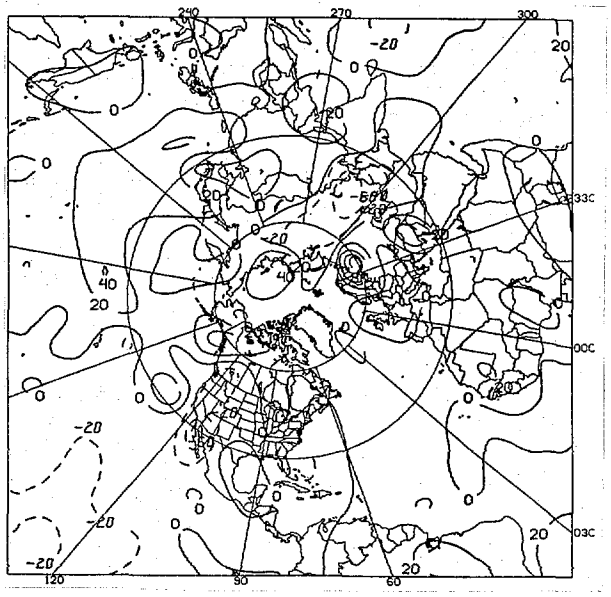

Figure 6. 120 hour differences (P-C), meters, between perturbed (P) and control (C) forecasts of 200 mb height for the summer experiments, northern hemisphere.

a) Total tropics STT

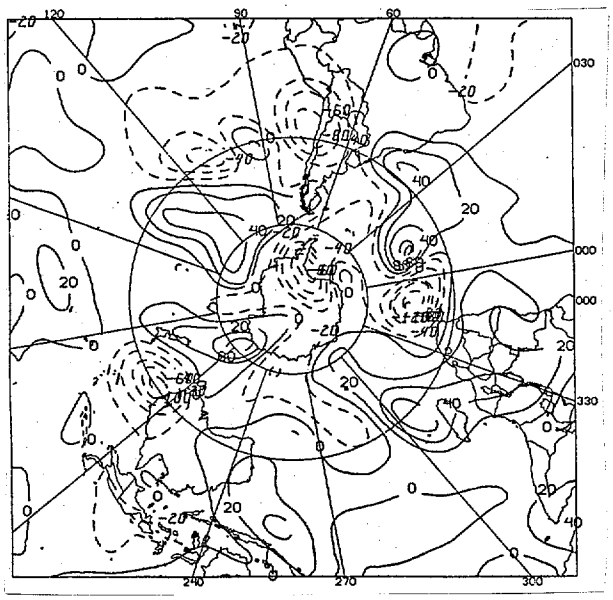

b) Eastern Pacific SEP

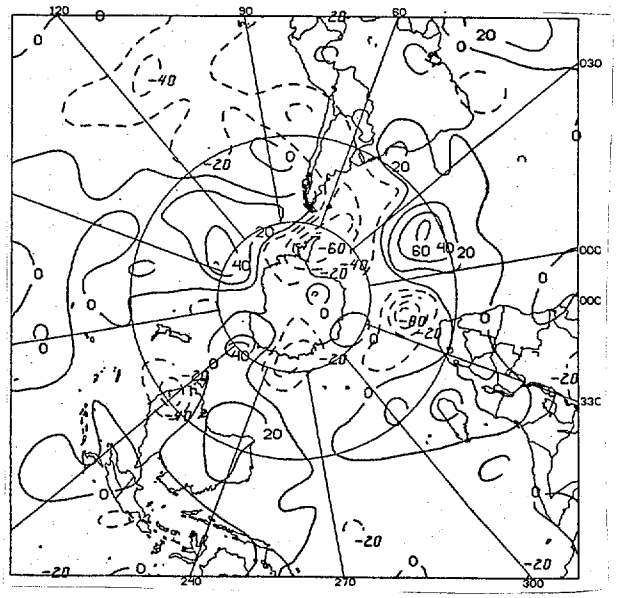

c) Indian Ocean SIO

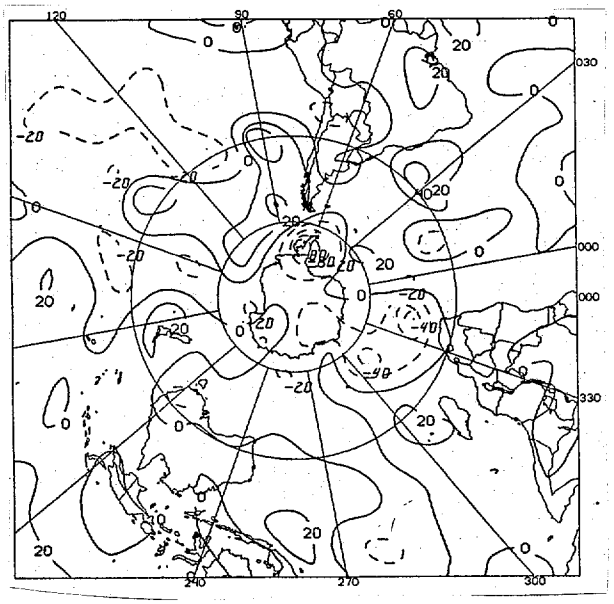

d) Western Pacific SWP

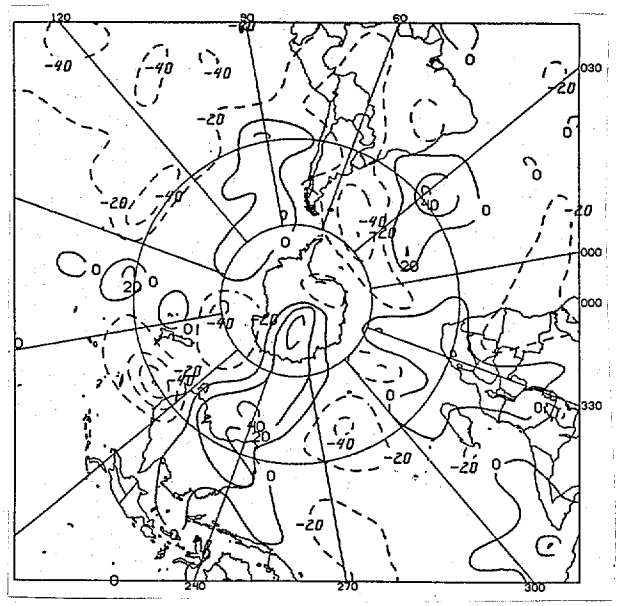

Figure 7. 120 hour differences (P-C), meters, between perturbed (P) and control (C) forecasts of 200 mb height for the summer experiments, southern hemisphere.

a)

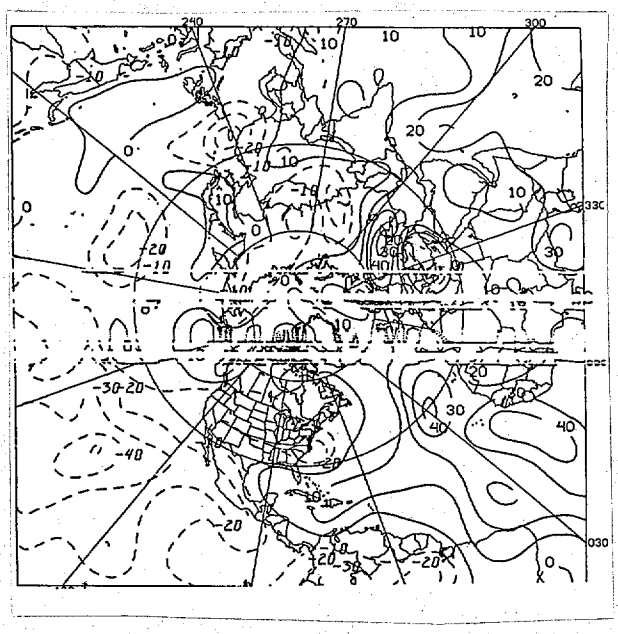

b)

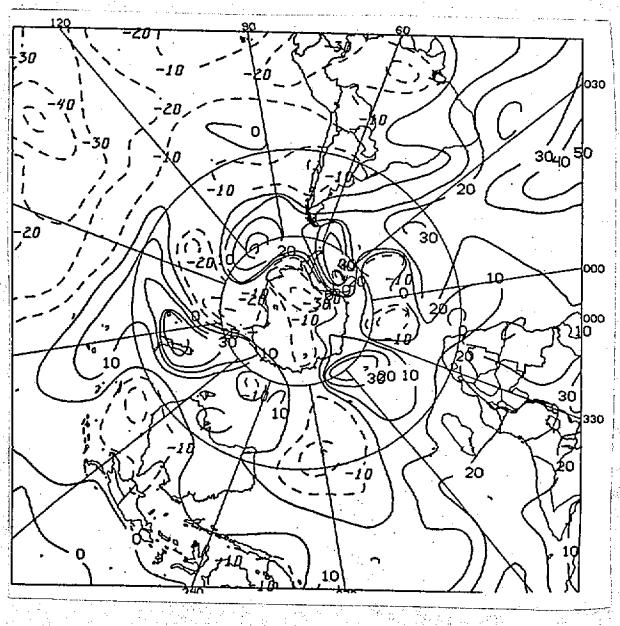

Figure 8. 120 hour differences (P-C), meters, between perturbed (P) and control (C) forecasts of 850 mb height, both hemispheres, summer total tropics experiment.

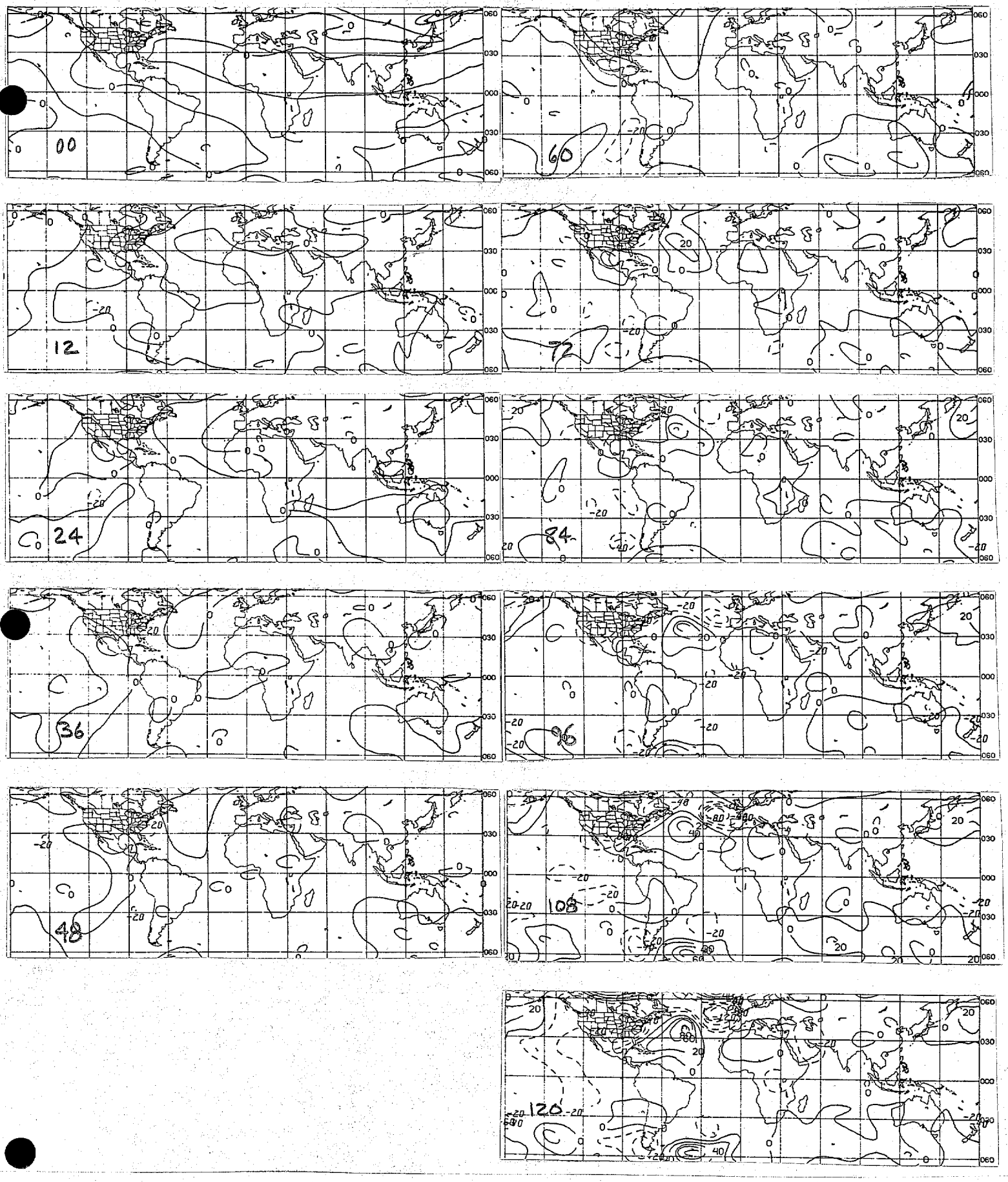

Figure 9. Evolution of 200 mb forecast height field differences (P-C), meters, at 12 hour intervals for the winter eastern Pacific experiment (WEP).

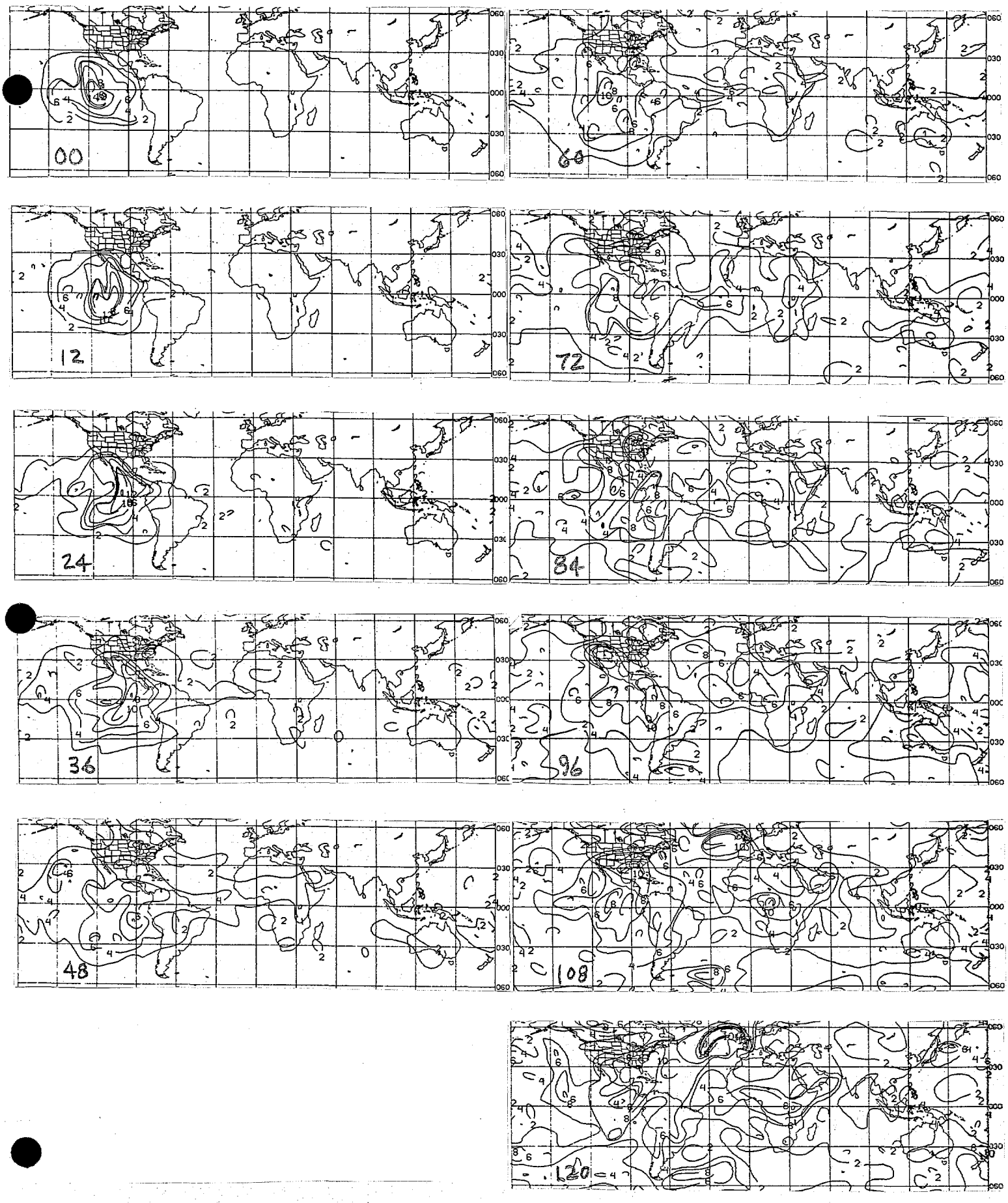

Figure 10. Evolution of 200 mb forecast wind field differences (P-C), ms^{-1}, at 12 hour intervals for the winter eastern Pacific experiment (WEP).

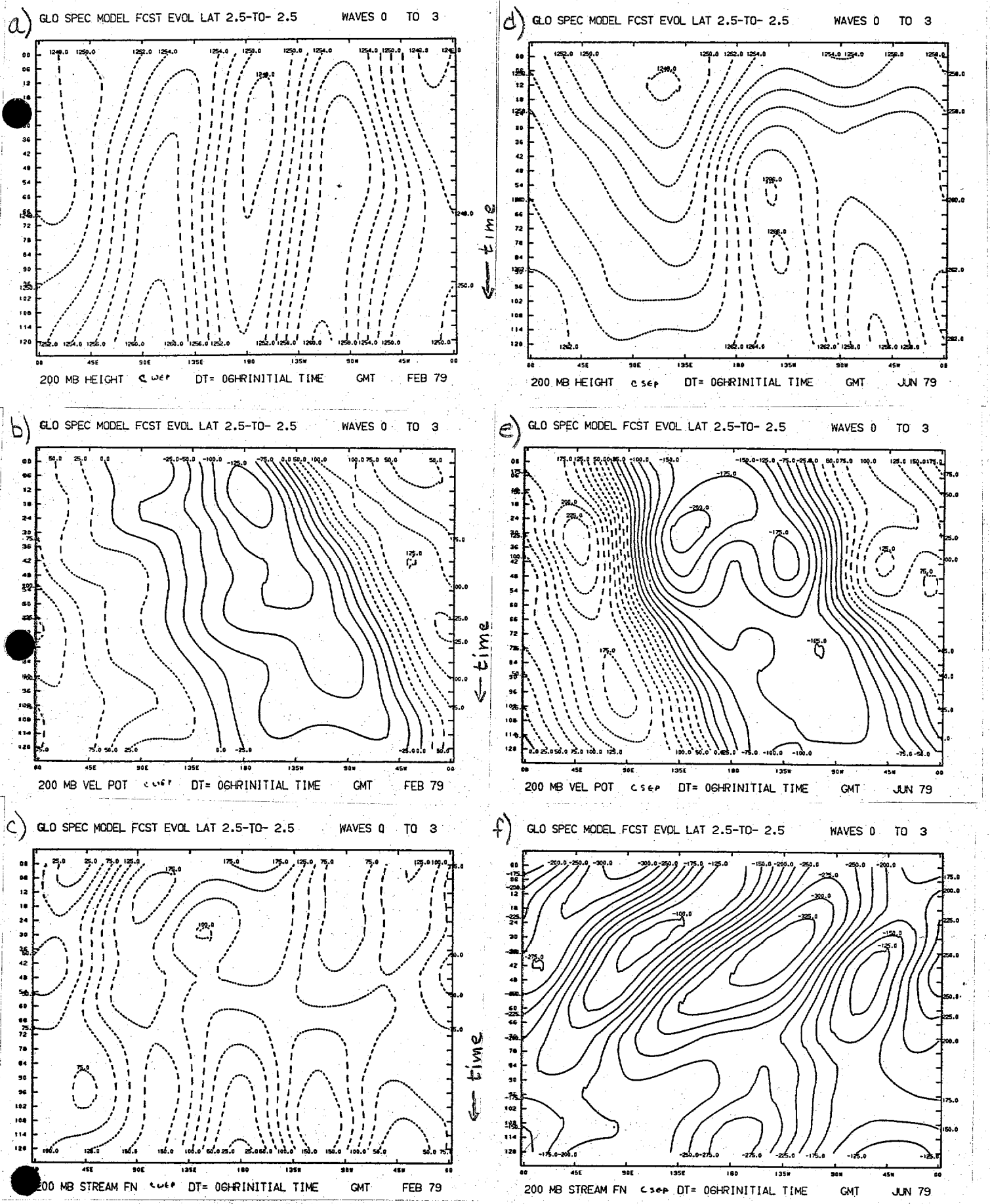

Figure 11. Hovmoller diagram of control forecasts of 200 mb height (Z), velocity potential (X), and stream function (ψ) for winter (a,b,c), and summer (d,e,f) cases, for 5 degree band centered on 0°.

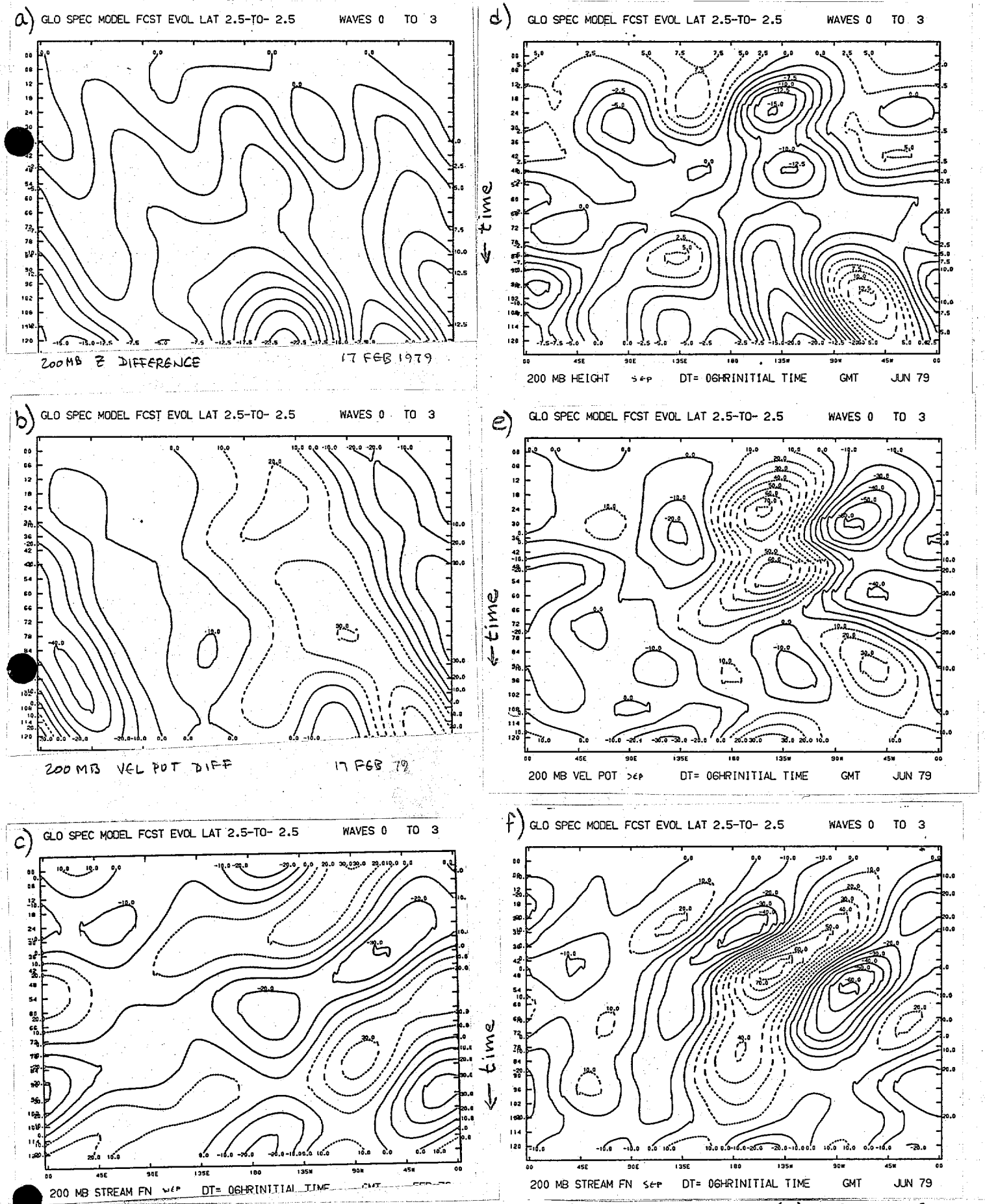

Figure 12. Hovmoller diagram of differences (P-C) between perturbed (P) and control (C) forecasts of 200 mb height (Z), velocity potential (X), and stream function (ψ) for winter (a,b,c) and summer (d,e,f) eastern Pacific experiments, for the 5 degree band centered on 0°.

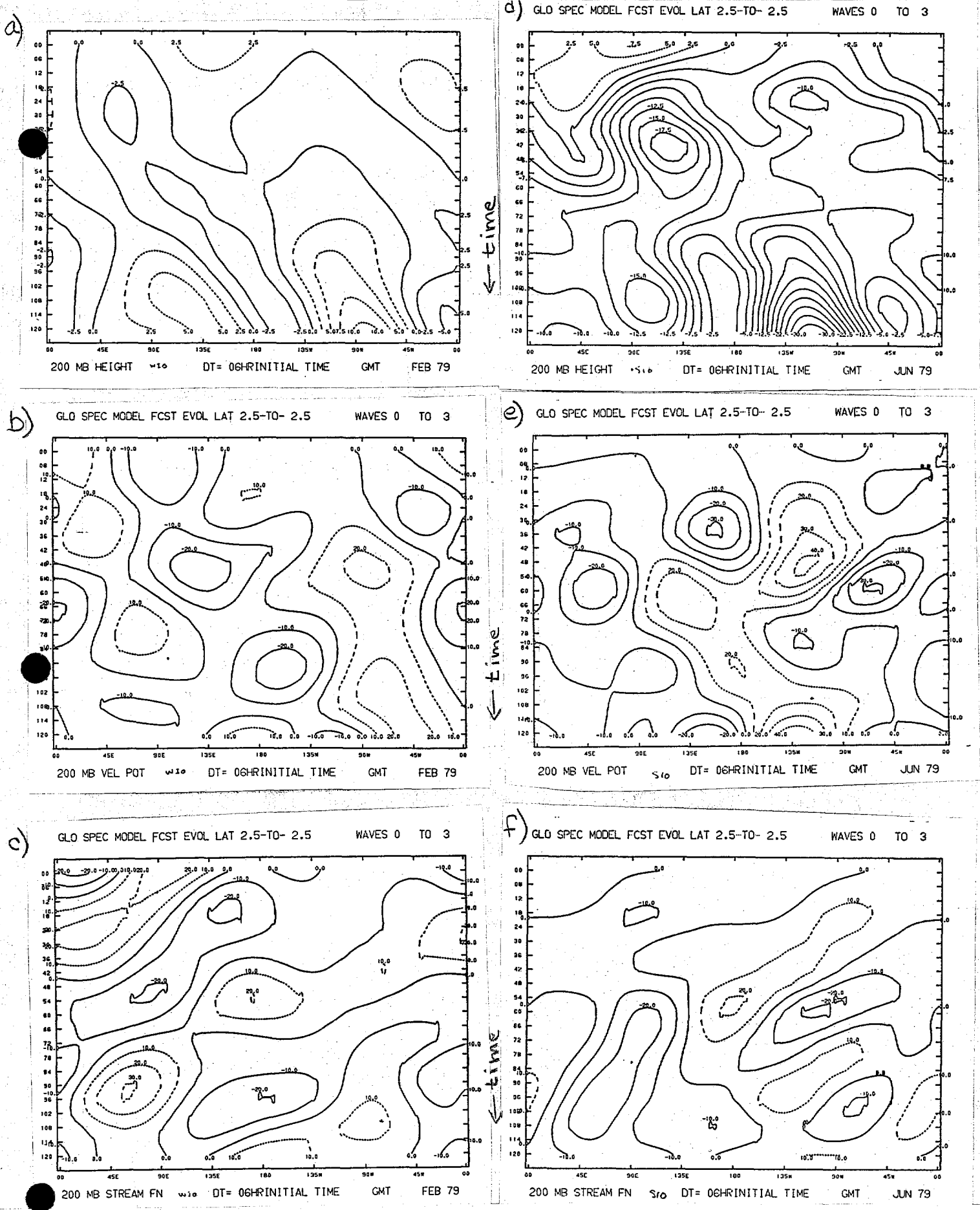

Figure 13. Hovmoller diagram of differences (P-C) between perturbed (P) and control (C) forecasts of 200 mb height (Z), velocity potential (X), and stream function (ψ) for the winter (a,b,c) and summer (d,e,f) Indian Ocean experiments, for the 5 degree band centered on 0°.

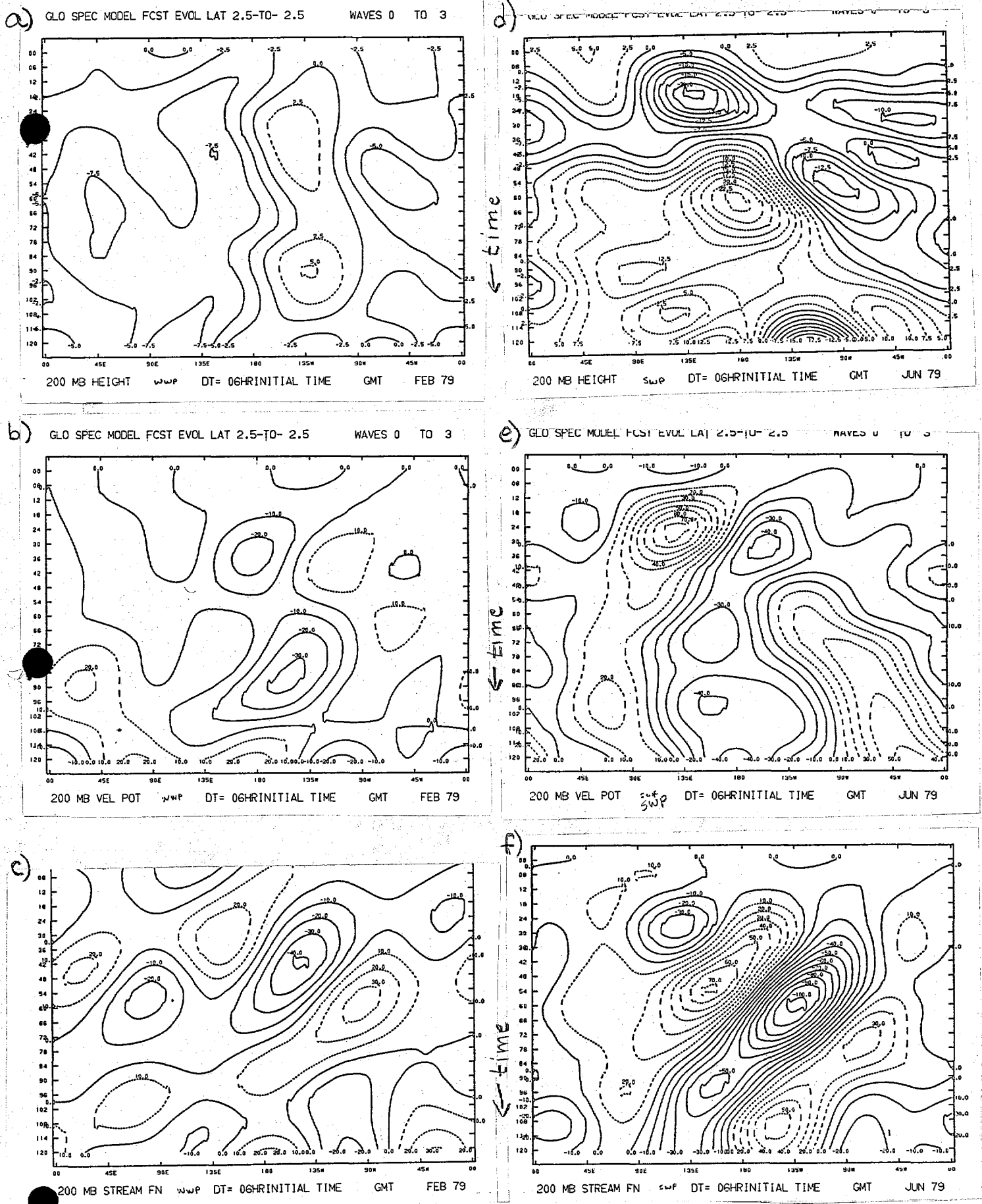

Figure 14. Hovmoller diagram of differences (P-C) between perturbed (P) and control (C) forecasts of 200 mb height (Z), velocity potential (X), and stream function (ψ) for the winter (a,b,c) and summer (d,e,f) western Pacific experiments, for the 5 degree band centered on 0°.

TOTAL FIELDS

GLO SPEC MODEL FCST EVOL LAT 2.5-TO- 2.5 WAVES 0 TO 3

P

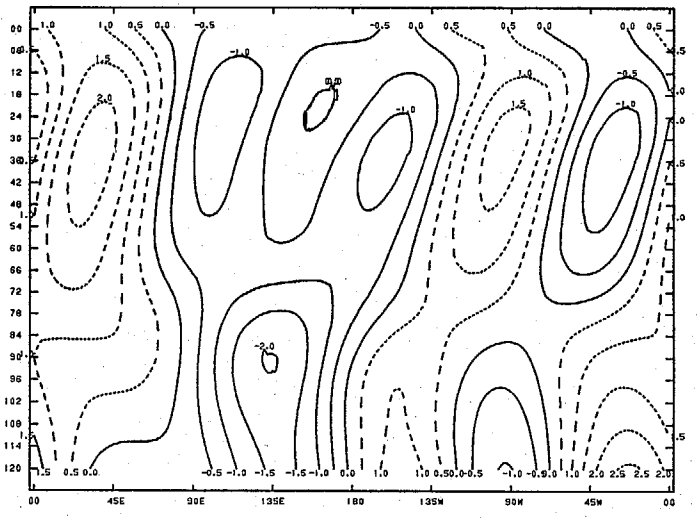

850 MB VORTICITY $P_{\omega 10}$ DT=06 HRINITIAL TIME GMT FEB 79

GLO SPEC MODEL FCST EVOL LAT 2.5-TO- 2.5 WAVES 0 TO 3

C

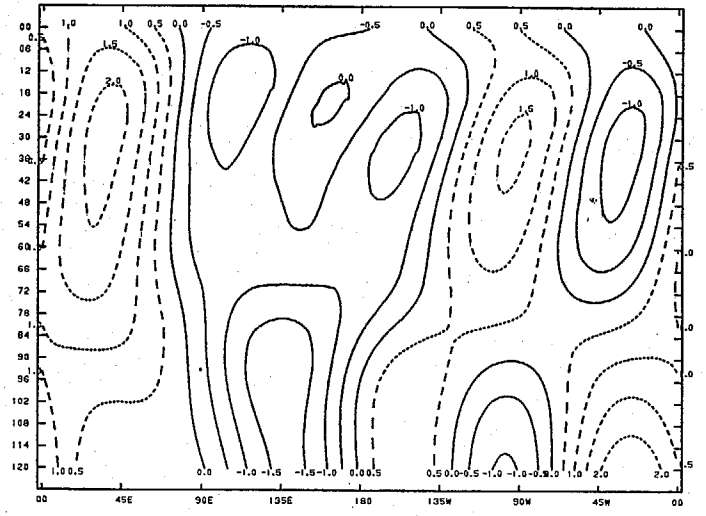

850 MB VORTICITY $C_{\omega 10}$ DT=06 HRINITIAL TIME GMT FEB 79

DIFFERENCE P-C

GLO SPEC MODEL FCST EVOL LAT 2.5-TO- 2.5 WAVES 0 TO 3

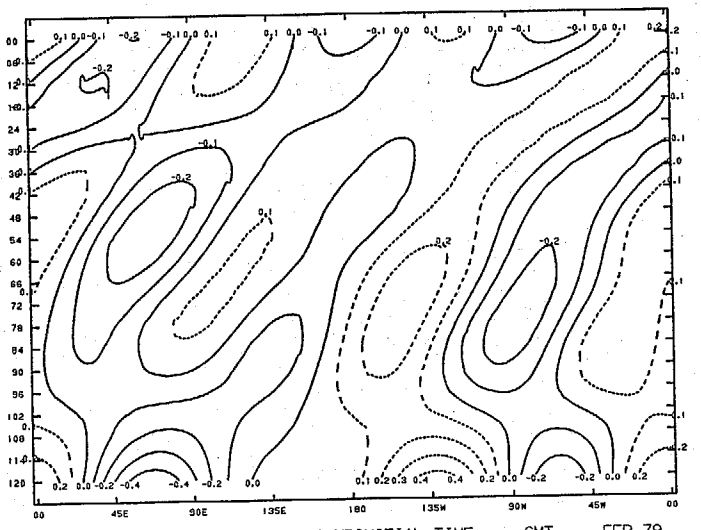

850 MB VORTICITY ω_{10} DT=06 HRINITIAL TIME GMT FEB 79

GLO SPEC MODEL FCST EVOL LAT 2.5-TO- 2.5 WAVES 0 TO 3

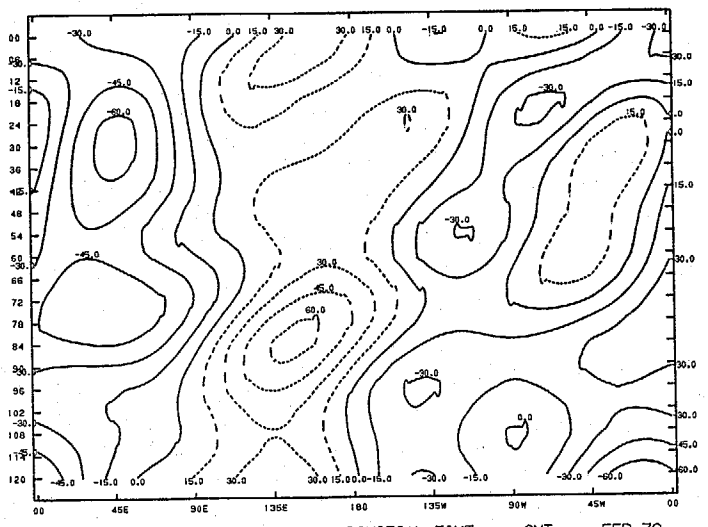

850 MB STREAM FN PWIO DT= 06HRINITIAL TIME GMT FEB 79

GLO SPEC MODEL FCST EVOL LAT 2.5-TO- 2.5 WAVES 0 TO 3

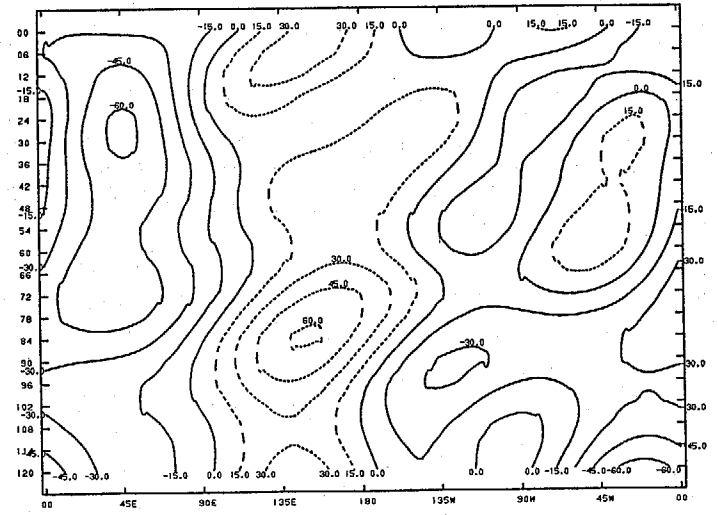

850 MB STREAM FN CWIO DT= 06HRINITIAL TIME GMT FEB 79

GLO SPEC MODEL FCST EVOL LAT 2.5-TO- 2.5 WAVES 0 TO 3

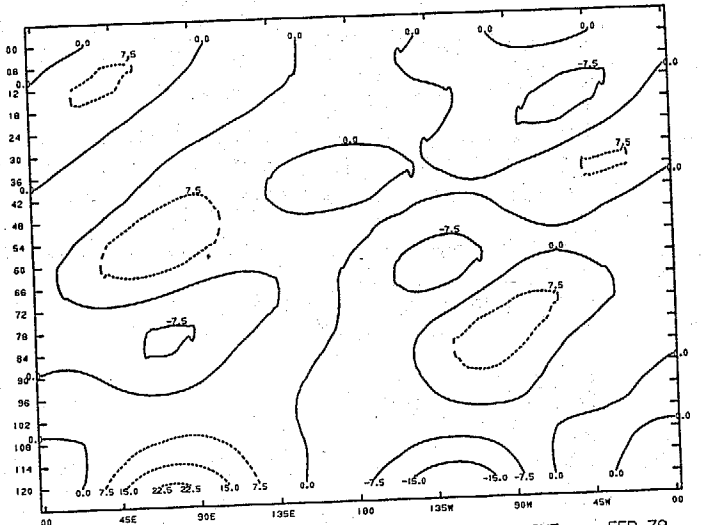

850 MB STREAM FN WIO DT= 06HRINITIAL TIME GMT FEB 79

GLO SPEC MODEL FCST EVOL LAT 2.5-TO- 2.5 WAVES 0 TO 3

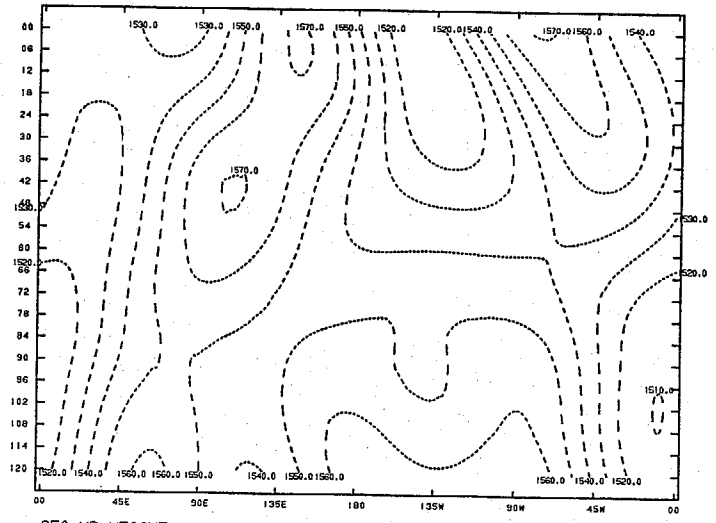

850 MB HEIGHT DT= 06HRINITIAL TIME GMT FEB 79

GLO SPEC MODEL FCST EVOL LAT 2.5-TO- 2.5 WAVES 0 TO 3

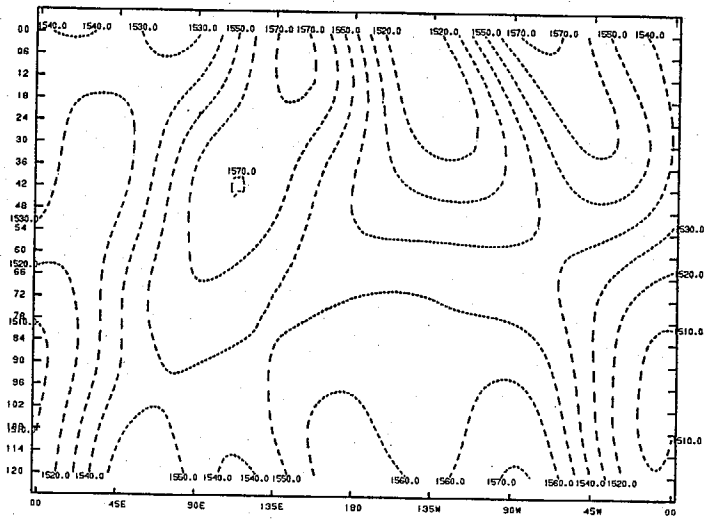

850 MB HEIGHT DT= 06HRINITIAL TIME GMT FEB 79

GLO SPEC MODEL FCST EVOL LAT 2.5-TO- 2.5 WAVES 0 TO 3

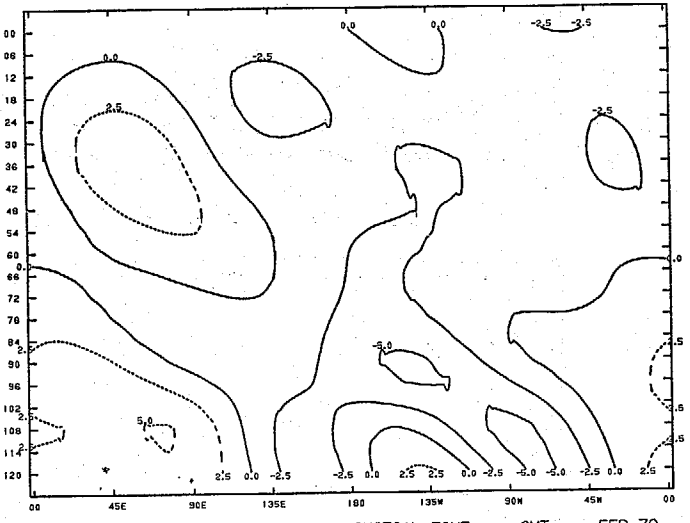

850 MB HEIGHT DT= 06HRINITIAL TIME GMT FEB 79

GLO SPEC MODEL FCST EVOL LAT 2.5-TO- 2.5 WAVES 0 TO 3

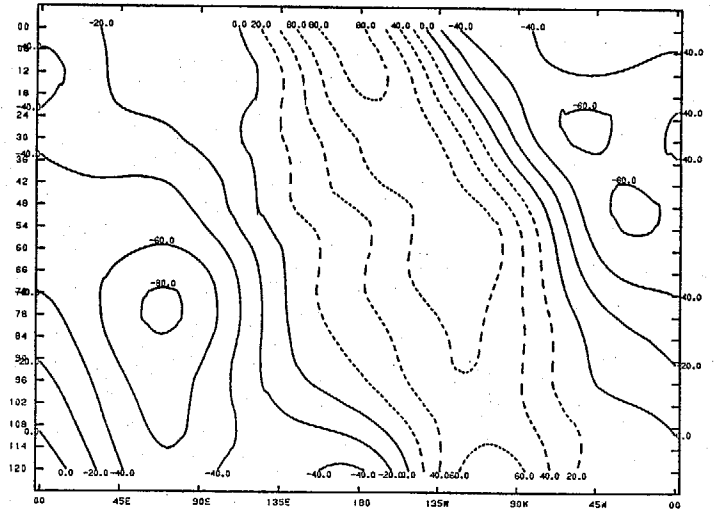

850 MB VEL POT DT= 06HRINITIAL TIME GMT FEB 79

GLO SPEC MODEL FCST EVOL LAT 2.5-TO- 2.5 WAVES 0 TO 3

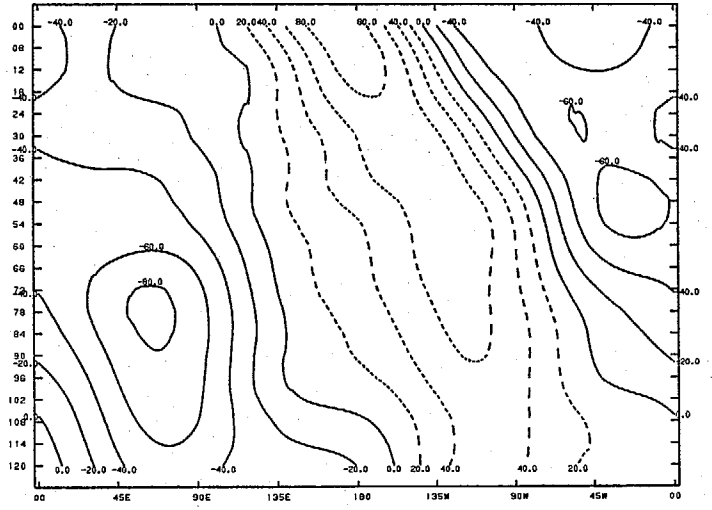

850 MB VEL POT DT= 06HRINITIAL TIME GMT FEB 79

GLO SPEC MODEL FCST EVOL LAT 2.5-TO- 2.5 WAVES 0 TO 3

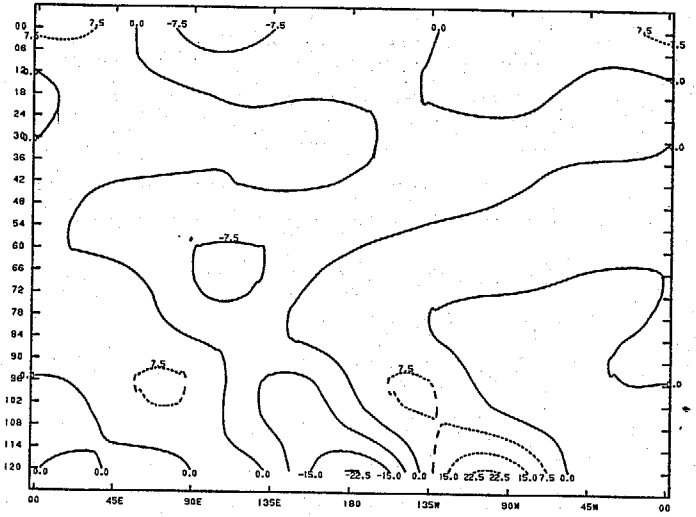

850 MB VEL POT DT= 06HRINITIAL TIME GMT FEB 79

GLO SPEC MODEL FCST EVOL LAT 2.5-TO- 2.5 WAVES 0 TO 3

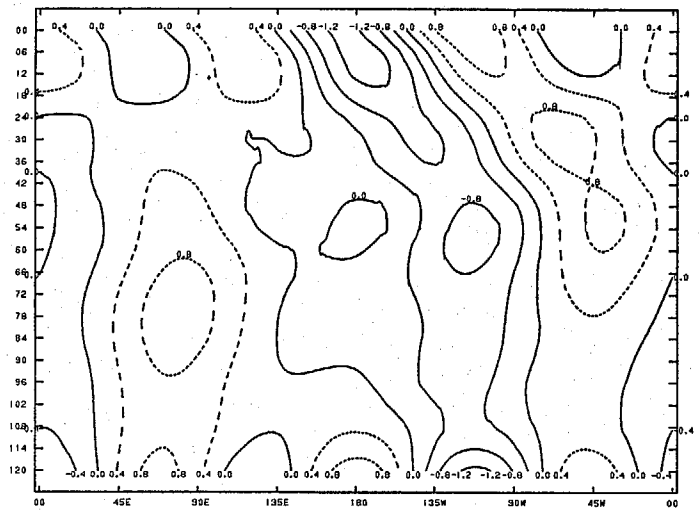

850 MB DIVERGENC ρω10 DT=06 HRINITIAL TIME GMT FEB 79

GLO SPEC MODEL FCST EVOL LAT 2.5-TO- 2.5 WAVES 0 TO 3

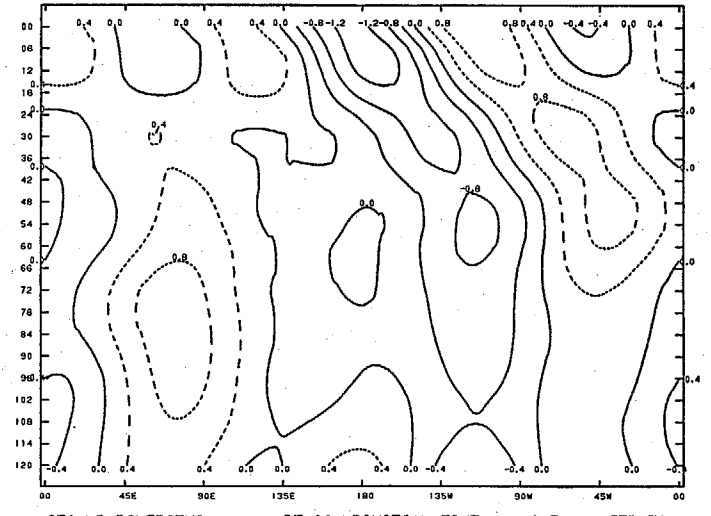

850 MB DIVERGENC cω10 DT=06 HRINITIAL TIME GMT FEB 79

GLO SPEC MODEL FCST EVOL LAT 2.5-TO- 2.5 WAVES 0 TO 3

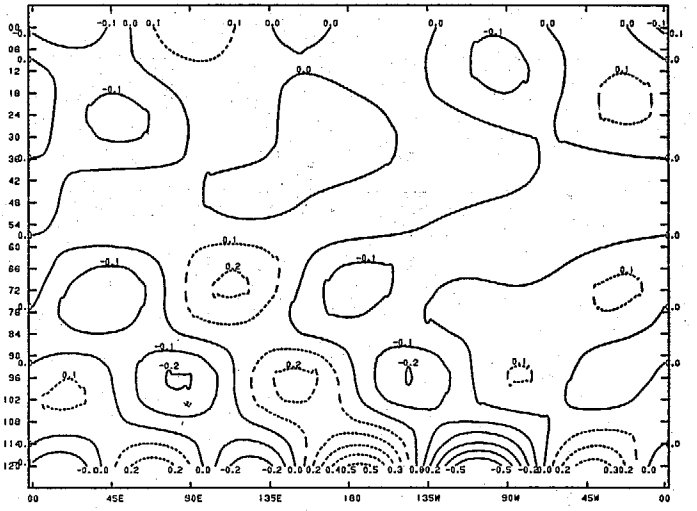

850 MB DIVERGENC ω10 DT=06 HRINITIAL TIME GMT FEB 79

GLO SPEC MODEL FCST EVOL LAT 2.5-TO- 2.5 WAVES 0 TO 3

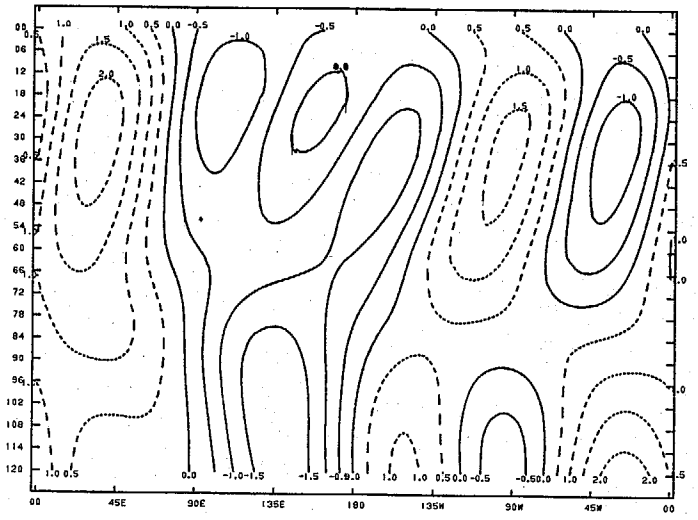

850 MB VORTICITY $\rho\omega\omega\rho$ DT=06 HRINITIAL TIME GMT FEB 79

GLO SPEC MODEL FCST EVOL LAT 2.5-TO- 2.5 WAVES 0 TO 3

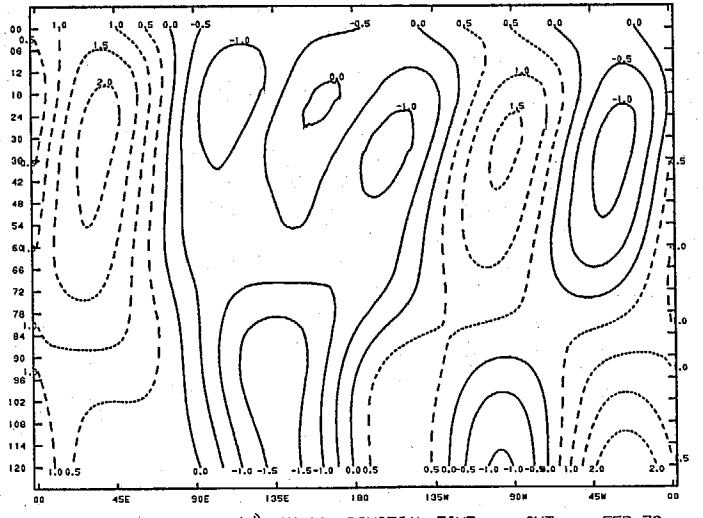

850 MB VORTICITY $\epsilon\omega\omega\rho$ DT=06 HRINITIAL TIME GMT FEB 79

GLO SPEC MODEL FCST EVOL LAT 2.5-TO- 2.5 WAVES 0 TO 3

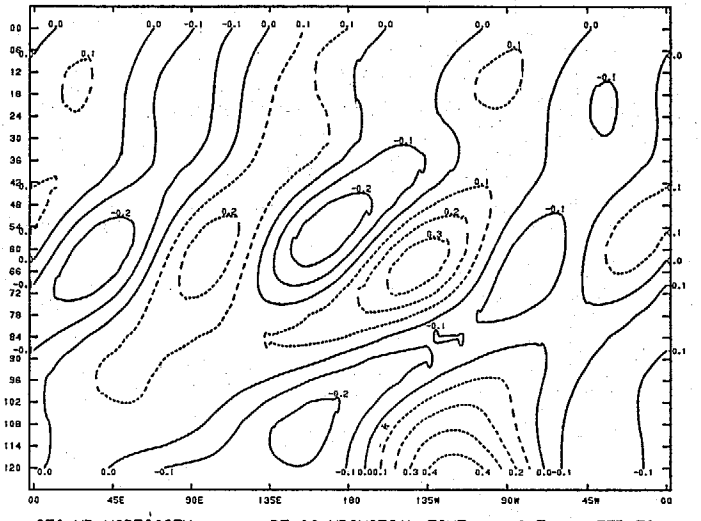

850 MB VORTICITY $\omega\omega\rho$ DT=06 HRINITIAL TIME GMT FEB 79

GLO SPEC MODEL FCST EVOL LAT 2.5-TO- 2.5 WAVES 0 TO 3

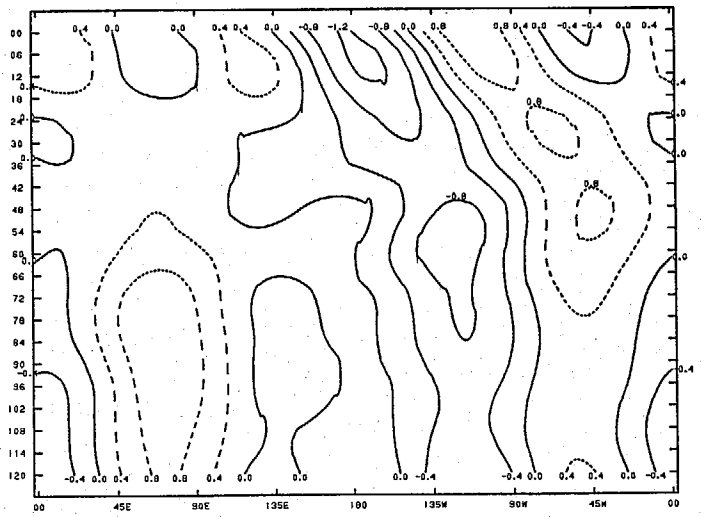

850 MB DIVERGENC ωωP DT=06 HRINITIAL TIME GMT FEB 79

GLO SPEC MODEL FCST EVOL LAT 2.5-TO- 2.5 WAVES 0 TO 3

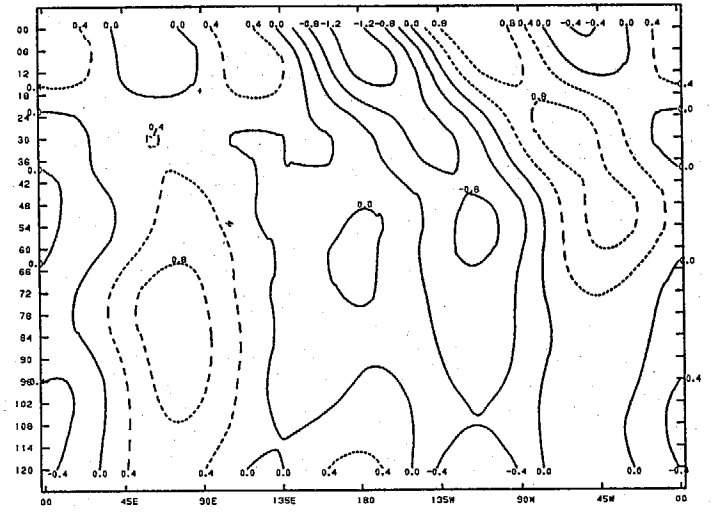

850 MB DIVERGENC ωωP DT=06 HRINITIAL TIME GMT FEB 79

GLO SPEC MODEL FCST EVOL LAT 2.5-TO- 2.5 WAVES 0 TO 3

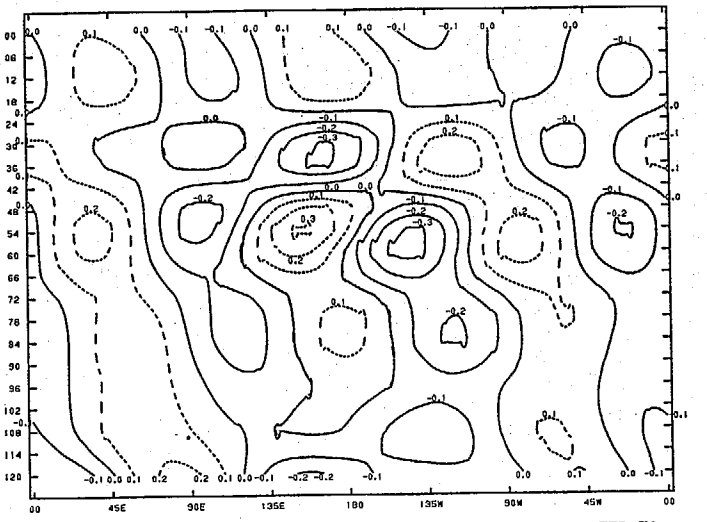

850 MB DIVERGENC ωωP DT=06 HRINITIAL TIME GMT FEB 79

GLO SPEC MODEL FCST EVOL LAT 2.5-TO- 2.5 WAVES 0 TO 3

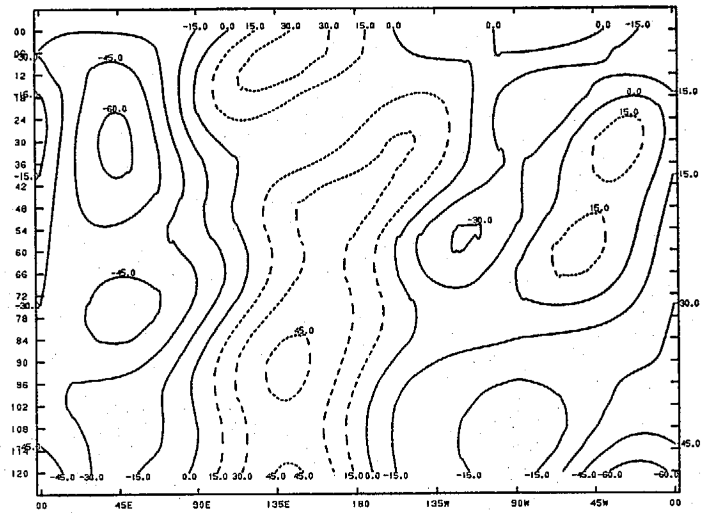

850 MB STREAM FN DT= 06HRINITIAL TIME GMT FEB 79

GLO SPEC MODEL FCST EVOL LAT 2.5-TO- 2.5 WAVES 0 TO 3

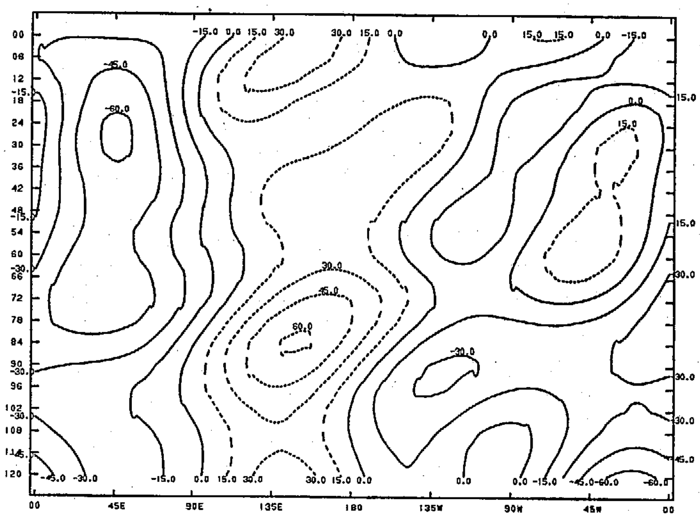

850 MB STREAM FN DT= 06HRINITIAL TIME GMT FEB 79

GLO SPEC MODEL FCST EVOL LAT 2.5-TO- 2.5 WAVES 0 TO 3

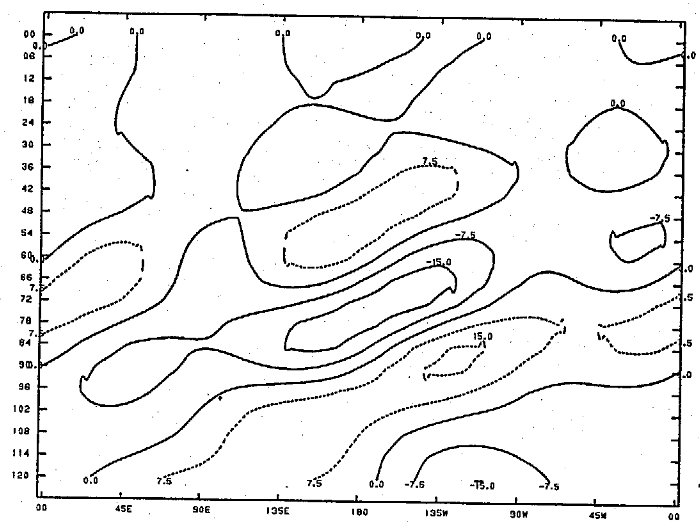

850 MB STREAM FN DT= 06HRINITIAL TIME GMT FEB 79

GLO SPEC MODEL FCST EVOL LAT 2.5-TO- 2.5 WAVES 0 TO 3

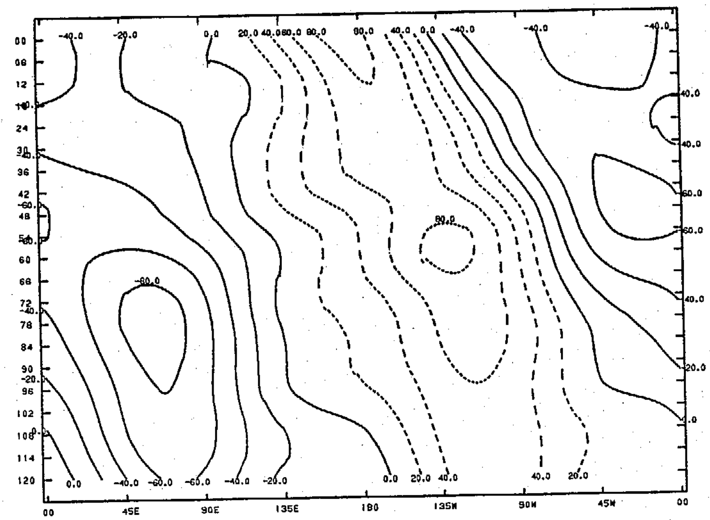

850 MB VEL POT Pwwp DT= 06HRINITIAL TIME GMT FEB 79

GLO SPEC MODEL FCST EVOL LAT 2.5-TO- 2.5 WAVES 0 TO 3

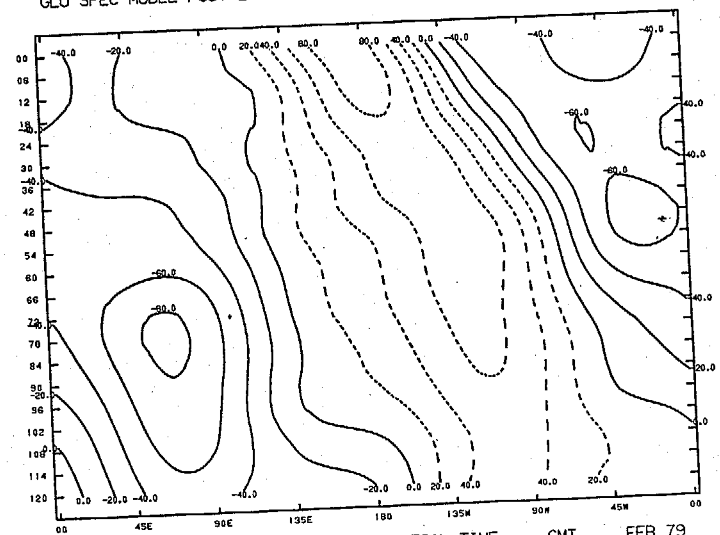

850 MB VEL POT cwwp DT= 06HRINITIAL TIME GMT FEB 79

GLO SPEC MODEL FCST EVOL LAT 2.5-TO- 2.5 WAVES 0 TO 3

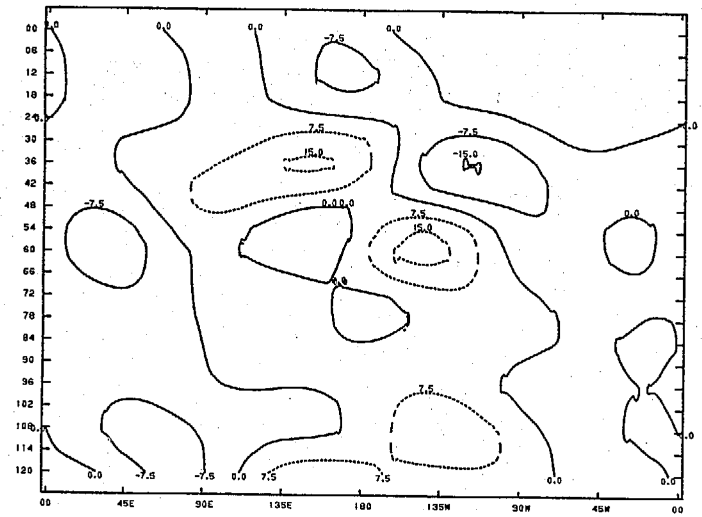

850 MB VEL POT wwp DT= 06HRINITIAL TIME GMT FEB 79

GLO SPEC MODEL FCST EVOL LAT 2.5-TO- 2.5 WAVES 0 TO 3

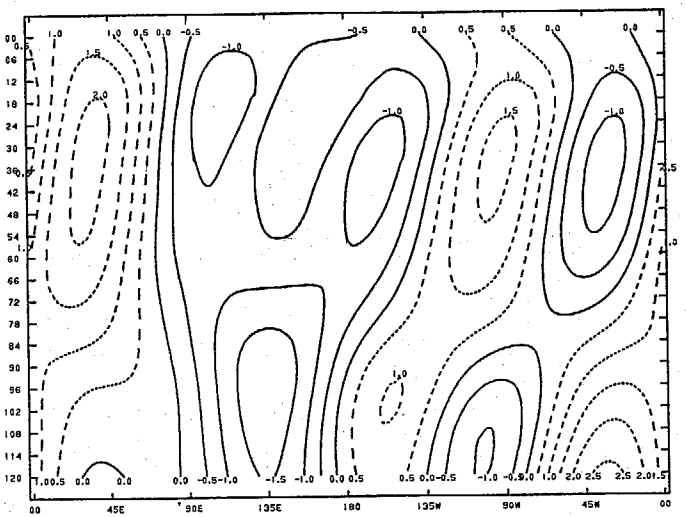

850 MB VORTICITY PWEP DT=06 HRINITIAL TIME GMT FEB 79

GLO SPEC MODEL FCST EVOL LAT 2.5-TO- 2.5 WAVES 0 TO 3

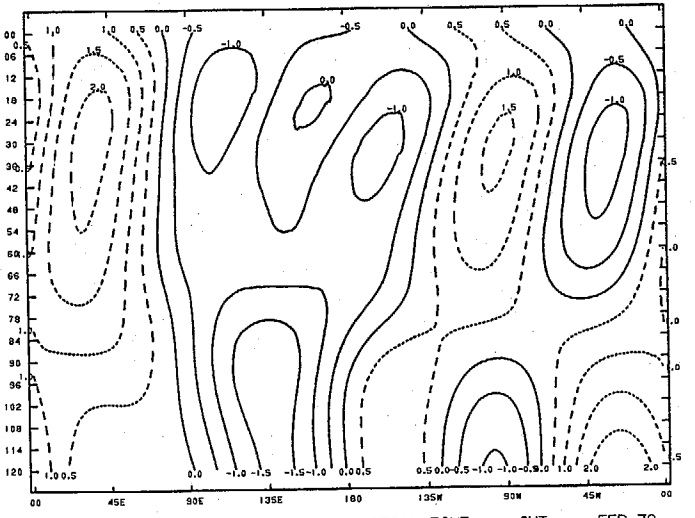

850 MB VORTICITY PWEP DT=06 HRINITIAL TIME GMT FEB 79

GLO SPEC MODEL FCST EVOL LAT 2.5-TO- 2.5 WAVES 0 TO 3

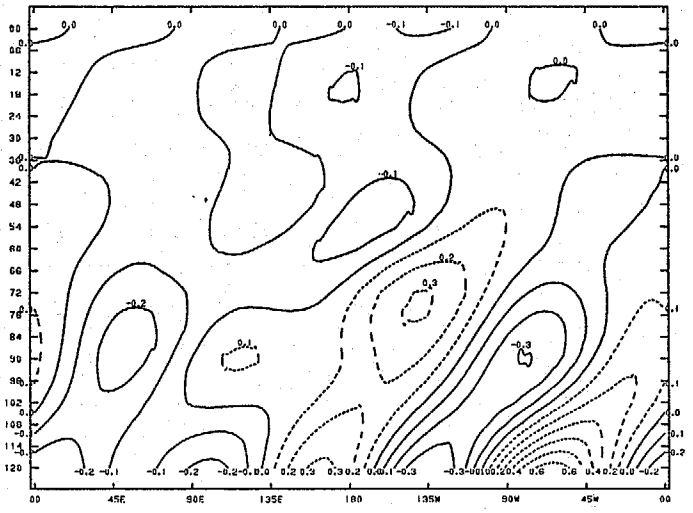

850 MB VORTICITY WEP DT=06 HRINITIAL TIME GMT FEB 79

GLO SPEC MODEL FCST EVOL LAT 2.5-TO- 2.5 WAVES 0 TO 3

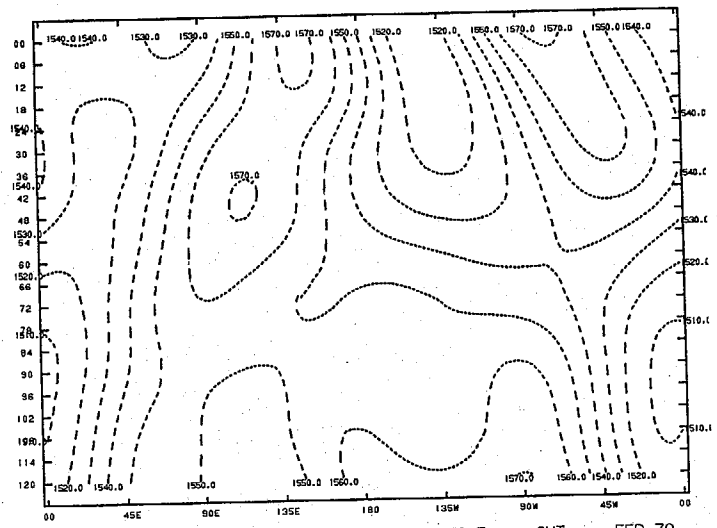

850 MB HEIGHT PWWP DT= 06HRINITIAL TIME GMT FEB 79

GLO SPEC MODEL FCST EVOL LAT 2.5-TO- 2.5 WAVES 0 TO 3

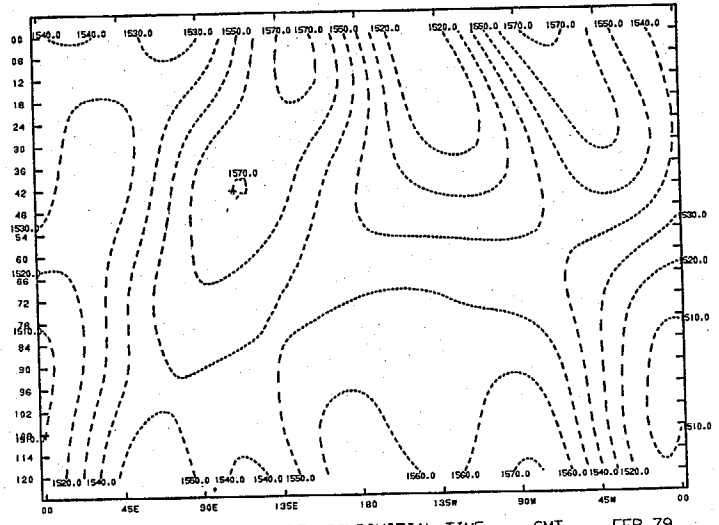

850 MB HEIGHT CWWP DT= 06HRINITIAL TIME GMT FEB 79

GLO SPEC MODEL FCST EVOL LAT 2.5-TO- 2.5 WAVES 0 TO 3

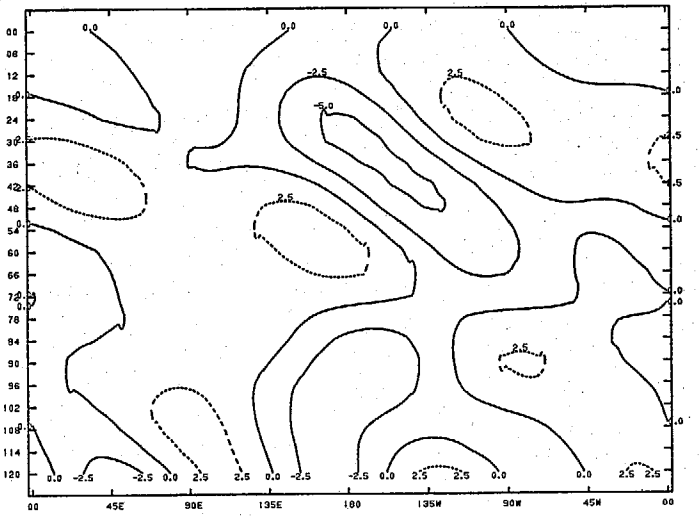

850 MB HEIGHT WWP DT= 06HRINITIAL TIME GMT FEB 79

GLO SPEC MODEL FCST EVOL LAT 2.5-TO- 2.5 WAVES 0 TO 3

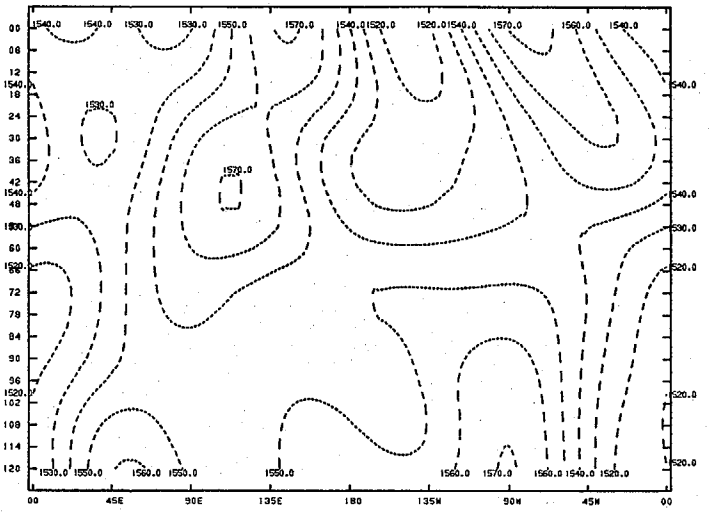

850 MB HEIGHT DT= 06HRINITIAL TIME GMT FEB 79

GLO SPEC MODEL FCST EVOL LAT 2.5-TO- 2.5 WAVES 0 TO 3

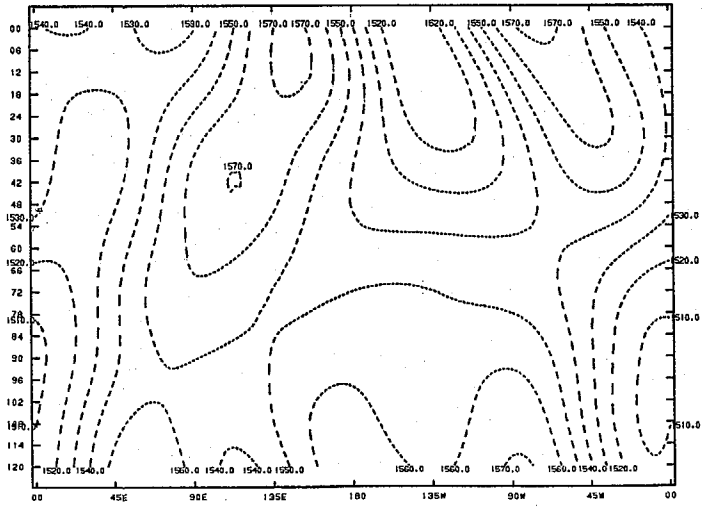

850 MB HEIGHT DT= 06HRINITIAL TIME GMT FEB 79

GLO SPEC MODEL FCST EVOL LAT 2.5-TO- 2.5 WAVES 0 TO 3

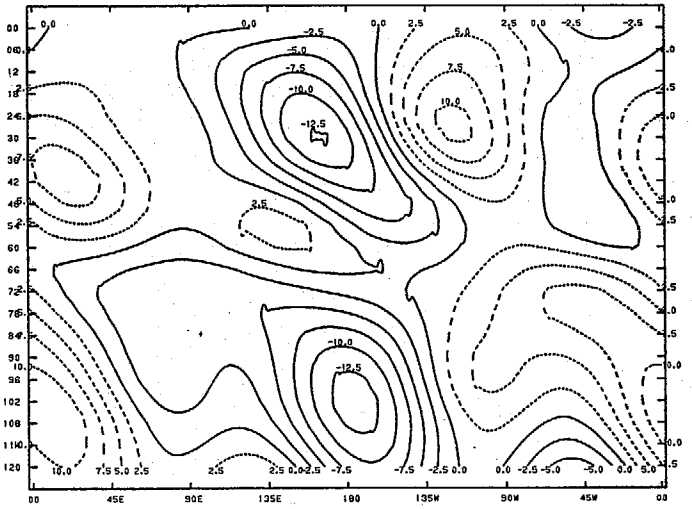

850 MB HEIGHT DT= 06HRINITIAL TIME GMT FEB 79

GLO SPEC MODEL FCST EVOL LAT 2.5-TO- 2.5 WAVES 0 TO 3

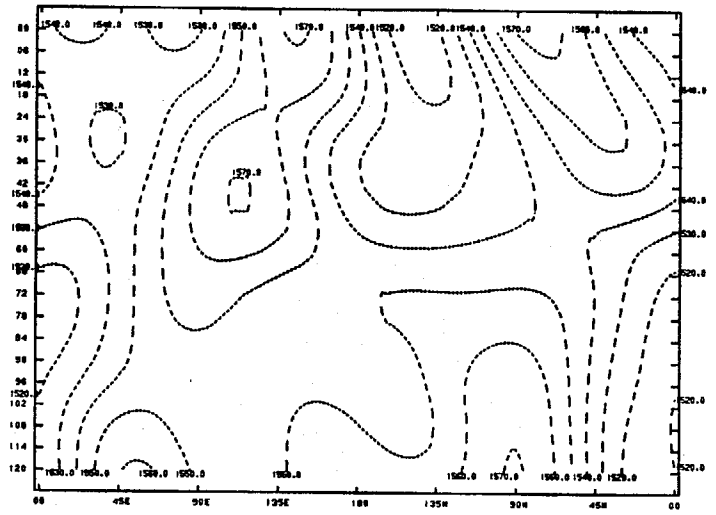

850 MB HEIGHT DT= 06HRINITIAL TIME GMT FEB 79

GLO SPEC MODEL FCST EVOL LAT 2.5-TO- 2.5 WAVES 0 TO 3

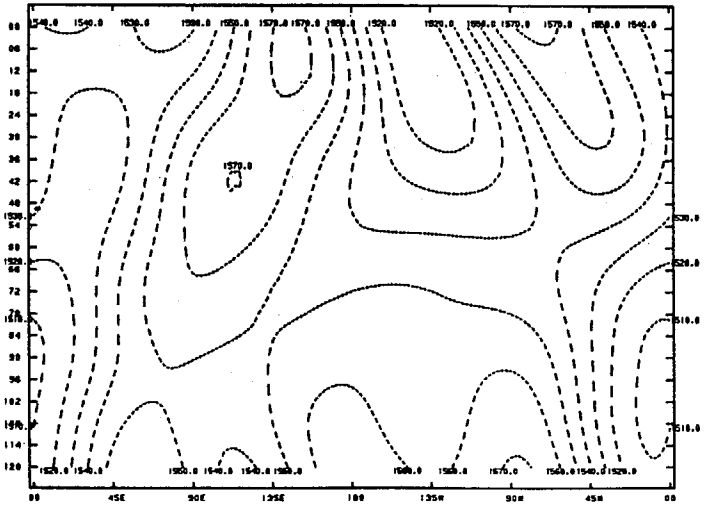

850 MB HEIGHT DT= 06HRINITIAL TIME GMT FEB 79

GLO SPEC MODEL FCST EVOL LAT 2.5-TO- 2.5 WAVES 0 TO 3

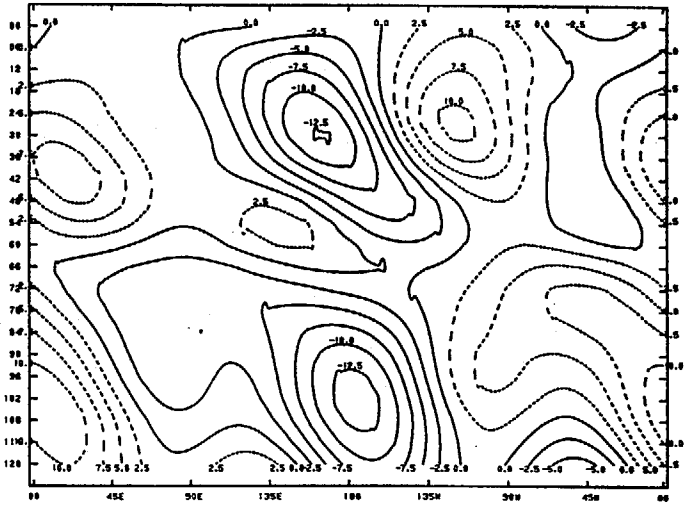

850 MB HEIGHT DT= 06HRINITIAL TIME GMT FEB 79

GLO SPEC MODEL FCST EVOL LAT 2.5-TO- 2.5 WAVES 0 TO 3

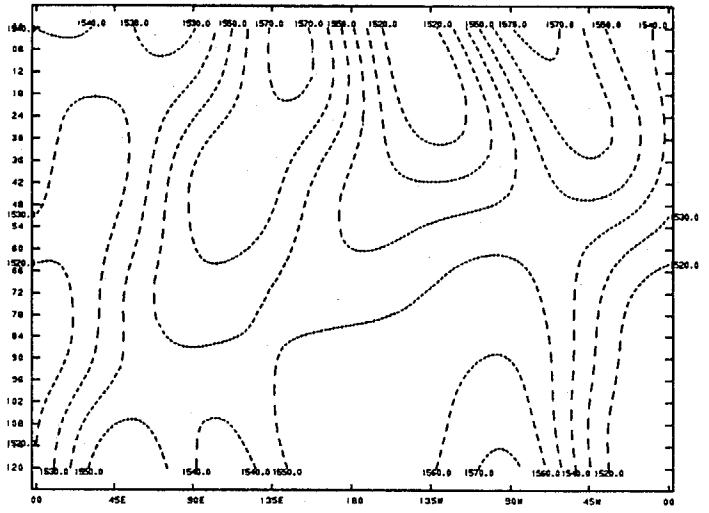

850 MB HEIGHT DT= 06HRINITIAL TIME GMT FEB 79

GLO SPEC MODEL FCST EVOL LAT 2.5-TO- 2.5 WAVES 0 TO 3

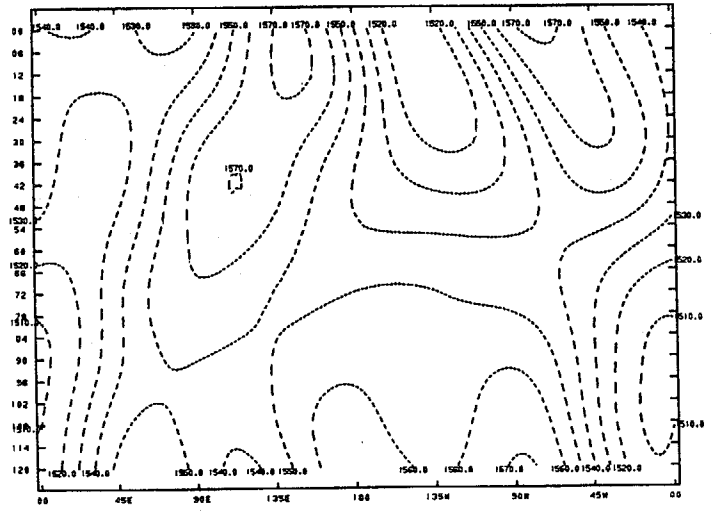

850 MB HEIGHT DT= 06HRINITIAL TIME GMT FEB 79

GLO SPEC MODEL FCST EVOL LAT 2.5-TO- 2.5 WAVES 0 TO 3

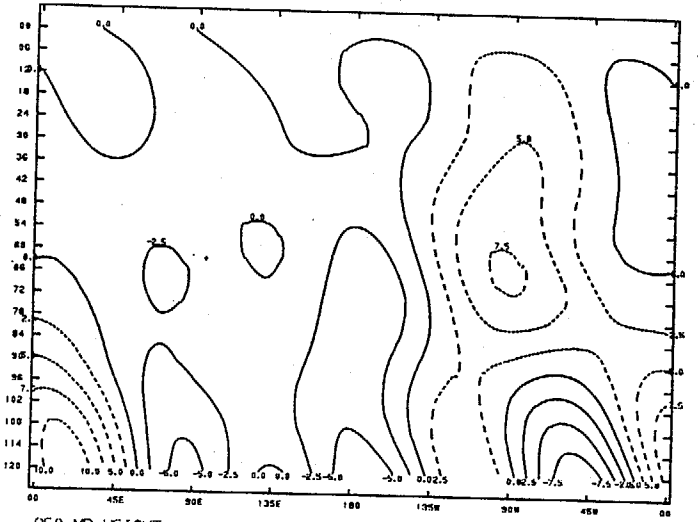

850 MB HEIGHT DT= 06HRINITIAL TIME GMT FEB 79

GLO SPEC MODEL FCST EVOL LAT 2.5-TO- 2.5 WAVES 0 TO 3

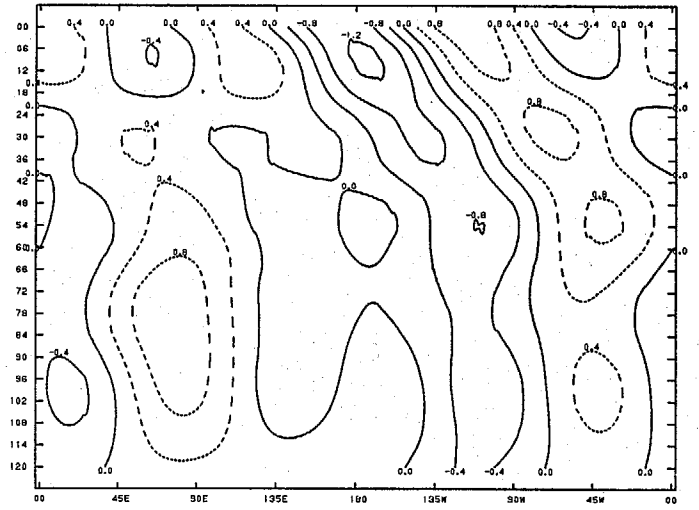

850 MB DIVERGENC DT=06 HRINITIAL TIME GMT FEB 79

GLO SPEC MODEL FCST EVOL LAT 2.5-TO- 2.5 WAVES 0 TO 3

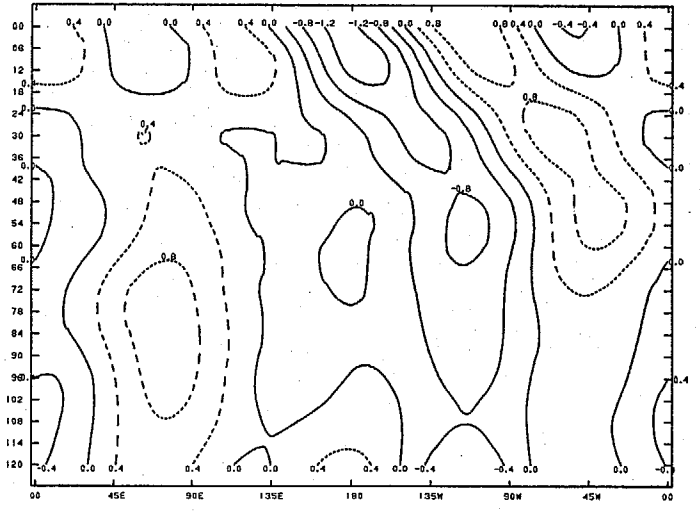

850 MB DIVERGENC DT=06 HRINITIAL TIME GMT FEB 79

GLO SPEC MODEL FCST EVOL LAT 2.5-TO- 2.5 WAVES 0 TO 3

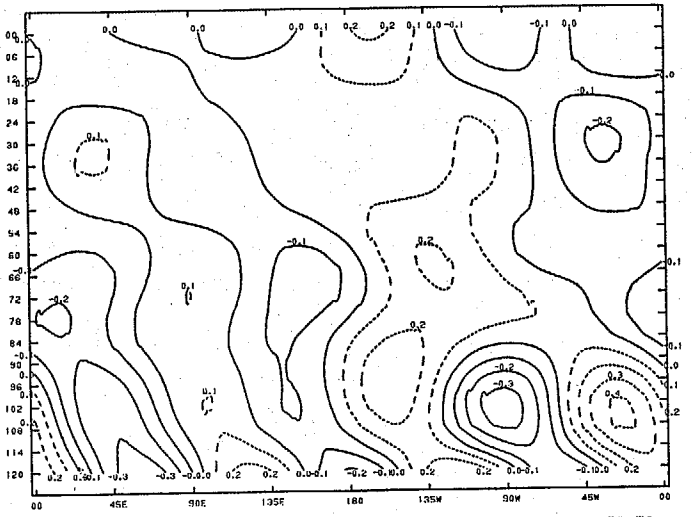

850 MB DIVERGENC DT=06 HRINITIAL TIME GMT FEB 79

GLO SPEC MODEL FCST EVOL LAT 2.5-TO- 2.5 WAVES 0 TO 3

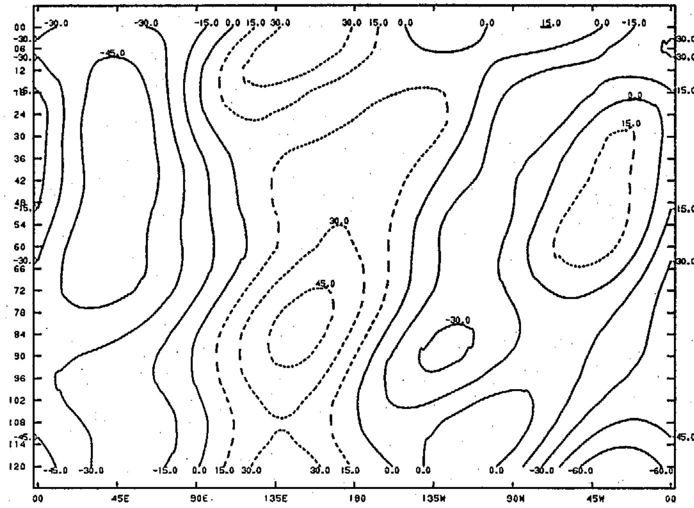

850 MB STREAM FN DT= 06HRINITIAL TIME GMT FEB 79

GLO SPEC MODEL FCST EVOL LAT 2.5-TO- 2.5 WAVES 0 TO 3

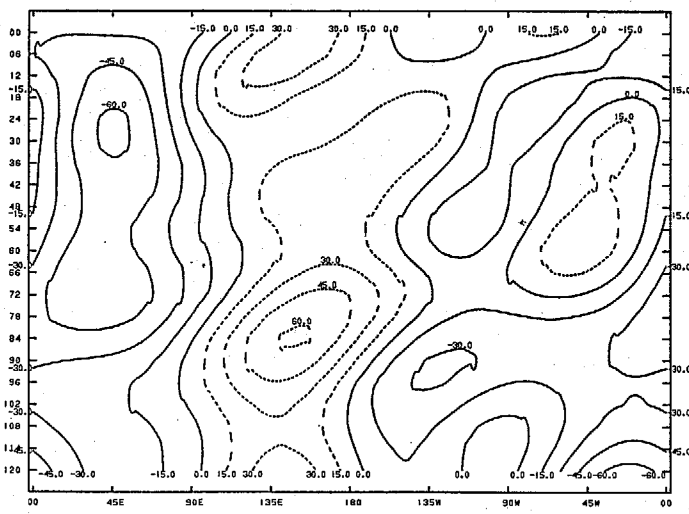

850 MB STREAM FN DT= 06HRINITIAL TIME GMT FEB 79

GLO SPEC MODEL FCST EVOL LAT 2.5-TO- 2.5 WAVES 0 TO 3

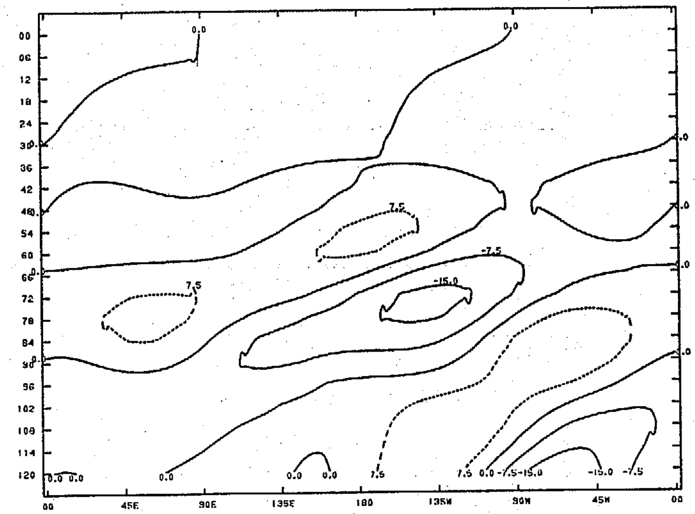

850 MB STREAM FN DT= 06HRINITIAL TIME GMT FEB 79

GLO SPEC MODEL FCST EVOL LAT 2.5-TO- 2.5 WAVES 0 TO 3

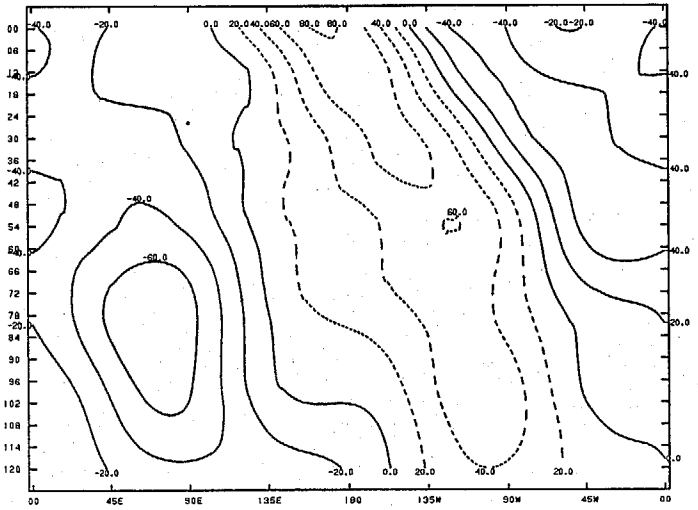

850 MB VEL POT ϕ ωεp DT= 06HRINITIAL TIME GMT FEB 79

GLO SPEC MODEL FCST EVOL LAT 2.5-TO- 2.5 WAVES 0 TO 3

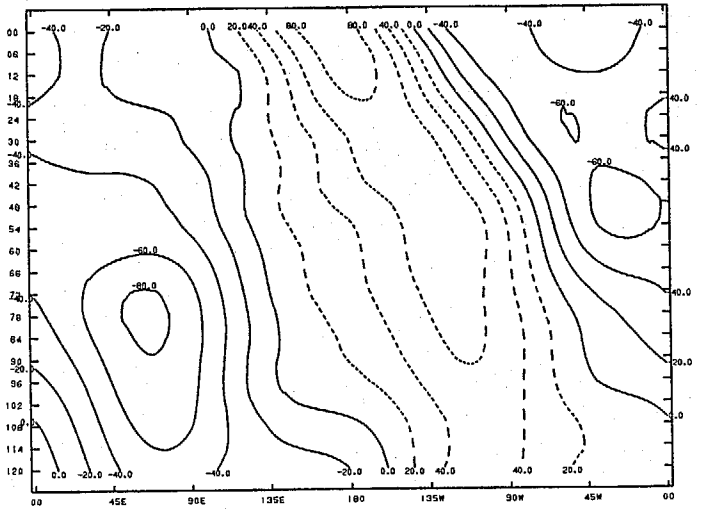

850 MB VEL POT ϕ ωεp DT= 06HRINITIAL TIME GMT FEB 79

GLO SPEC MODEL FCST EVOL LAT 2.5-TO- 2.5 WAVES 0 TO 3

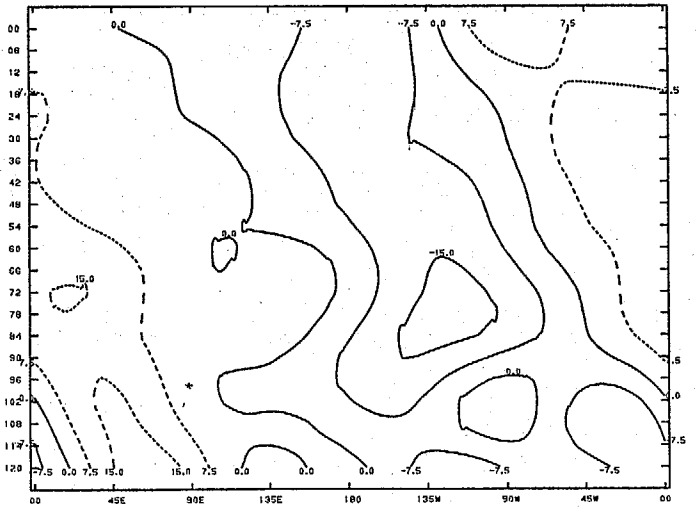

850 MB VEL POT ωεp DT= 06HRINITIAL TIME GMT FEB 79

GLO SPEC MODEL FCST EVOL LAT 2.5-TO- 2.5 WAVES 0 TO 3

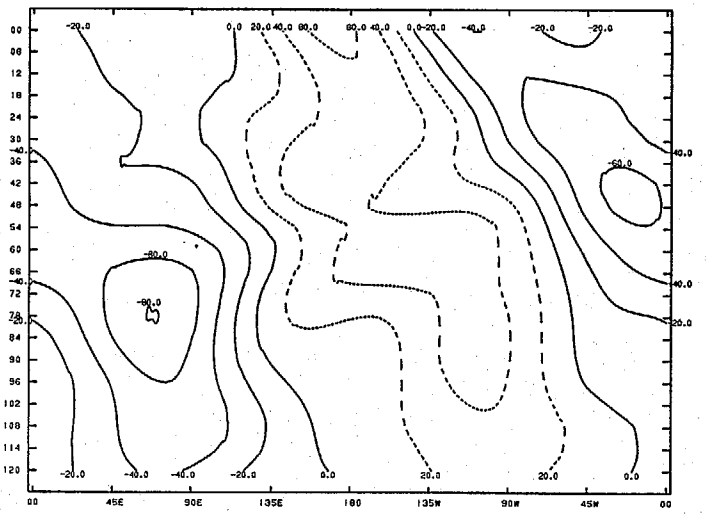

850 MB VEL POT ω_{TT} DT= 06HRINITIAL TIME GMT FEB 79

GLO SPEC MODEL FCST EVOL LAT 2.5-TO- 2.5 WAVES 0 TO 3

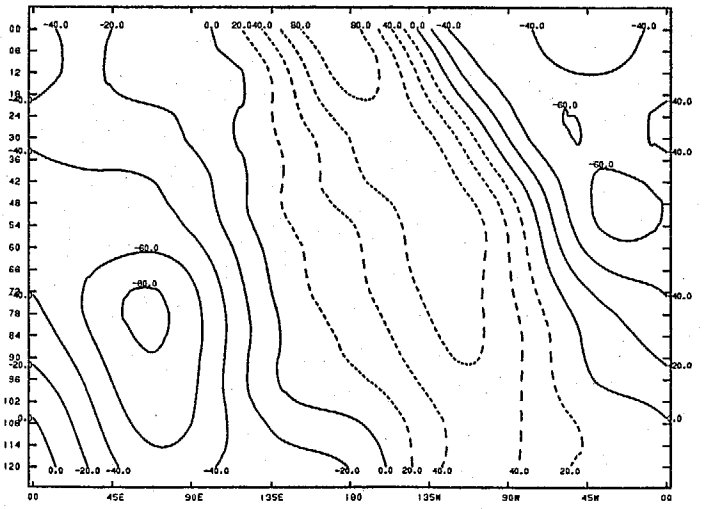

850 MB VEL POT ω_{WEP} DT= 06HRINITIAL TIME GMT FEB 79

GLO SPEC MODEL FCST EVOL LAT 2.5-TO- 2.5 WAVES 0 TO 3

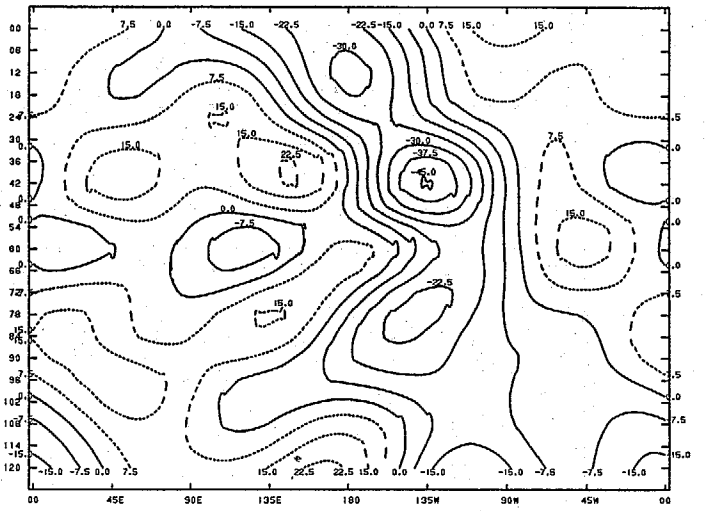

850 MB VEL POT ω_{TT} DT= 06HRINITIAL TIME GMT FEB 79

GLO SPEC MODEL FCST EVOL LAT 2.5-TO- 2.5 WAVES 0 TO 3

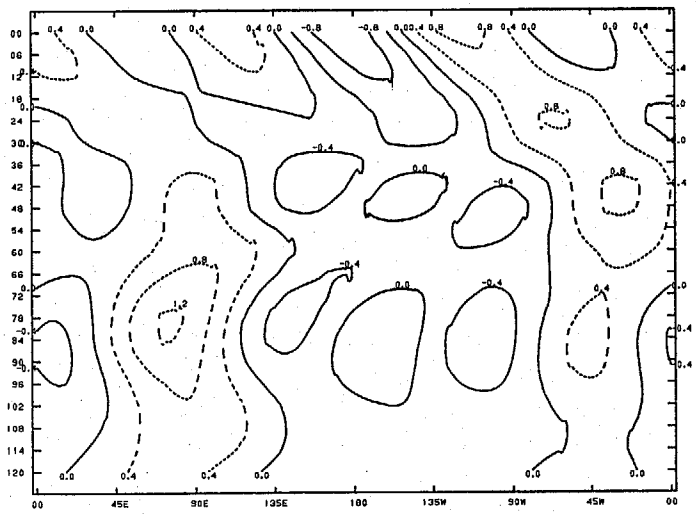

850 MB DIVERGENC ρ WTT DT=06 HRINITIAL TIME GMT FEB 79

GLO SPEC MODEL FCST EVOL LAT 2.5-TO- 2.5 WAVES 0 TO 3

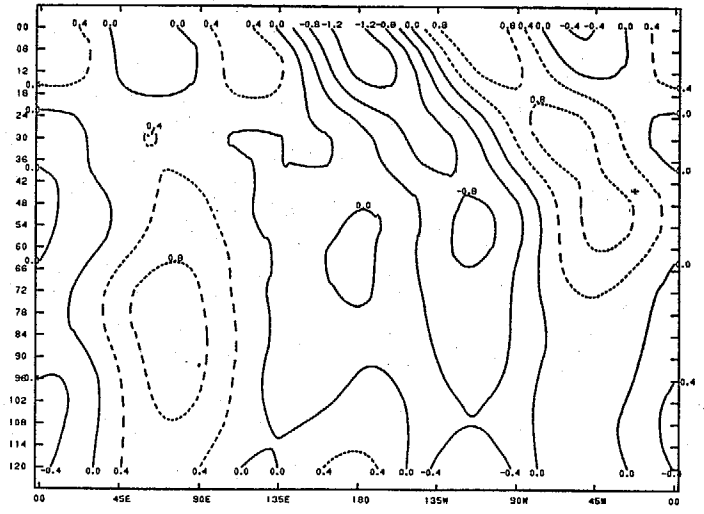

850 MB DIVERGENC WEP DT=06 HRINITIAL TIME GMT FEB 79

GLO SPEC MODEL FCST EVOL LAT 2.5-TO- 2.5 WAVES 0 TO 3

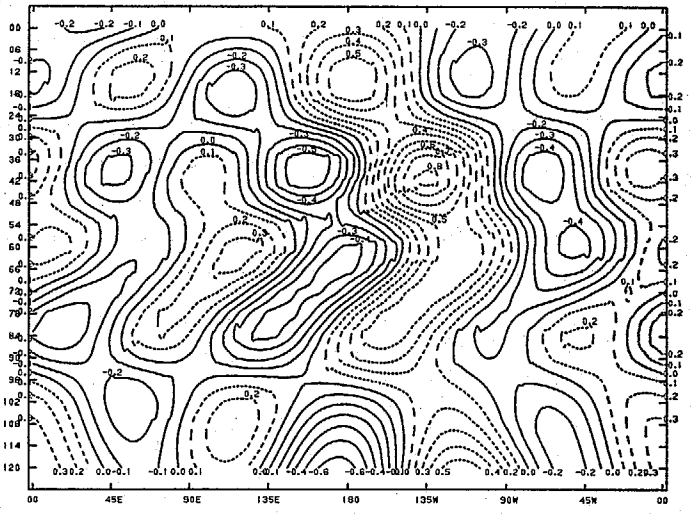

850 MB DIVERGENC WTT DT=06 HRINITIAL TIME GMT FEB 79

GLO SPEC MODEL FCST EVOL LAT 2.5-TO- 2.5 WAVES 0 TO 3

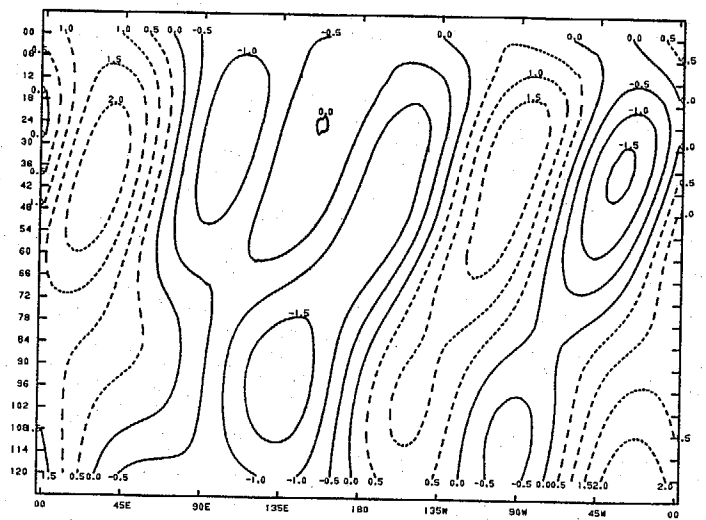

850 MB VORTICITY PωTT DT=06 HRINITIAL TIME GMT FEB 79

GLO SPEC MODEL FCST EVOL LAT 2.5-TO- 2.5 WAVES 0 TO 3

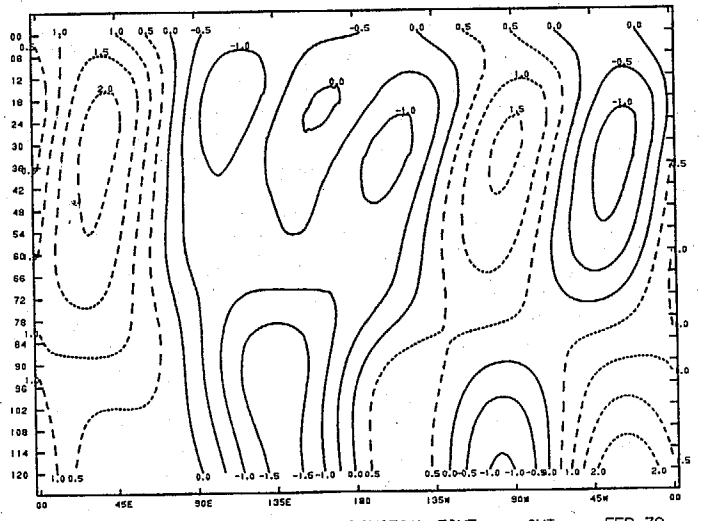

850 MB VORTICITY ωTT DT=06 HRINITIAL TIME GMT FEB 79

GLO SPEC MODEL FCST EVOL LAT 2.5-TO- 2.5 WAVES 0 TO 3

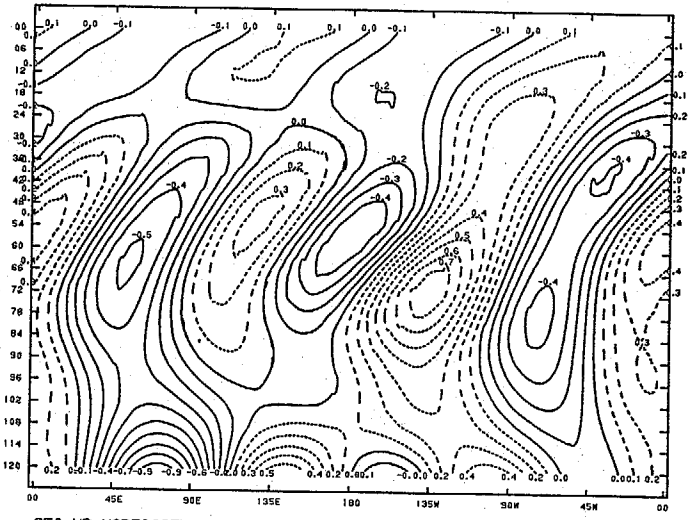

850 MB VORTICITY ωTT DT=06 HRINITIAL TIME GMT FEB 79

GLO SPEC MODEL FCST EVOL LAT 2.5-TO- 2.5 WAVES 0 TO 3

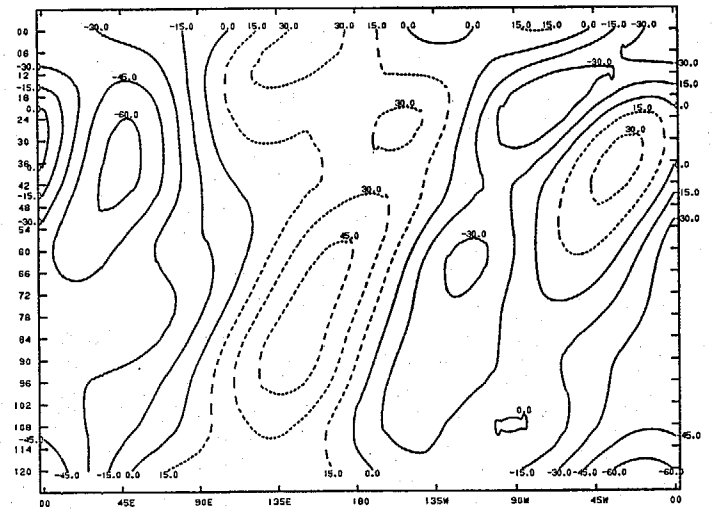

850 MB STREAM FN ψ_{TT} DT= 06HRINITIAL TIME GMT FEB 79

54

GLO SPEC MODEL FCST EVOL LAT 2.5-TO- 2.5 WAVES 0 TO 3

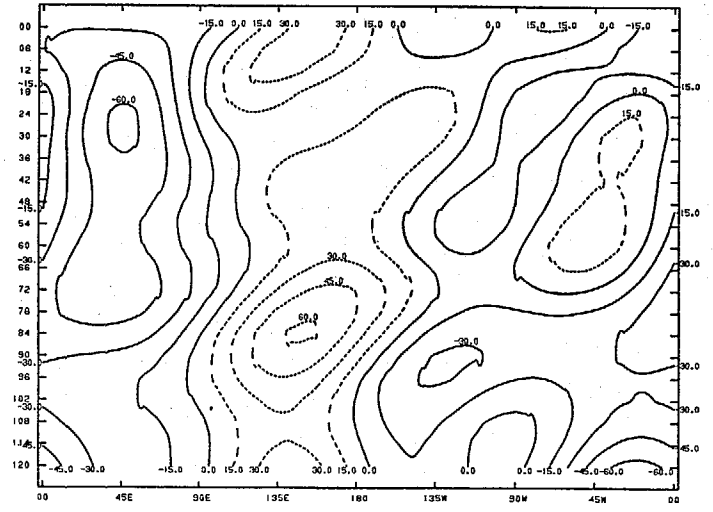

850 MB STREAM FN χ_{VEP} DT= 06HRINITIAL TIME GMT FEB 79

GLO SPEC MODEL FCST EVOL LAT 2.5-TO- 2.5 WAVES 0 TO 3

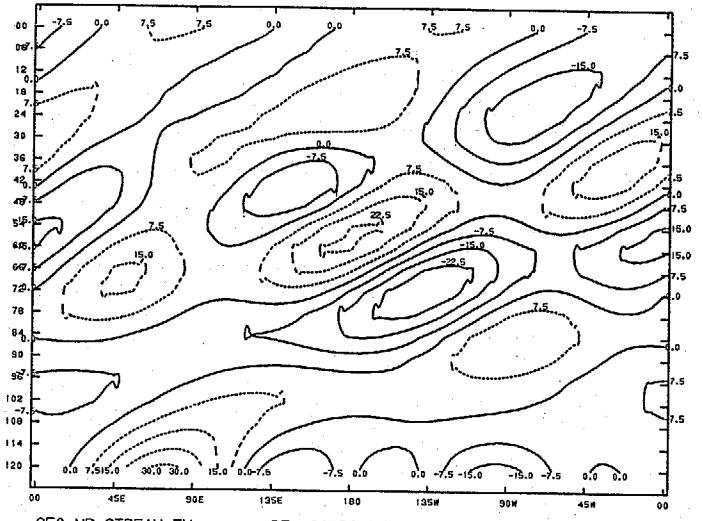

850 MB STREAM FN ω_{TT} DT= 06HRINITIAL TIME GMT FEB 79

GLO SPEC MODEL FCST EVOL LAT 2.5-TO- 2.5 WAVES 0 TO 3

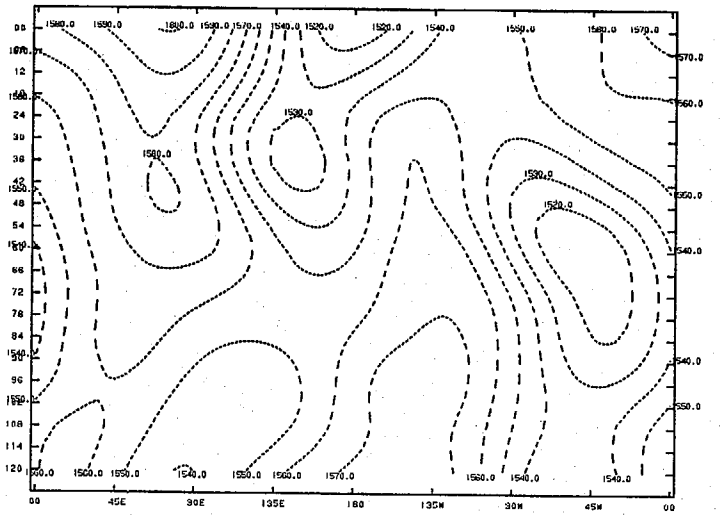

850 MB HEIGHT psup DT= 06HRINITIAL TIME GMT JUN 79

GLO SPEC MODEL FCST EVOL LAT 2.5-TO- 2.5 WAVES 0 TO 3

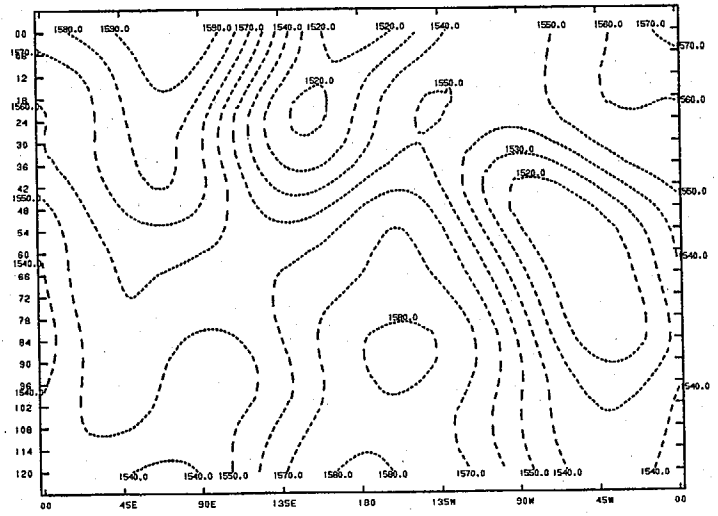

850 MB HEIGHT c sep DT= 06HRINITIAL TIME GMT JUN 79

55

GLO SPEC MODEL FCST EVOL LAT 2.5-TO- 2.5 WAVES 0 TO 3

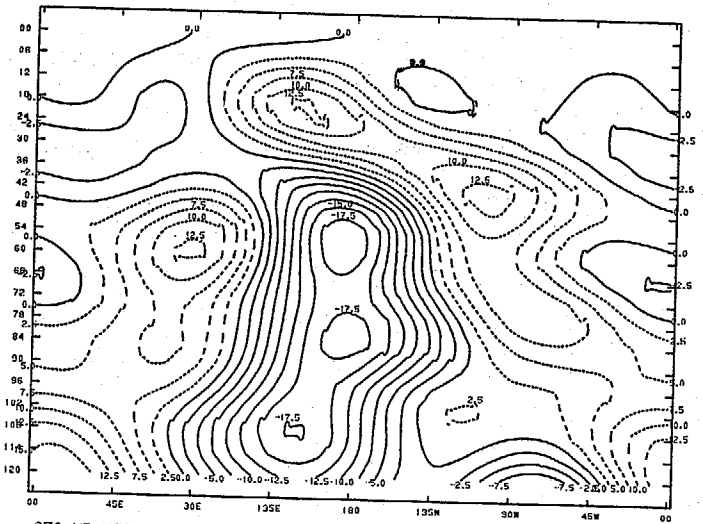

850 MB HEIGHT sup DT= 06HRINITIAL TIME GMT JUN 79

GLO SPEC MODEL FCST EVOL LAT 2.5-TO- 2.5 WAVES 0 TO 3

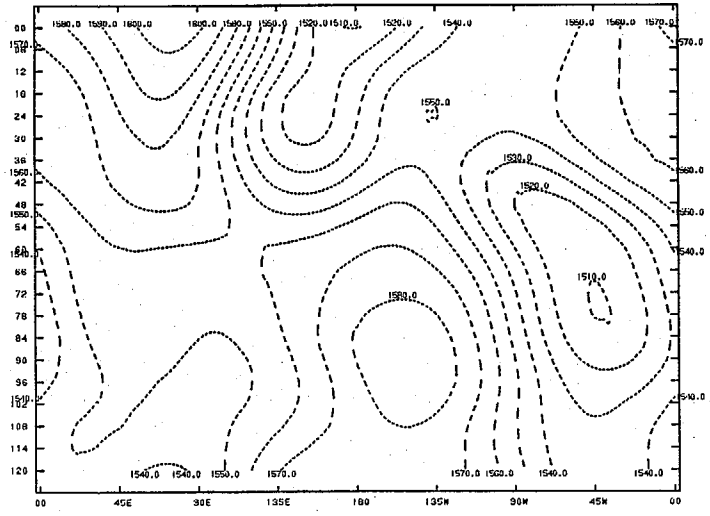

850 MB HEIGHT 6 sep DT= 06HRINITIAL TIME GMT JUN 79

GLO SPEC MODEL FCST EVOL LAT 2.5-TO- 2.5 WAVES 0 TO 3

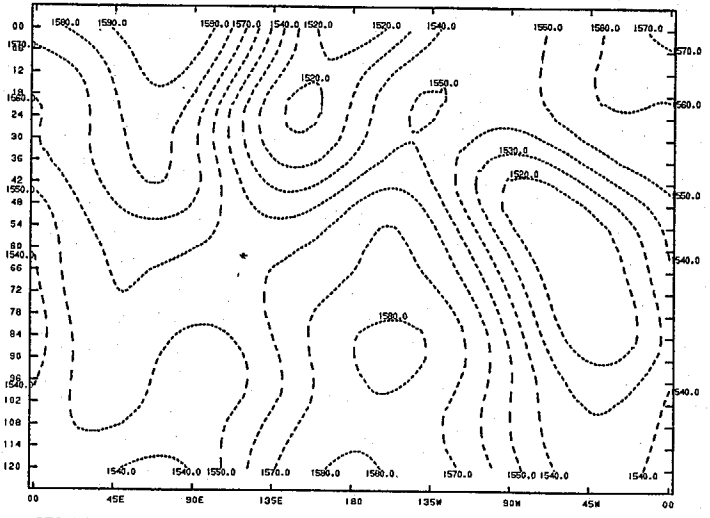

850 MB HEIGHT 6 sep DT= 06HRINITIAL TIME GMT JUN 79

GLO SPEC MODEL FCST EVOL LAT 2.5-TO- 2.5 WAVES 0 TO 3

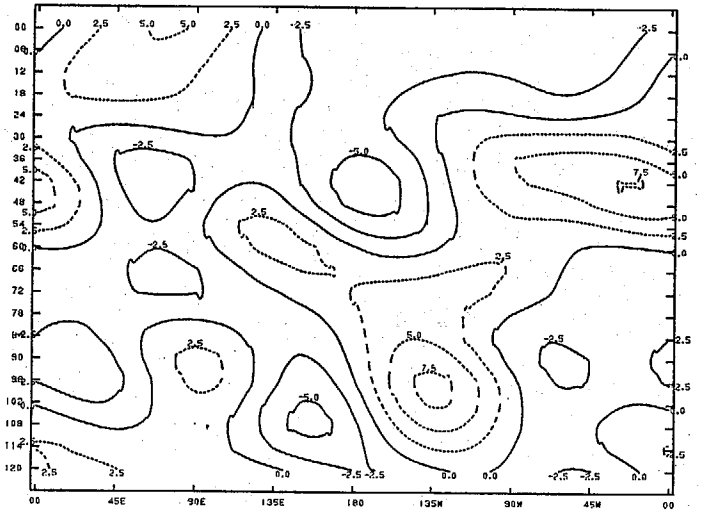

850 MB HEIGHT 5 sep DT= 06HRINITIAL TIME GMT JUN 79

GLO SPEC MODEL FCST EVOL LAT 2.5-TO- 2.5 WAVES 0 TO 3

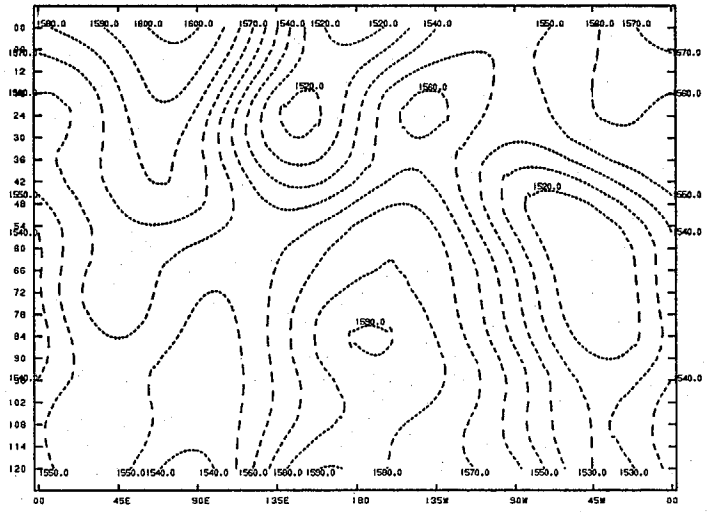

850 MB HEIGHT PSGP DT= 06HRINITIAL TIME GMT JUN 79

GLO SPEC MODEL FCST EVOL LAT 2.5-TO- 2.5 WAVES 0 TO 3

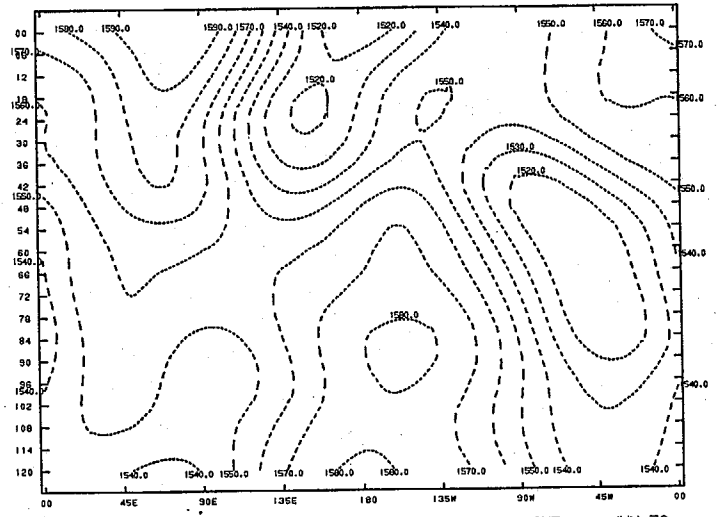

850 MB HEIGHT c sep DT= 06HRINITIAL TIME GMT JUN 79

57

GLO SPEC MODEL FCST EVOL LAT 2.5-TO- 2.5 WAVES 0 TO 3

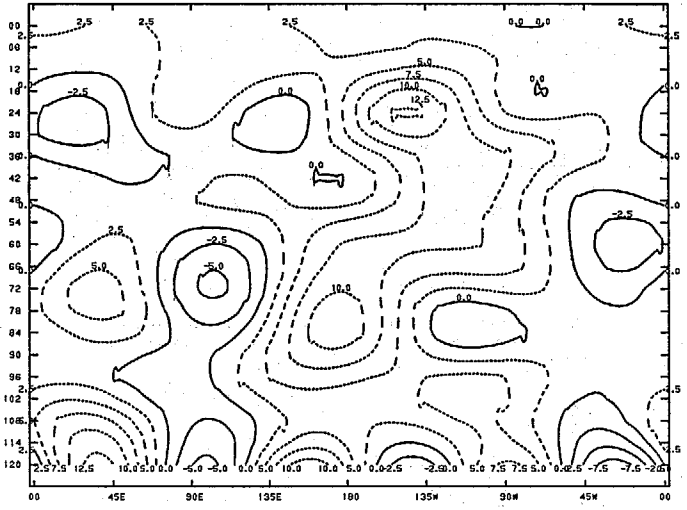

850 MB HEIGHT sep DT= 06HRINITIAL TIME GMT JUN 79

GLO SPEC MODEL FCST EVOL LAT 2.5-TO- 2.5 WAVES 0 TO 3

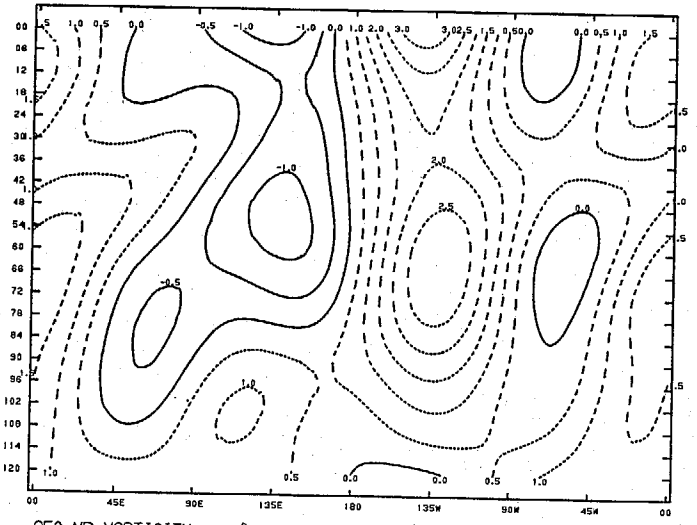

850 MB VORTICITY psvp DT=06 HRINITIAL TIME GMT JUN 79

GLO SPEC MODEL FCST EVOL LAT 2.5-TO- 2.5 WAVES 0 TO 3

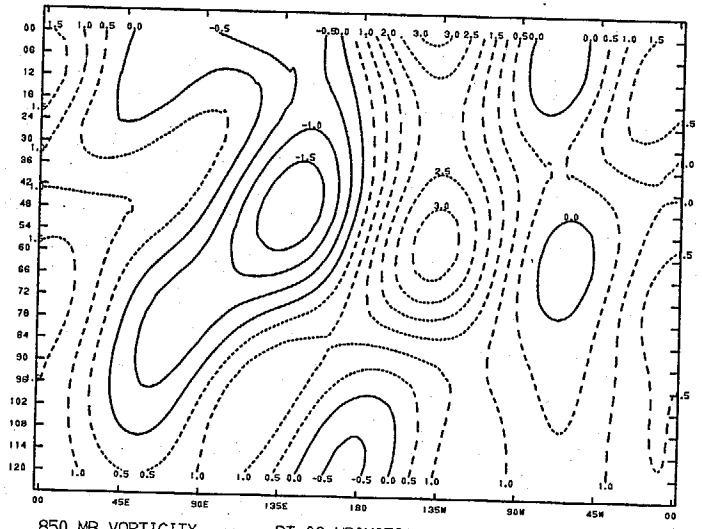

850 MB VORTICITY csep DT=06 HRINITIAL TIME GMT JUN 79

GLO SPEC MODEL FCST EVOL LAT 2.5-TO- 2.5 WAVES 0 TO 3

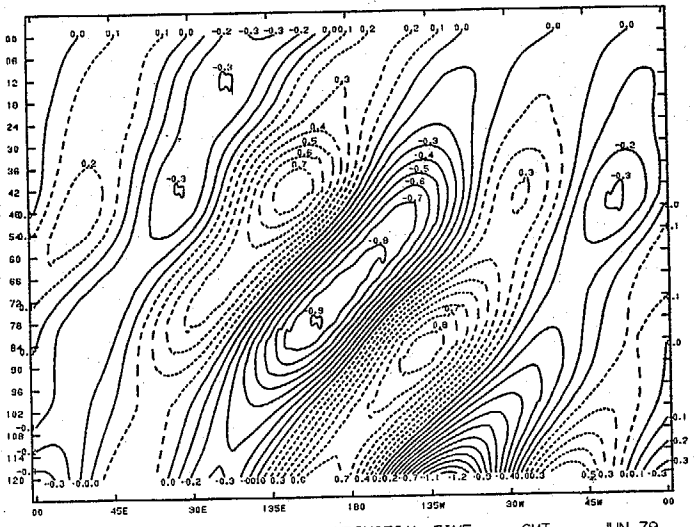

850 MB VORTICITY swp DT=06 HRINITIAL TIME GMT JUN 79

GLO SPEC MODEL FCST EVOL LAT 2.5-TO- 2.5 WAVES 0 TO 3

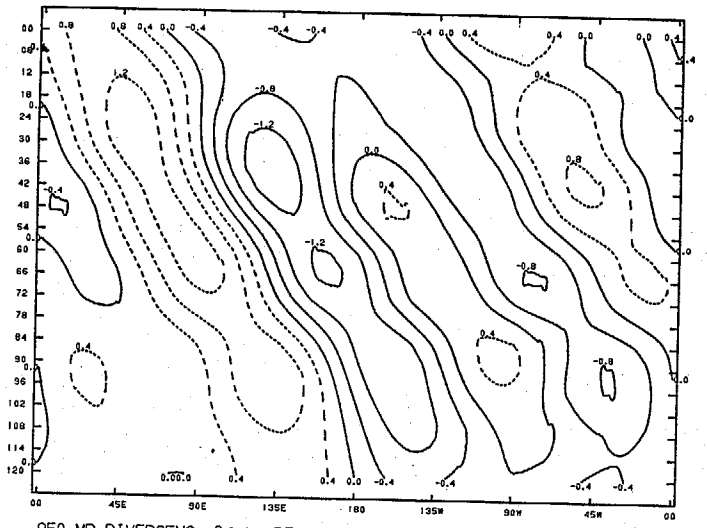

850 MB DIVERGENC P SWP DT=06 HRINITIAL TIME GMT JUN 79

GLO SPEC MODEL FCST EVOL LAT 2.5-TO- 2.5 WAVES 0 TO 3

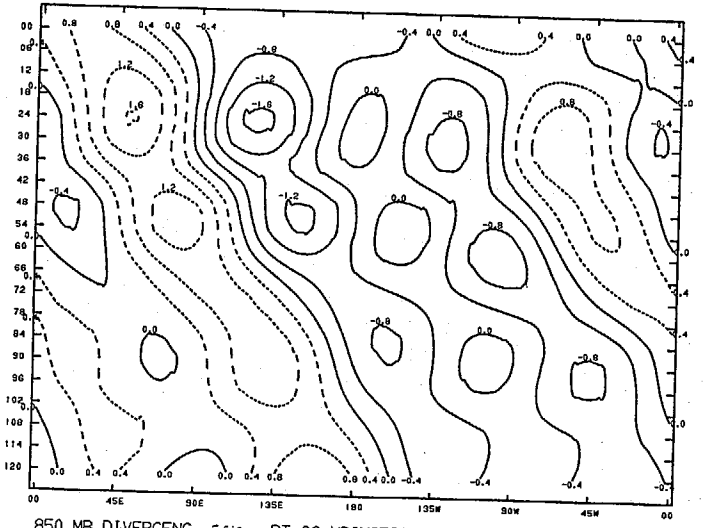

850 MB DIVERGENC C SEP DT=06 HRINITIAL TIME GMT JUN 79

GLO SPEC MODEL FCST EVOL LAT 2.5-TO- 2.5 WAVES 0 TO 3

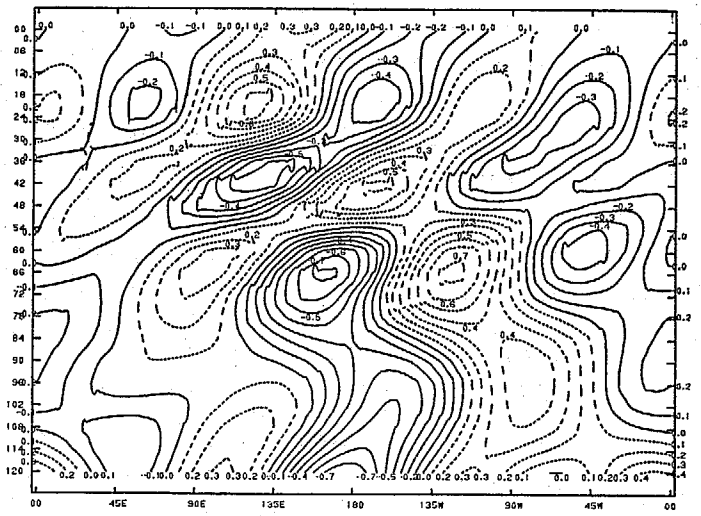

850 MB DIVERGENC SWP DT=06 HRINITIAL TIME GMT JUN 79

GLO SPEC MODEL FCST EVOL LAT 2.5-TO- 2.5 WAVES 0 TO 3

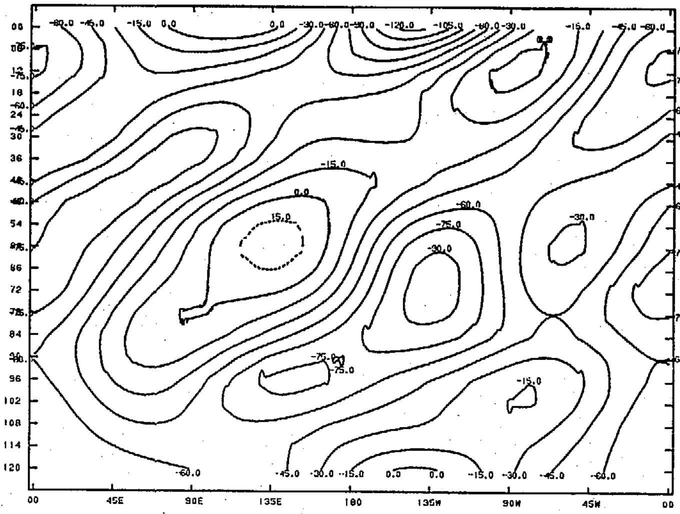

850 MB STREAM FN ρ SWP DT= 06HRINITIAL TIME GMT JUN 79

GLO SPEC MODEL FCST EVOL LAT 2.5-TO- 2.5 WAVES 0 TO 3

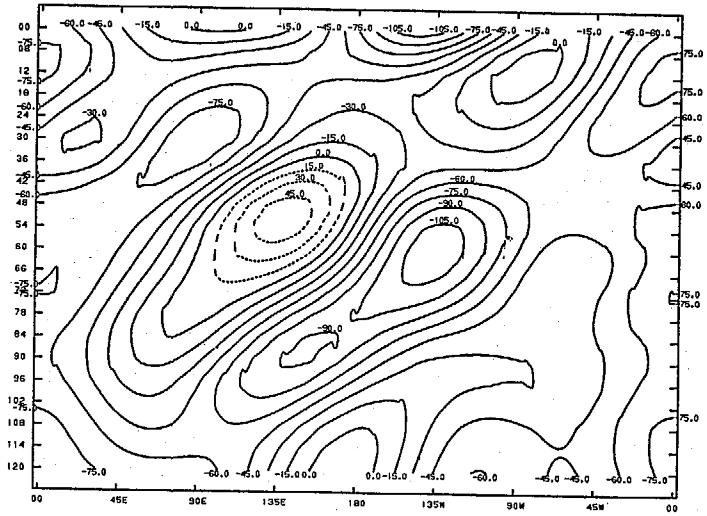

850 MB STREAM FN CSGP DT= 06HRINITIAL TIME GMT JUN 79

GLO SPEC MODEL FCST EVOL LAT 2.5-TO- 2.5 WAVES 0 TO 3

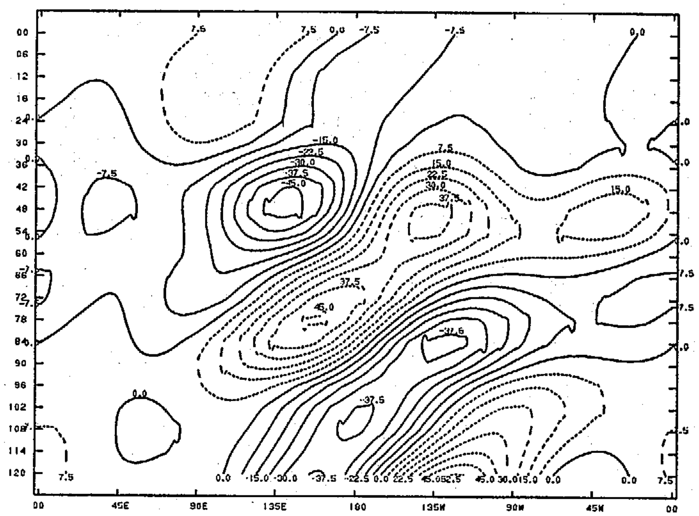

850 MB STREAM FN SWP DT= 06HRINITIAL TIME GMT JUN 79

GLO SPEC MODEL FCST EVOL LAT 2.5-TO- 2.5 WAVES 0 TO 3

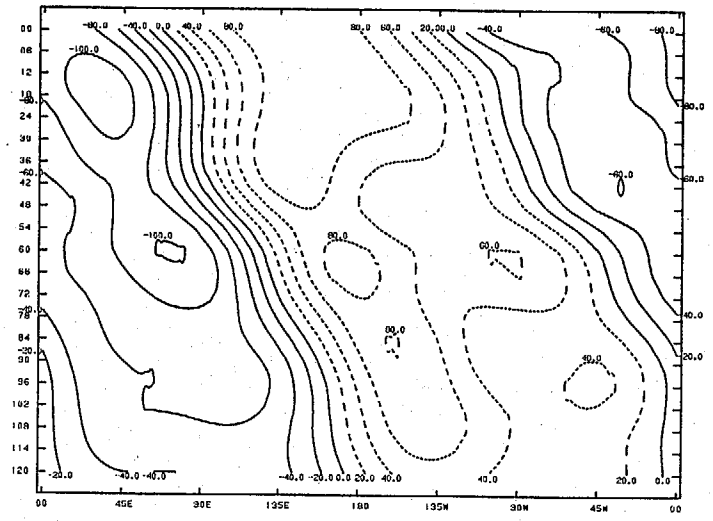

850 MB VEL POT psup DT= 06HRINITIAL TIME GMT JUN 79

GLO SPEC MODEL FCST EVOL LAT 2.5-TO- 2.5 WAVES 0 TO 3

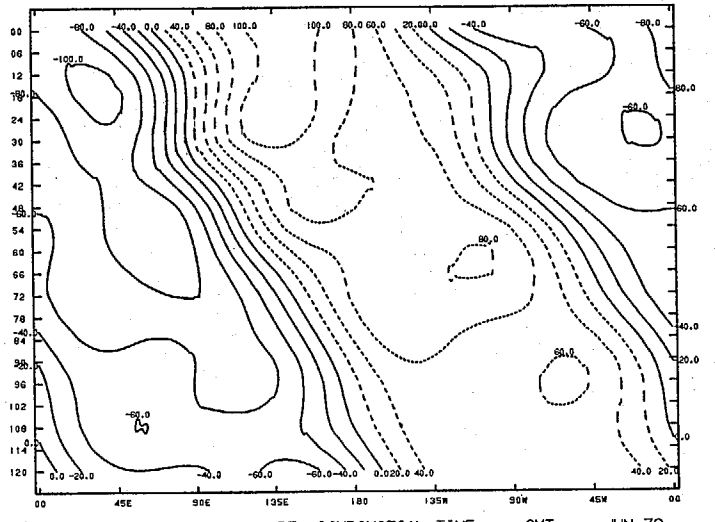

850 MB VEL POT csep DT= 06HRINITIAL TIME GMT JUN 79

GLO SPEC MODEL FCST EVOL LAT 2.5-TO- 2.5 WAVES 0 TO 3

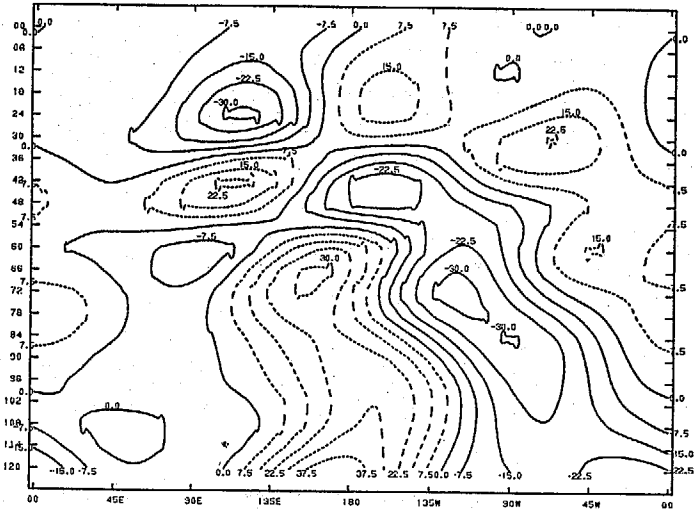

850 MB VEL POT swp DT= 06HRINITIAL TIME GMT JUN 79

GLO SPEC MODEL FCST EVOL LAT 2.5-TO- 2.5 WAVES 0 TO 3

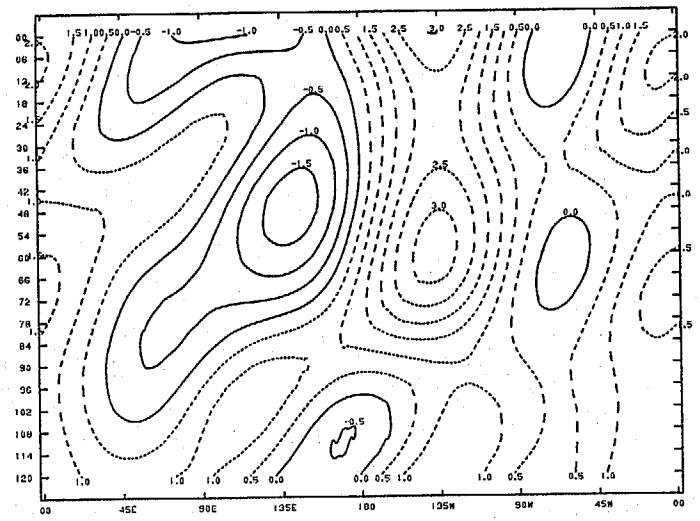

850 MB VORTICITY Psio DT=06 HRINITIAL TIME GMT JUN 79

GLO SPEC MODEL FCST EVOL LAT 2.5-TO- 2.5 WAVES 0 TO 3

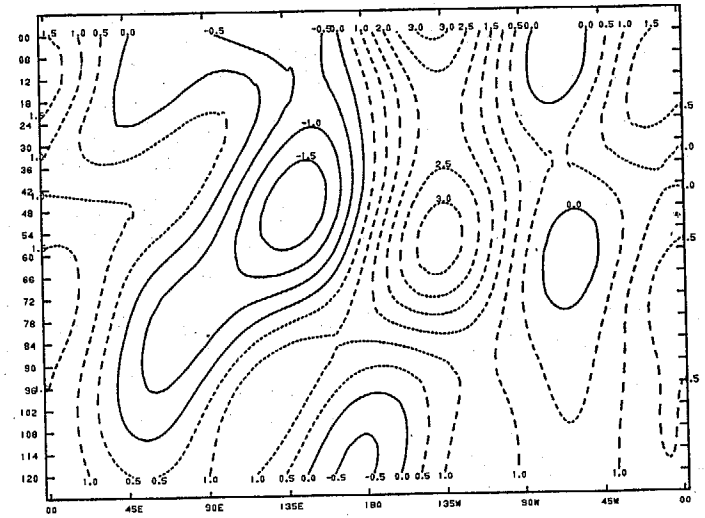

850 MB VORTICITY csep DT=06 HRINITIAL TIME GMT JUN 79

62

GLO SPEC MODEL FCST EVOL LAT 2.5-TO- 2.5 WAVES 0 TO 3

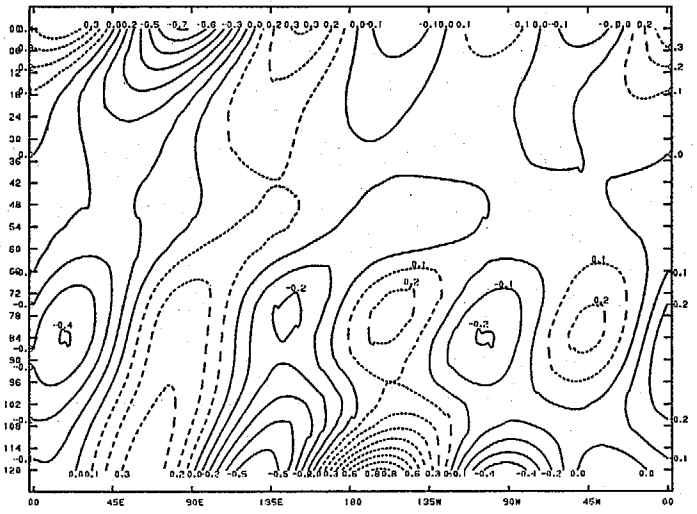

850 MB VORTICITY S1o DT=06 HRINITIAL TIME GMT JUN 79

GLO SPEC MODEL FCST EVOL LAT 2.5-TO- 2.5 WAVES 0 TO 3

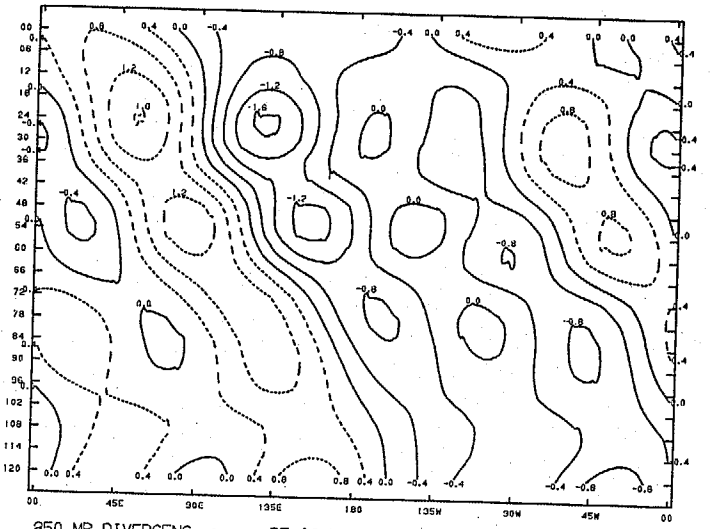

850 MB DIVERGENC P s/o DT=06 HRINITIAL TIME GMT JUN 79

GLO SPEC MODEL FCST EVOL LAT 2.5-TO- 2.5 WAVES 0 TO 3

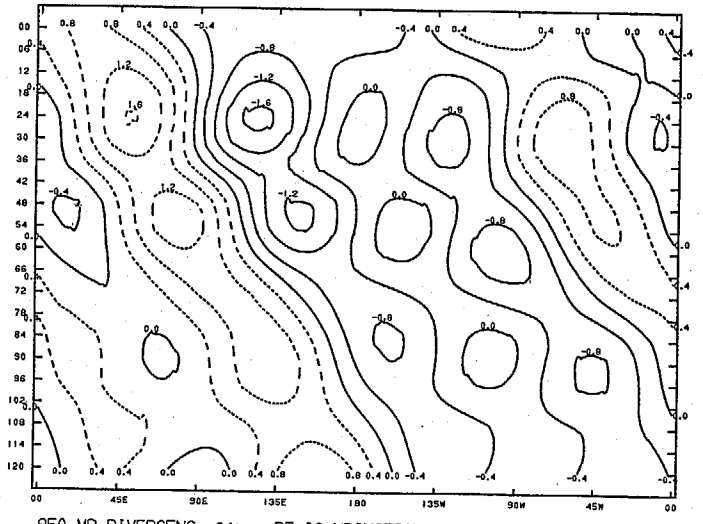

850 MB DIVERGENC Sep DT=06 HRINITIAL TIME GMT JUN 79

GLO SPEC MODEL FCST EVOL LAT 2.5-TO- 2.5 WAVES 0 TO 3

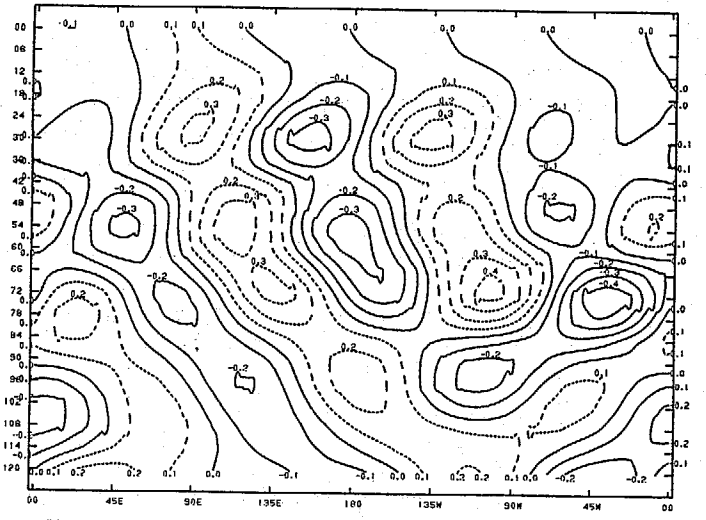

850 MB DIVERGENC s/o DT=06 HRINITIAL TIME GMT JUN 79

GLO SPEC MODEL FCST EVOL LAT 2.5-TO- 2.5 WAVES 0 TO 3

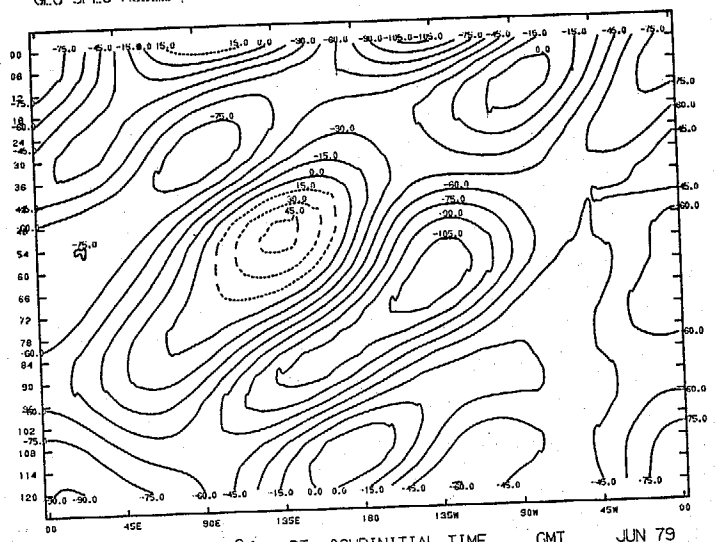

850 MB STREAM FN P510 DT= 06HRINITIAL TIME GMT JUN 79

GLO SPEC MODEL FCST EVOL LAT 2.5-TO- 2.5 WAVES 0 TO 3

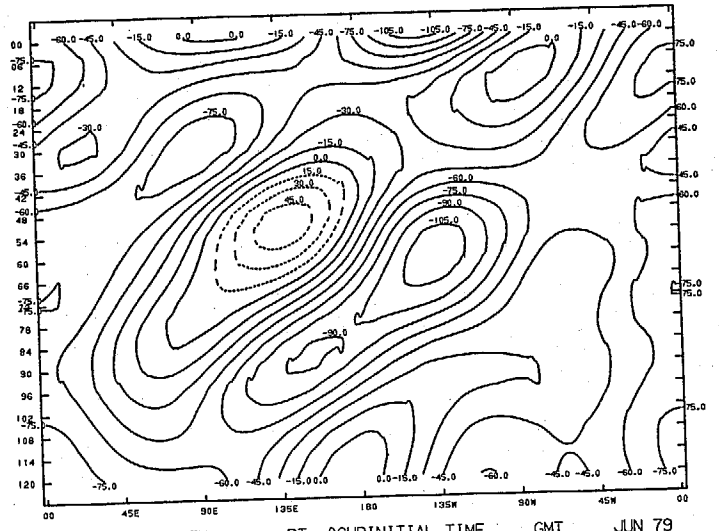

850 MB STREAM FN C566 DT= 06HRINITIAL TIME GMT JUN 79

64

GLO SPEC MODEL FCST EVOL LAT 2.5-TO- 2.5 WAVES 0 TO 3

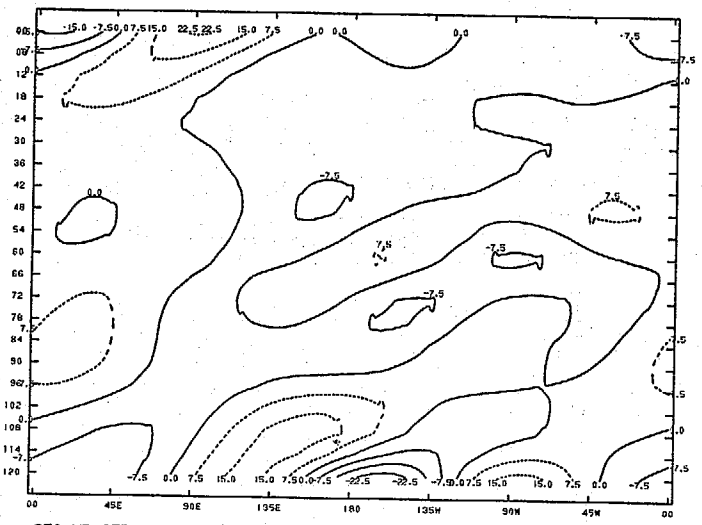

850 MB STREAM FN 510 DT= 06HRINITIAL TIME GMT JUN 79

GLO SPEC MODEL FCST EVOL LAT 2.5-TO- 2.5 WAVES 0 TO 3

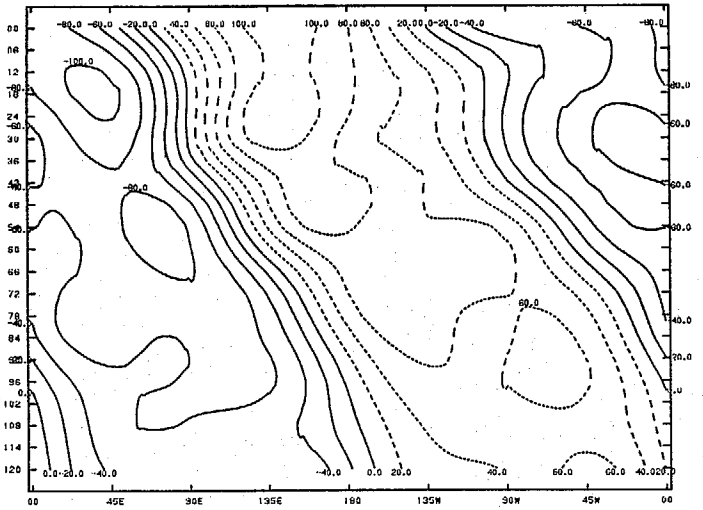

850 MB VEL POT χ_{10} DT= 06HRINITIAL TIME GMT JUN 79

GLO SPEC MODEL FCST EVOL LAT 2.5-TO- 2.5 WAVES 0 TO 3

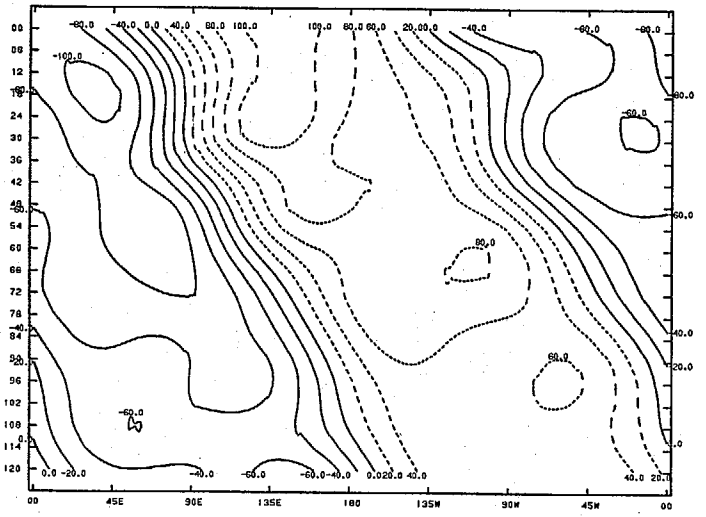

850 MB VEL POT χ_{sep} DT= 06HRINITIAL TIME GMT JUN 79

GLO SPEC MODEL FCST EVOL LAT 2.5-TO- 2.5 WAVES 0 TO 3

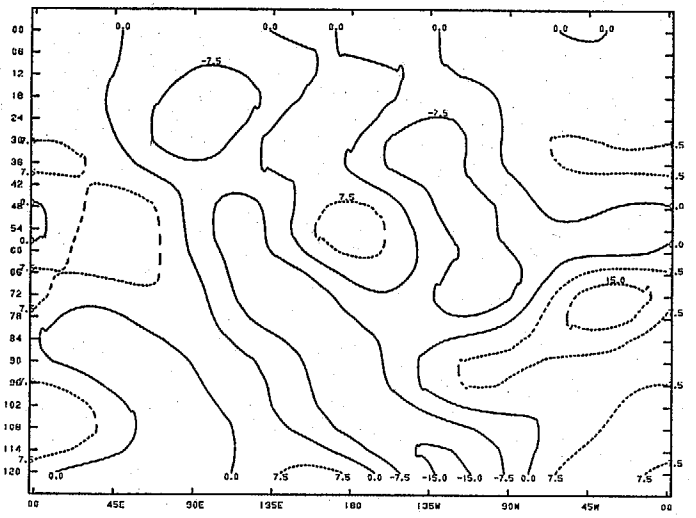

850 MB VEL POT χ_{10} DT= 06HRINITIAL TIME GMT JUN 79

GLO SPEC MODEL FCST EVOL LAT 2.5-TO- 2.5 WAVES 0 TO 3

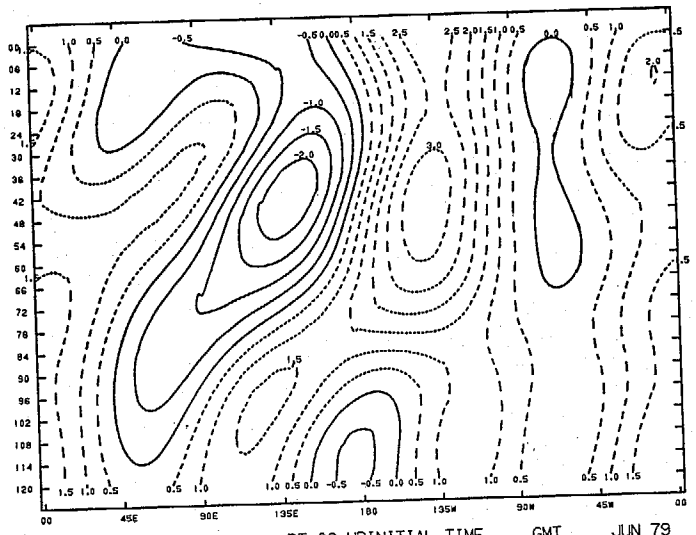

850 MB VORTICITY psep DT=06 HRINITIAL TIME GMT JUN 79

GLO SPEC MODEL FCST EVOL LAT 2.5-TO- 2.5 WAVES 0 TO 3

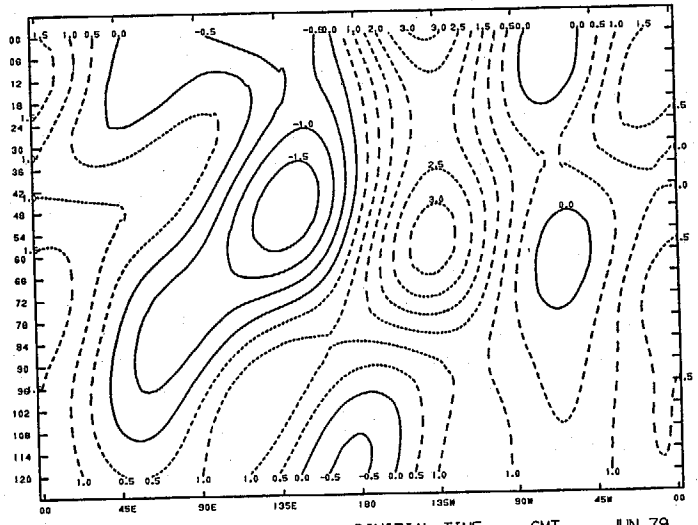

850 MB VORTICITY csep DT=06 HRINITIAL TIME GMT JUN 79

GLO SPEC MODEL FCST EVOL LAT 2.5-TO- 2.5 WAVES 0 TO 3

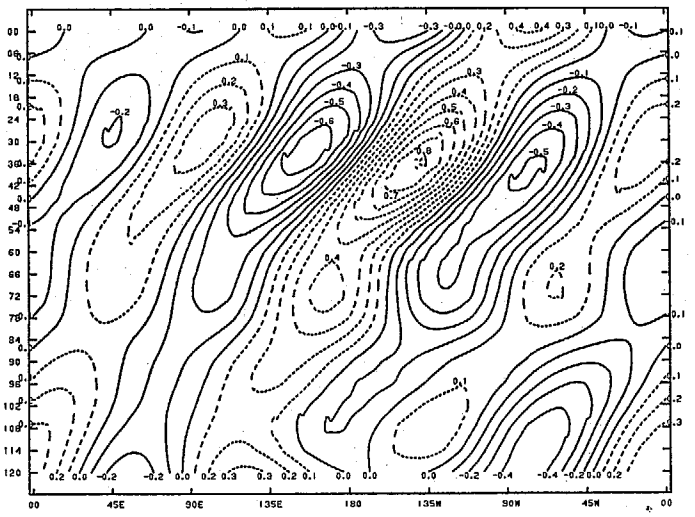

850 MB VORTICITY sep DT=06 HRINITIAL TIME GMT JUN 79

GLO SPEC MODEL FCST EVOL LAT 2.5-TO- 2.5 WAVES 0 TO 3

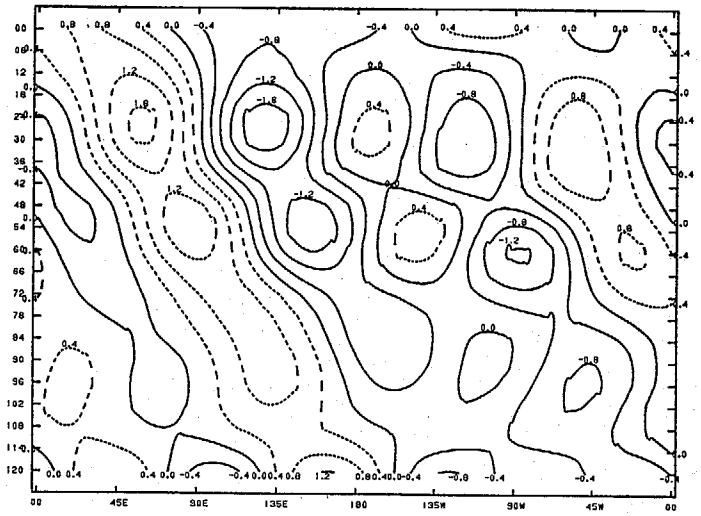

850 MB DIVERGENC SEP DT=06 HRINITIAL TIME GMT JUN 79

GLO SPEC MODEL FCST EVOL LAT 2.5-TO- 2.5 WAVES 0 TO 3

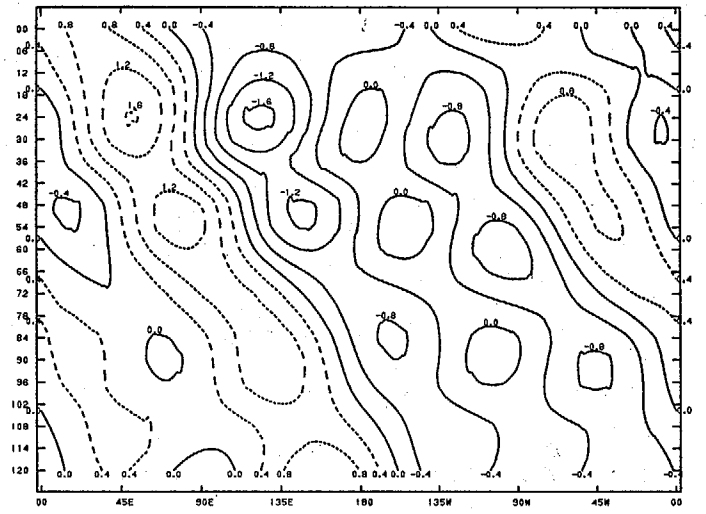

850 MB DIVERGENC SEP DT=06 HRINITIAL TIME GMT JUN 79

GLO SPEC MODEL FCST EVOL LAT 2.5-TO- 2.5 WAVES 0 TO 3

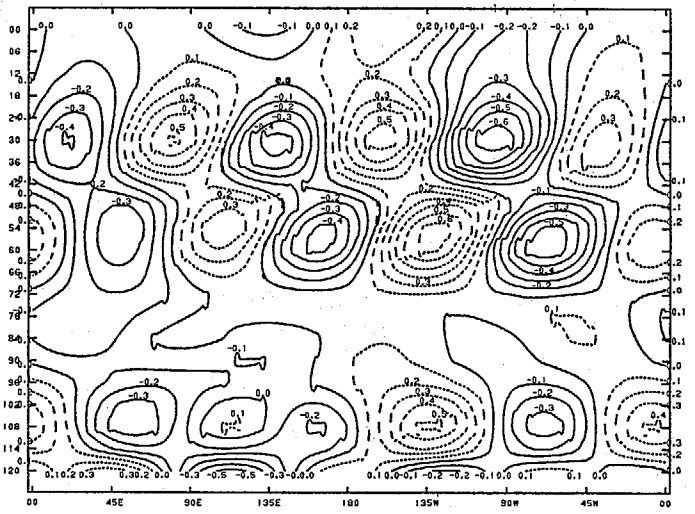

850 MB DIVERGENC SEP DT=06 HRINITIAL TIME GMT JUN 79

GLO SPEC MODEL FCST EVOL LAT 2.5-TO- 2.5 WAVES 0 TO 3

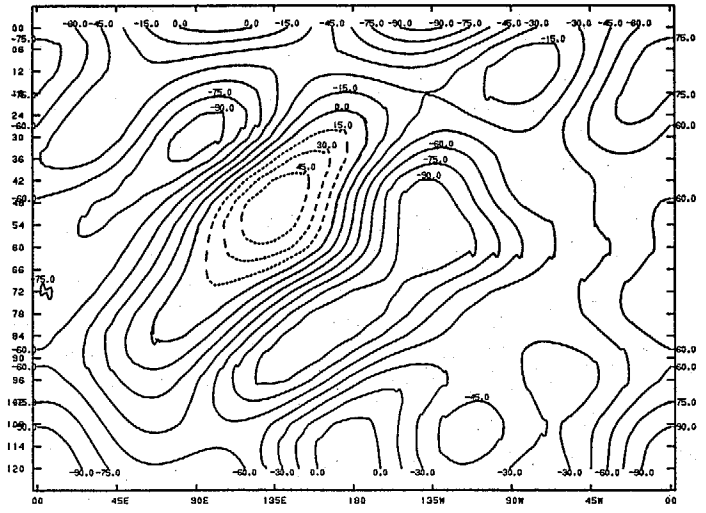

850 MB STREAM FN PSEP DT= 06HRINITIAL TIME GMT JUN 79

GLO SPEC MODEL FCST EVOL LAT 2.5-TO- 2.5 WAVES 0 TO 3

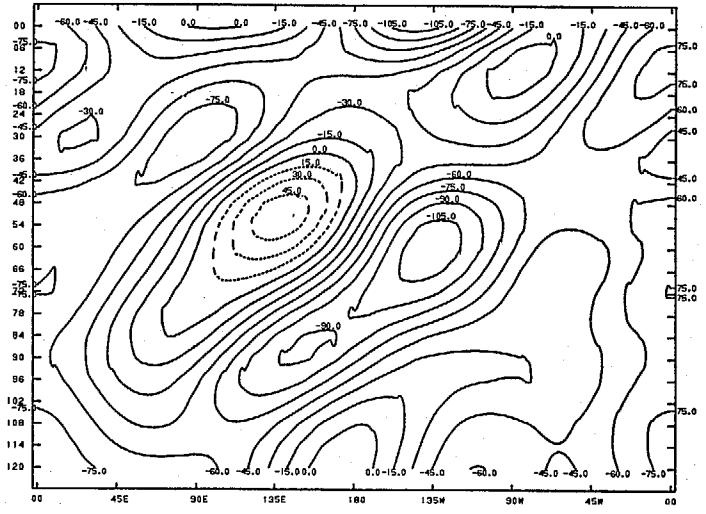

850 MB STREAM FN CSEP DT= 06HRINITIAL TIME GMT JUN 79

GLO SPEC MODEL FCST EVOL LAT 2.5-TO- 2.5 WAVES 0 TO 3

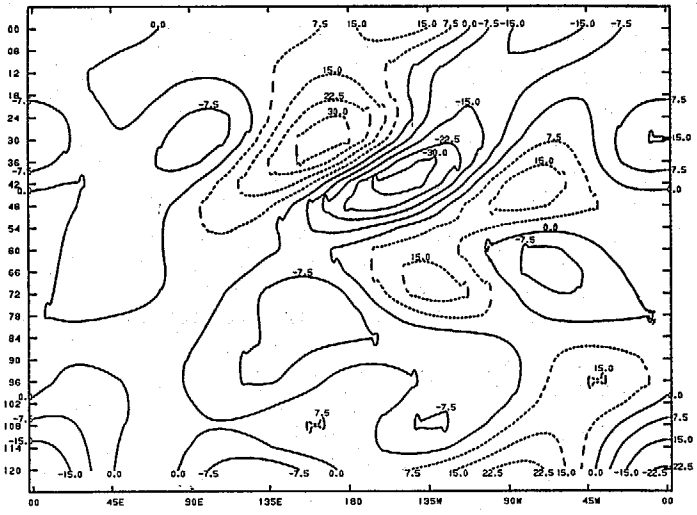

850 MB STREAM FN SEP DT= 06HRINITIAL TIME GMT JUN 79

GLO SPEC MODEL FCST EVOL LAT 2.5-TO- 2.5 WAVES 0 TO 3

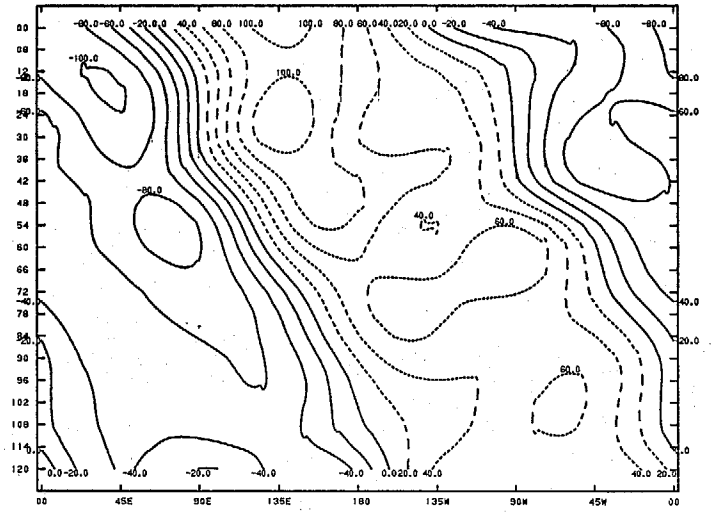

850 MB VEL POT psep DT= 06HRINITIAL TIME GMT JUN 79

GLO SPEC MODEL FCST EVOL LAT 2.5-TO- 2.5 WAVES 0 TO 3

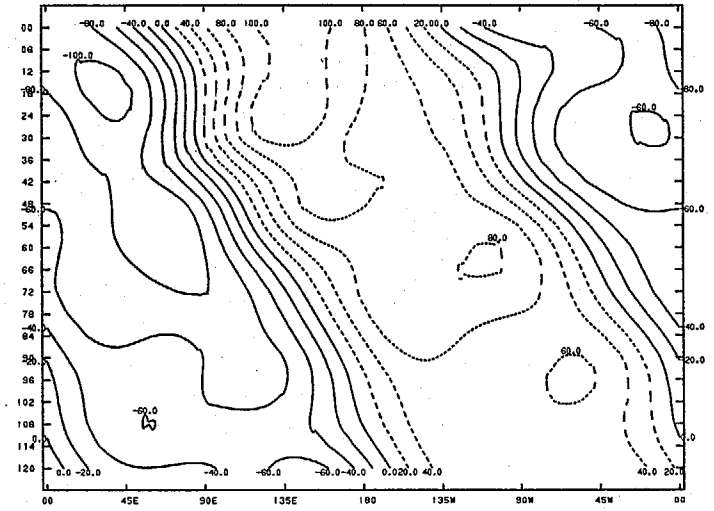

850 MB VEL POT csep DT= 06HRINITIAL TIME GMT JUN 79

69

GLO SPEC MODEL FCST EVOL LAT 2.5-TO- 2.5 WAVES 0 TO 3

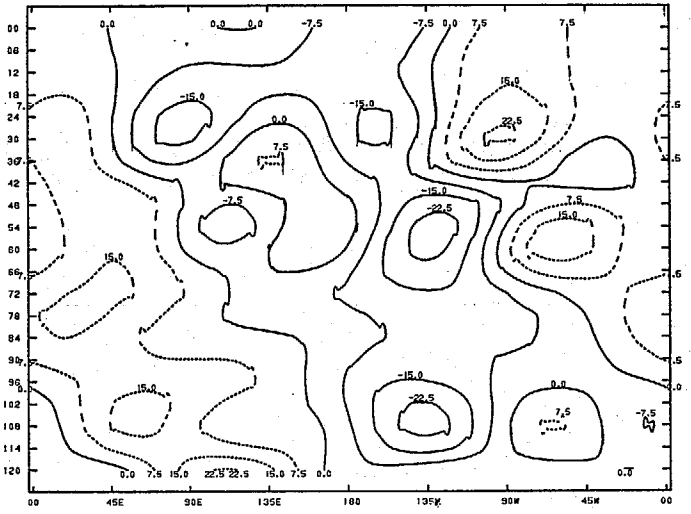

850 MB VEL POT ssep DT= 06HRINITIAL TIME GMT JUN 79

GLO SPEC MODEL FCST EVOL LAT 2.5-TO- 2.5 WAVES 0 TO 3

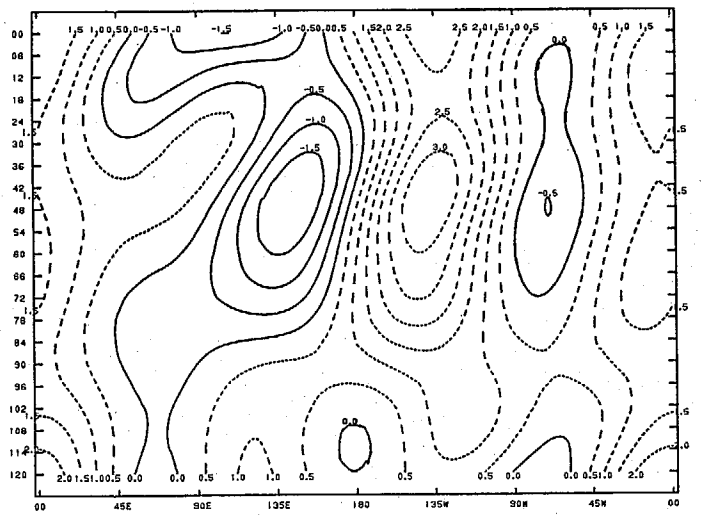

850 MB VORTICITY PSTT DT=06 HRINITIAL TIME GMT JUN 79

GLO SPEC MODEL FCST EVOL LAT 2.5-TO- 2.5 WAVES 0 TO 3

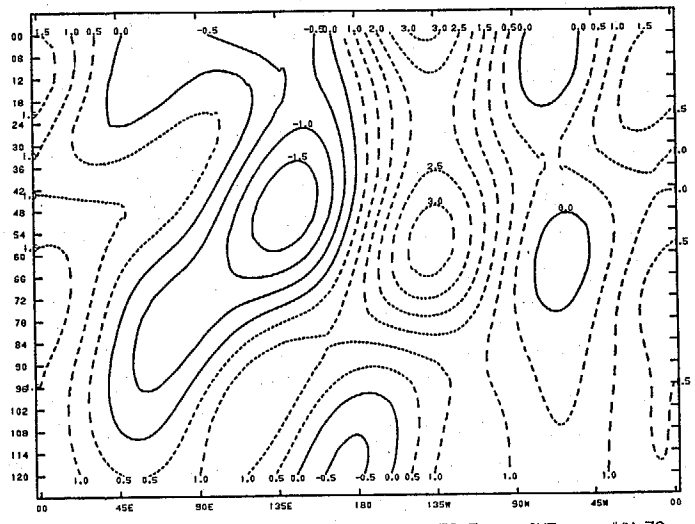

850 MB VORTICITY CSEE DT=06 HRINITIAL TIME GMT JUN 79

GLO SPEC MODEL FCST EVOL LAT 2.5-TO- 2.5 WAVES 0 TO 3

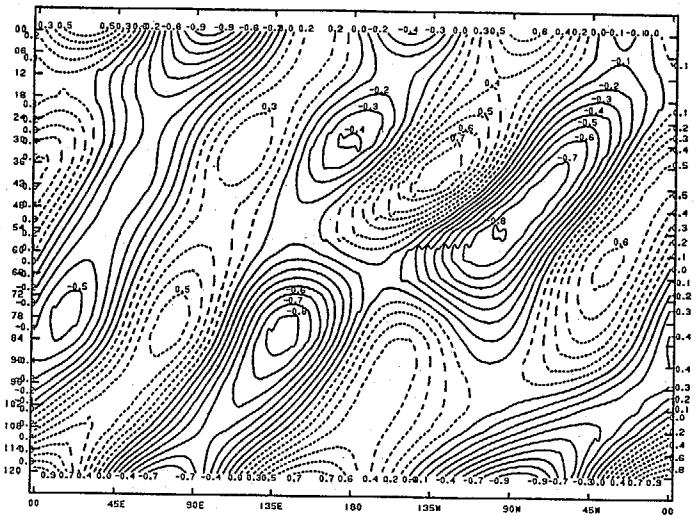

850 MB VORTICITY STT DT=06 HRINITIAL TIME GMT JUN 79

GLO SPEC MODEL FCST EVOL LAT 2.5-TO- 2.5 WAVES 0 TO 3

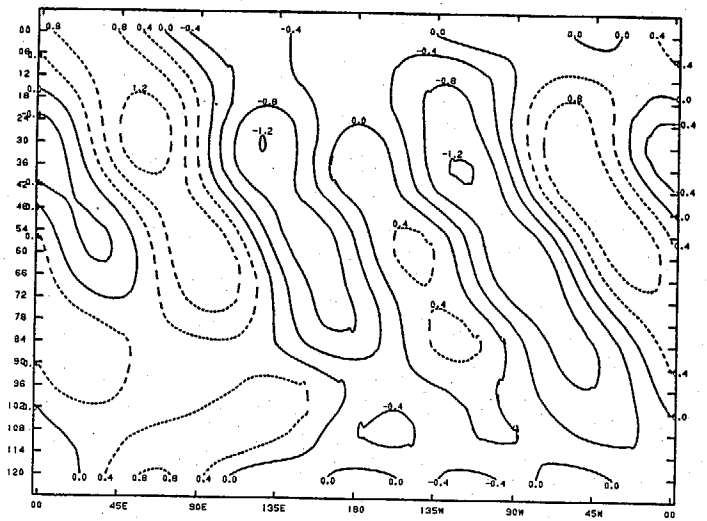

850 MB DIVERGENC PSTT DT=06 HRINITIAL TIME GMT JUN 79

GLO SPEC MODEL FCST EVOL LAT 2.5-TO- 2.5 WAVES 0 TO 3

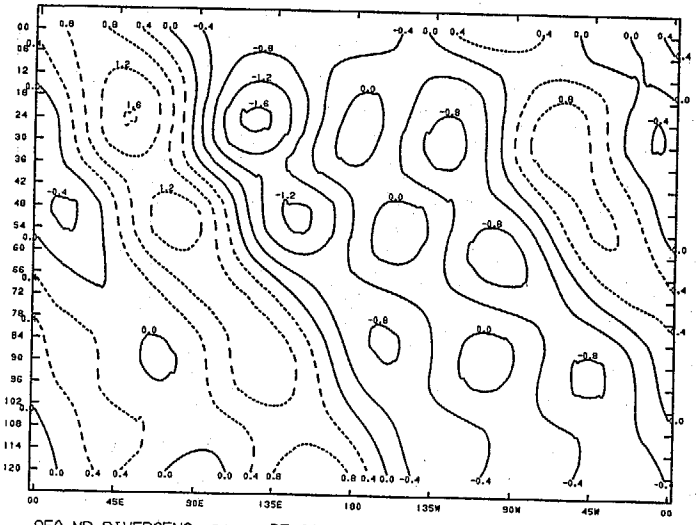

850 MB DIVERGENC PSTT DT=06 HRINITIAL TIME GMT JUN 79

GLO SPEC MODEL FCST EVOL LAT 2.5-TO- 2.5 WAVES 0 TO 3

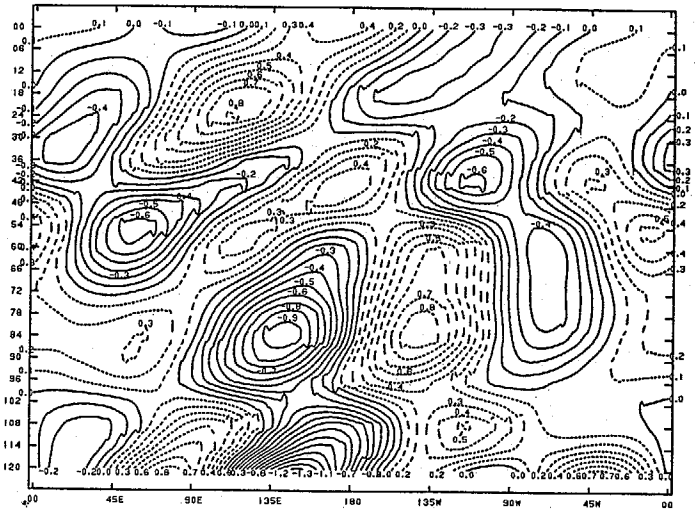

850 MB DIVERGENC PSTT DT=06 HRINITIAL TIME GMT JUN 79

GLO SPEC MODEL FCST EVOL LAT 2.5-TO- 2.5 WAVES 0 TO 3

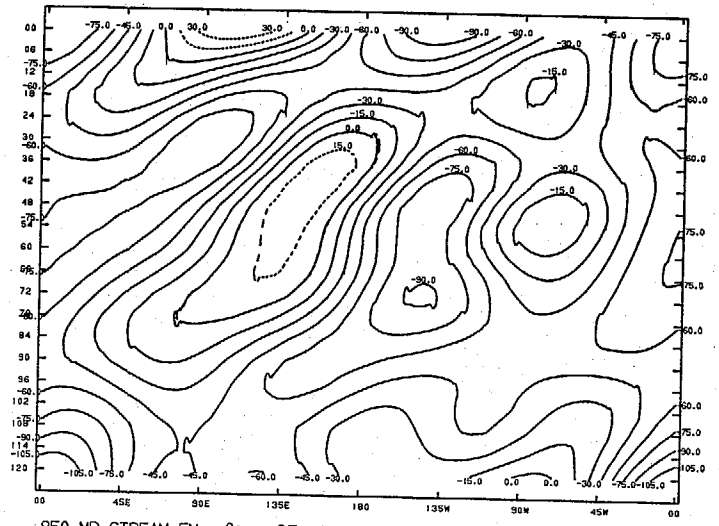

850 MB STREAM FN ψ_{STT} DT= 06HRINITIAL TIME GMT JUN 79

GLO SPEC MODEL FCST EVOL LAT 2.5-TO- 2.5 WAVES 0 TO 3

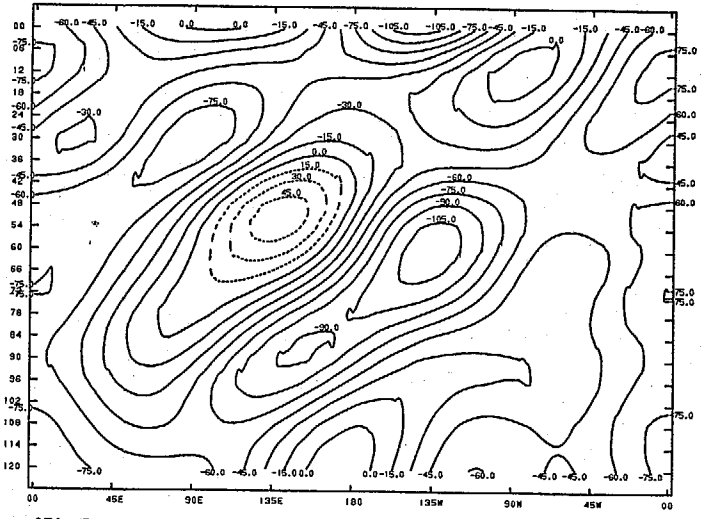

850 MB STREAM FN ψ_{SGP} DT= 06HRINITIAL TIME GMT JUN 79

GLO SPEC MODEL FCST EVOL LAT 2.5-TO- 2.5 WAVES 0 TO 3

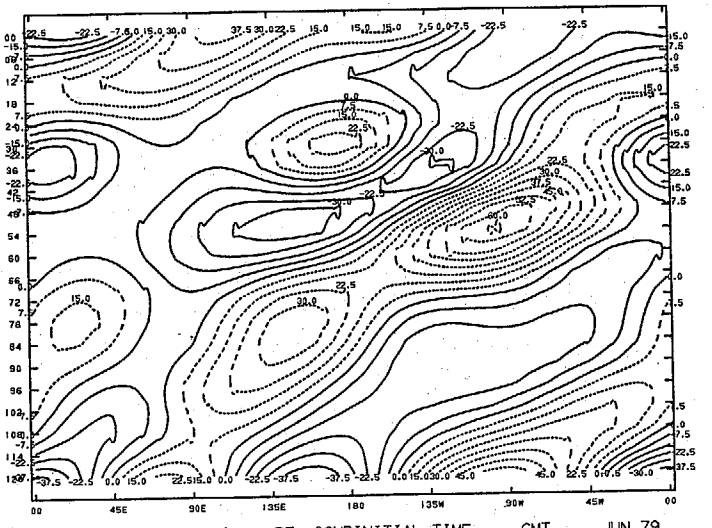

850 MB STREAM FN ψ_{STT} DT= 06HRINITIAL TIME GMT JUN 79

GLO SPEC MODEL FCST EVOL LAT 2.5-TO- 2.5 WAVES 0 TO 3

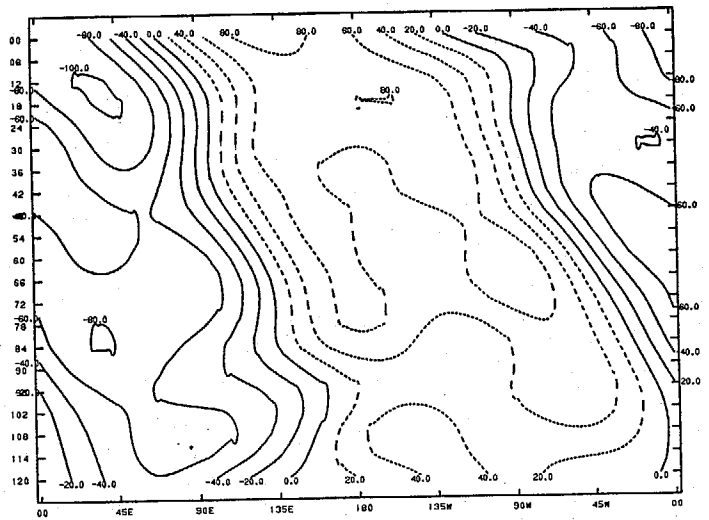

850 MB VEL POT PSTT DT= 06HRINITIAL TIME GMT JUN 79

GLO SPEC MODEL FCST EVOL LAT 2.5-TO- 2.5 WAVES 0 TO 3

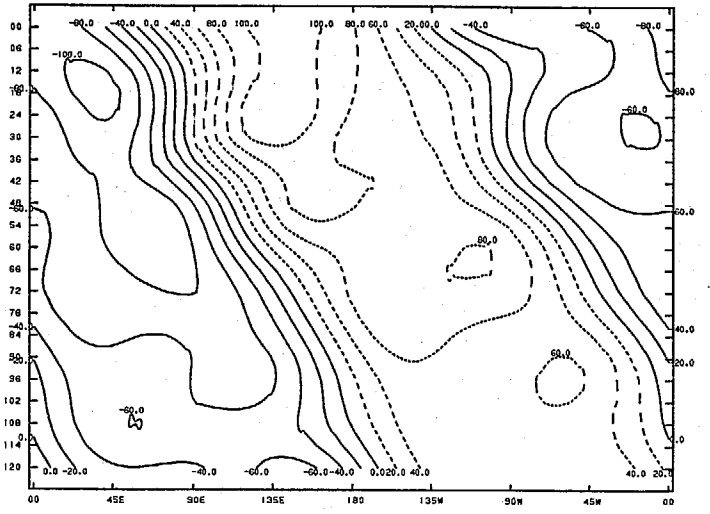

850 MB VEL POT CSEP DT= 06HRINITIAL TIME GMT JUN 79

GLO SPEC MODEL FCST EVOL LAT 2.5-TO- 2.5 WAVES 0 TO 3

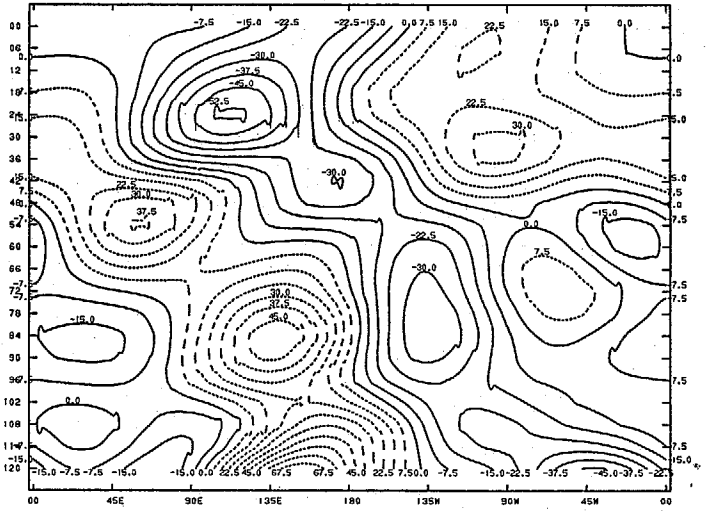

850 MB VEL POT STT DT= 06HRINITIAL TIME GMT JUN 79

GLO SPEC MODEL FCST EVOL LAT 2.5-TO- 2.5 WAVES 0 TO 3

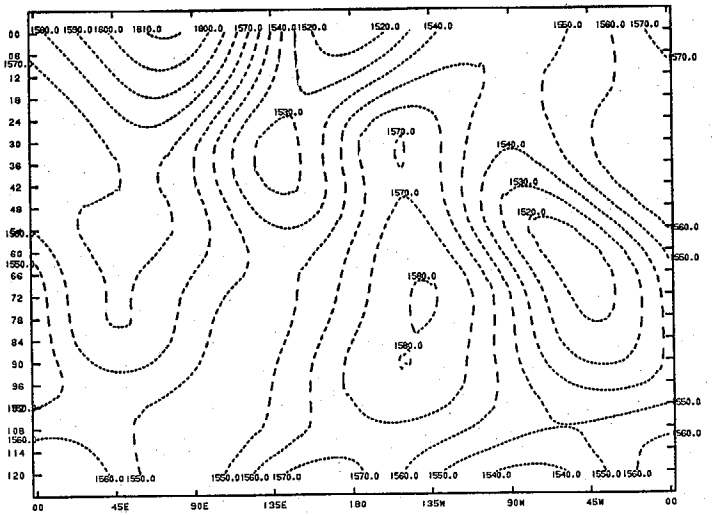

850 MB HEIGHT Psττ DT= 06HRINITIAL TIME GMT JUN 79

GLO SPEC MODEL FCST EVOL LAT 2.5-TO- 2.5 WAVES 0 TO 3

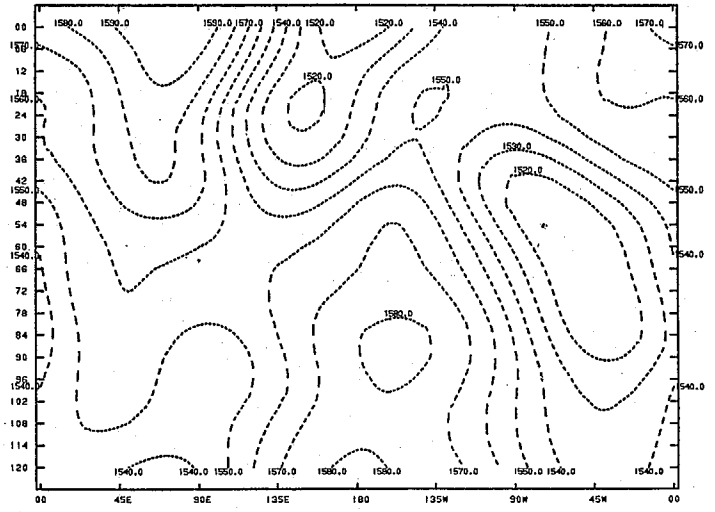

850 MB HEIGHT c sep DT= 06HRINITIAL TIME GMT JUN 79

GLO SPEC MODEL FCST EVOL LAT 2.5-TO- 2.5 WAVES 0 TO 3

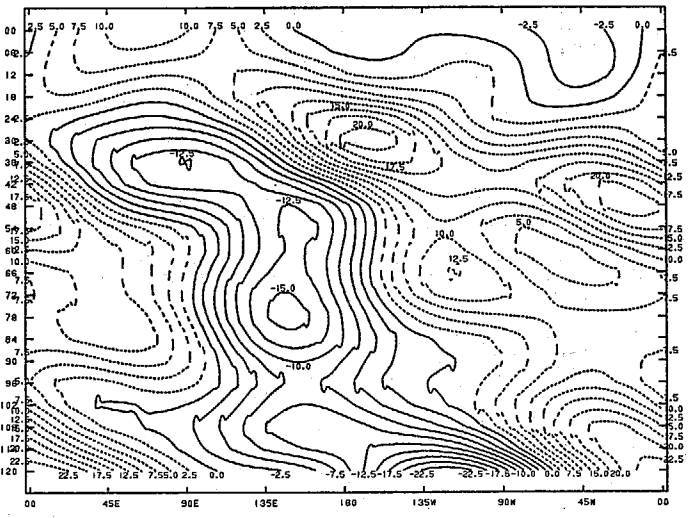

850 MB HEIGHT ϕsττ DT= 06HRINITIAL TIME GMT JUN 79

74